Development of a novel methodology for the determination of the total solar energy transmittance of Building-Integrated Photovoltaic window technologies using outdoor measurements

by

Sara Eskandar

A thesis

presented to the University of Waterloo

in fulfilment of the

thesis requirement for the degree of

Master of Applied Science

in

Civil Engineering

Waterloo, Ontario, Canada, 2023

Author's declaration

I hereby declare that I am the sole author of this thesis. This is a true copy of the thesis, including any required final revisions, as accepted by my examiners.

I understand that my thesis may be made electronically available to the public.

Abstract

The urgent need to combat global warming and transition towards sustainable energy sources has focused attention on the building sector, a major contributor to energy consumption and greenhouse gas emissions. To achieve net-zero energy building performance, a comprehensive approach is essential, involving energy conservation measures, enhanced building systems efficiency, and integrating on-site renewable energy generation. Within this context, the integration of photovoltaic window technologies become essential for the generation of renewable electricity and reduction of solar heat gains which impacts building heating, cooling, and electric lighting loads as well as visual and thermal comfort.

The aim of this thesis is to introduce the theoretical background of a novel experimental methodology for the determination of total solar energy transmittance (TSET) of building-integrated photovoltaic (BIPV) windows using outdoor measurements. Existing studies and standards dictate the use of indoor test facilities consisting primarily of a hot box calorimeter where the window is mounted and characterized under a steady state solar simulator. The calorimetric (thermal) methods require steady state conditions that have been proven challenging to achieve for windows that incorporate advanced shading devices or photovoltaic cells, potentially resulting to significant measurement errors of the TSET. Also, these studies rarely characterize the angular dependency of TSET.

To overcome these challenges, a novel experimental methodology is proposed to measure TSET using optical measurements under outdoor conditions. The experimental setup uses pyranometers (for solar transmittance measurements), pyrheliometer (for direct incident measurements), several Resistance Temperature Detector (RTD) sensors and infrared cameras (for surface temperature measurements), allowing the determination of TSET (and its angular dependency) based on a series of instantaneous outdoor measurements under sunny conditions that could result to reliable and repeatable TSET values. For the case of BIPV windows, a load at maximum power point (MPP) is connected to the window, allowing the maximum fraction of the absorbed solar energy to be converted into electricity. Finally, a new approach is proposed for the conversion of measured TSET to TSET under standard conditions, using a reference window of known TSET.

The unique aspects of the proposed TSET methodology are: i) the use of optical measurements ii) performed under transient outdoor test conditions. Current standard TSET calorimetric tests use thermal measurements that require long window conditioning under steady state conditions. The new methodology is also able to perform TSET measurements under a range of solar angle of incidence (i.e., 0 to 60 degrees), including normal TSET. The limitation of the proposed methodology is that it is not applicable to products with angular selective properties (e.g., microshade film). While it is developed for BIPV windows, and can be applied for TSET determination of coated, reflective, and electrochromic windows, under outdoor test conditions.

In summary, a novel experimental methodology is proposed for the determination of the total solar energy transmittance of Building-Integrated Photovoltaic windows using outdoor measurements. The proposed methodology aims to provide a framework to quick, accurate, consistent, and repeatable approach to TSET testing that can potentially be standardized for BIPV windows and other advanced window technologies. The proposed methodology intends to support the advancement of sustainable building practices, enhance energy efficiency, and foster the integration of renewable energy technologies into building design and construction, paving the way for a more sustainable built environment.

Key words:

Acknowledgements

Table of Contents

List of Figures

List of Tables

List of Abbreviations

AOI	Angle of incidence
a-Si	Amorphous silicon
BIPV	Building-Integrated Photovoltaic
CdTe	Cadmium telluride
CIGS	Copper indium gallium (di) selenide
c-Si	Crystalline silicon (Mono-crystalline, Multi-crystalline, Micro-crystalline)
EVA	Ethylene-vinyl acetate
MPP	Maximum power point (refers to electrical I-V characteristics of PV devices)
NOCT	Nominal operating cell temperature
OC	Open circuit
pf	Packing factor
POA	Plane of array (plane of the module)
PV	Photovoltaic
PVB	Polyvinyl butyral
SC	Short circuit
SHGC	Solar heat gain coefficient
STC	Standard test conditions (irradiance 1 kW/m2, ambient temperature 25 °C, AM 1.5G solar spectrum)
TSET	Total solar energy transmittance
VLT	Visible light transmittance
WWR	Window-to-Wall Ratio

List of symbols

A	Surface area (m^2)
E	Irradiance ($\frac{W}{m^2}$)
E_{DN}	Direct normal irradiance ($\frac{W}{m^2}$)
E_{Direct}	Direct irradiance ($\frac{W}{m^2}$)
$E_{Diffuse}$	Diffuse irradiance ($\frac{W}{m^2}$)
E_t	Total irradiance ($\frac{W}{m^2}$)
E_{POA}	Irradiance on plane of array ($\frac{W}{m^2}$)
h	Surface coefficient of heat transfer($\frac{W}{m^2K}$)
h_i	Interior heat transfer coefficient ($\frac{W}{m^2K}$)
h_e	Exterior heat transfer coefficient ($\frac{W}{m^2K}$)
I	Current (A)
η	Electrical conversion efficiency (%)
$η_{STC}$	Efficiency at STC (%)
P_{max}	Power at maximum power point (W)
Q	Instantaneous energy flow (W)
R	Thermal resistance ($\frac{m^2K}{W}$)
T	Temperature (K, °C)
U	Thermal transmittance($\frac{W}{m^2K}$)
V	Voltage (V)
σ	$5.67 \cdot 10^{-8} \frac{W}{m^2K^4}$, Stefan-Boltzmann constant

Chapter 1. Introduction

1.1 Introduction

Global warming has raised awareness toward renewable energies and sustainable development strategies. The building sector accounts for 40% of all energy use and greenhouse gas emissions (GHG)[1]. Many studies have been conducted regarding sustainable and energy efficient buildings, aiming to reduce energy consumption in buildings, especially in major areas of energy consumption (heating, cooling, and lighting). Electrification and decarbonization of buildings and the built environment have become of paramount importance, primarily through the construction of net-zero energy, fully electric buildings.

To achieve net-zero energy buildings (NZEBs) performance goals, existing standards and practice has demonstrated three distinct linear steps, in building design, construction and operation: 1) energy conservation measures through high performance envelope design, 2) energy efficiency measures through efficient building systems, equipment and controls, and 3) onsite renewable energy generation [2]. Energy conservation and efficiency measures aim to reduce the energy consumption and peak power demand of the building through the implementation of well insulated, airtight building envelope with moderate Window-to-Wall-Ratio (WWR) and effective solar shading, energy efficient HVAC, lighting and plug loads. Onsite renewable energy aims to offset the building energy consumption of the building within a period of a year. While there is a wide range of cost-effective and reliable technological solutions regarding energy conservation and efficiency, when it comes to onsite renewable electricity generation, the only available solution is the use of photovoltaic technologies. Note that solar photovoltaic power is highly growing in Canada and has seen an average growth rate of 13.8% per year since 2004 [3].

With population rise, rapid growth in global building floor area and rise of buildings' glazing area in new architecture styles, the impact of the glazing optical and thermal characteristics on yearly energy load becomes prominent under every climate. The emergence of Building Integrated Photovoltaics (BIPV) technology, with full envelope functionality, enables building surfaces to generate electricity acting as environmental separators. BIPV is a subset of PV. As it refers to building envelope technologies, it can directly impact the energy (cooling, heating, and lighting) performance of buildings and occupant comfort. Picture 1 shows different BIPV systems and their impact on building energy and occupants' comfort [4].
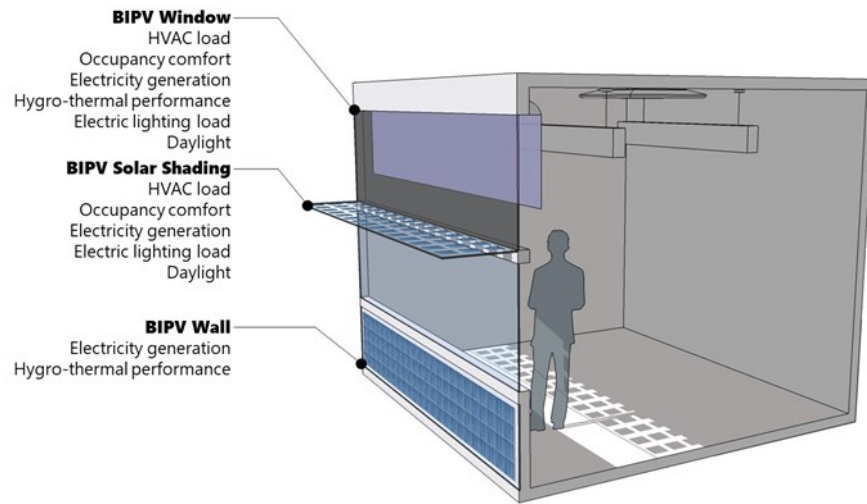
Figure 1 The application of BIPV converts sunlight directly into onsite electricity and it can affect building performance in terms of heating, cooling and daylighting [4].

Similar to conventional window technologies, BIPV windows are available in various configurations from single glazed to multi-glazing assemblies providing electricity generation and great potential on effective shading, thermal management, light management, and glare protection. Note that increasing solar cell area coverage (in spaced cell BIPV windows) or increasing absorption (in see-through BIPV windows) leads to higher electricity generation but reduction of TSET [5]. For highly glazed buildings, one of the main contributors to the energy consumption is the total solar energy transmittance (TSET) through the windows. While the visible transmittance (VLT) demonstrates the optical behavior of a window as perceived by the occupants, TSET measures the part of solar energy that passes (i.e., directly transmitted and absorbed and reemitted toward indoors) through the window. Whereas the solar heat gain of windows and glazing units is experimentally investigated with the use of calorimetric hot box and solar simulator as an existing method, obtaining the TSET values for a BIPV window remains problematic due to: 1) electricity generation and 2) the inhomogeneous nature of some of the BIPV window technologies. Recently, the International Electrotechnical Commission (IEC) Technical Committee has announced the development of an international standard for the reliable determination of TSET of BIPV windows. The theoretical study presented under this thesis aims to provide input to TC 82[1] and guide the development of a new TSET experimental standard using optical measurements.

---

[1] TC 82 scope is to prepare international standards for systems of photovoltaic conversion of solar energy into electrical energy and for all the elements in the entire photovoltaic energy system.

1.2 Problem statement

The need to reduce energy consumption and GHG emissions in the building sector has focused attention on onsite energy generation technologies. BIPV windows can be considered an effective solution for highly glazed buildings as they can reduce energy use up to 40% [1]. BIPV windows not only actively generate electricity but also, they passively regulate glare and solar heat gains, effectively reducing cooling loads. For highly glazed buildings, one of the main contributors to the energy consumption is the total solar energy transmitted (TSET) through the windows that is commonly reported in the form of a performance metric known as total solar energy transmittance (TSET).Currently, TSET is calculated either with simulation models and programs like LBNL WINDOW [6] or is experimentally measured using calorimetric hot box apparatus. Current experimental standard methods cannot accurately determine the TSET for active technologies such as BIPV windows.

The main difference between BIPV and conventional windows is that BIPV windows generate electricity. For BIPV windows part of the absorbed solar irradiance is converted to electrical power output and not heat. In general, TSET depends on angle of incidence and the spectral distribution of the incident solar radiation. For BIPV windows, TSET also depends on electricity generation (and electrical conversion efficiency). Thus, BIPV technologies pose challenges on the determination of solar heat gain based upon the use of existing experimental methods as they do not account for any electricity generation, they tend to measure TSET only under normal incidence angle (i.e., perpendicular to the surface of window). On the other hand, simulation software do not consider the electricity generation of the BIPV windows and thus, overestimate the TSET value.

As BIPV technologies are becoming more popular, a reliable methodology of evaluating TSET to account for angular dependency and electricity generation in BIPV windows is needed. Current standard TSET calorimetric tests use thermal measurements that require long window conditioning under steady state conditions. However, the BIPV window electrical output, hence the TSET, is outdoor temperature dependent, and using steady state standard test conditions does not generate realistic results.

Meanwhile, outdoor experimental methods, using radiometers and optical instruments, have been commonly used to determine the thermal, optical, and electrical performance of different BIPV windows based upon real-time environmental conditions. Similar methods can be deployed to determine TSET for BIPV windows based on outdoor conditions and under a range of solar angle of incidence.

The scope of this research is the reliable and repeatable measurement of TSET for BIPV windows. The main objective is to develop a methodology for TSET determination which is angular-dependent and generation-dependent. The proposed methodology aims to provide a framework for quick, accurate, consistent, and repeatable approach to TSET testing that can potentially be standardized for BIPV windows and other advanced window technologies.

In summary, existing calorimetric standards used for the determination of TSET on (inactive) conventional windows cannot be applied for BIPV window technologies, as they are both angular-dependent and generation-dependent. In this thesis, a new experimental TSET methodology is proposed, suited for both conventional and BIPV windows. In this first effort, the theoretical background, methodology and limitations are presented, including a critical review of existing procedures for the determination of the TSET.

1.3 Thesis Overview

This thesis presents development of an innovative methodology designed to assess the total solar energy transmittance (TSET) of BIPV windows experimentally through outdoor optical measurements. Chapter 2 delves into an extensive literature review, and presents evolution of BIPV technology, specifically BIPV windows and their impact on heating, cooling, and occupant comfort within the built environment. This chapter presents fundamentals about TSET and its numerical and experimental determination, followed by the literature review regarding the outdoor and indoor experimental measurement of TSET for BIPV windows. Literature review of TSET experimental measurement in BIPV windows is grouped under two categories of i) solar calorimetric method, and ii) solar optical method with their advantages and limitations. The solar calorimetric method primarily relies on the measurement of heat transfer through BIPV window under steady state experimental condition. While the solar optical method employs radiometric instruments to measure TSET.

In Chapter 3, the novel methodology is explained, providing a detailed exposition of TSET determination process utilizing optical measurement. By applying this method in a dynamic condition of outdoor setting, it promises a more accurate and realistic representation of BIPV window performance, thus setting the stage for a shift in TSET experimental determination. Furthermore, Chapter 4 offers an in-depth discussion regarding the new methodology and its practical applications, focusing on a prototype sample of CdTe-based BIPV window. This exploration not only underscores the methodology's viability but also addresses potential limitations and challenges that could arise. The thesis contributes not only to the advancement of BIPV window technology but also to the energy performance assessment of other glazing systems and transparent technologies. Finally, Chapter 5 summarizes the main contribution of this thesis and research needs.

Chapter 2. Literature Review

2.1 BIPV window categorization

Building Integrated Photovoltaics (BIPV) are building envelope technologies that convert solar irradiance into electricity and provide on-site renewable electricity [3]. BIPV products can be integrated in roof, exterior walls, externally integrated systems (e.g., solar shades, balconies, canopy) or fenestration. The terms solar windows, BIPV windows, semi-transparent photovoltaics (BIPV) window, photovoltaic fenestration systems, while they have slightly different meanings, they are all typically referring to a broad range of active solar energy harvesting window solutions which also fulfill daylighting and view requirements. In this study, they will be referred to as BIPV windows (Figure 2).
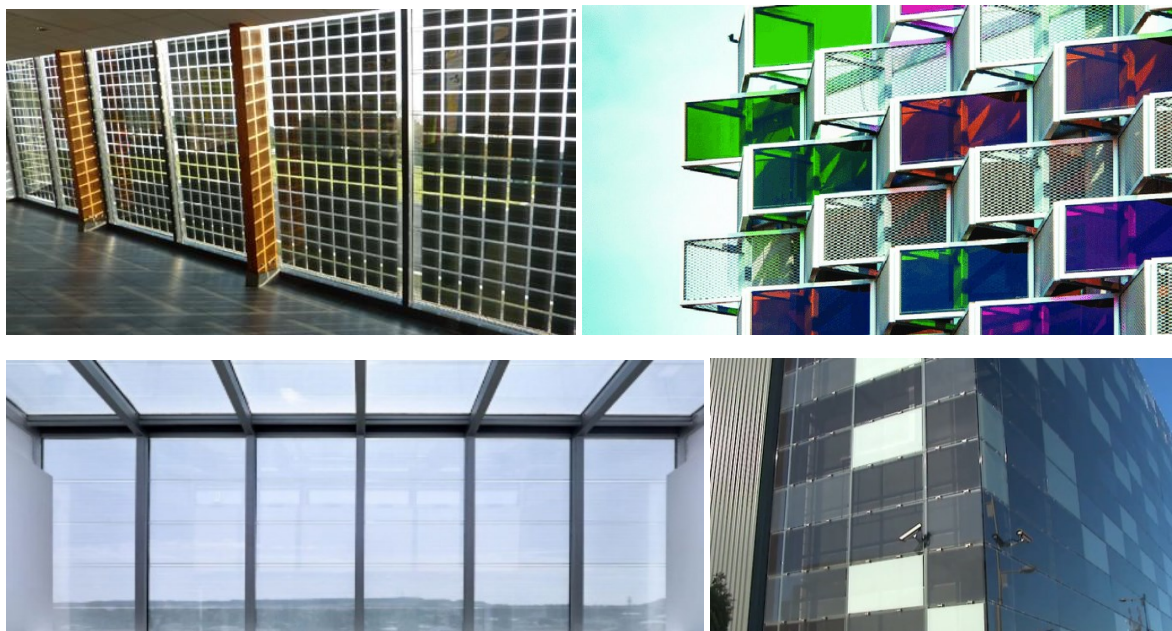
Figure 2 BIPV curtainwall with c-Si solar cells (top Left, source: Ertex Solar), Transparent glazing with dye-sentitised solar cells (Top right, source: Soltech in Sweden), Amorphous silicon glass panes (bottom source: Onyx Solar)

BIPV windows need to meet function requirements associated to i) building construction products (i.e. thermal protection, weather protection, safety, daylight control, and noise protection), ii) electrotechnical products, and iii) fire safety [7]. In addition, the electrical efficiency of any BIPV window product is recommended to be equal or more than 5% [3], in order to provide any substantial electricity generation for use in buildings.

BIPV windows can directly impacts the energy (cooling, heating, and lighting) performance of buildings and occupant comfort (visual and thermal). The most advantageous performance of this technology lies in onsite electricity generation, daylighting glare control, and solar heat gain reduction [4].

While reducing energy consumption in buildings and the built environment have become of paramount importance, the use of solar photovoltaic power has seen an average growth rate of 13.8% per year since 2004 [8]. BIPV technologies are growing quickly in Canada and contribute to electrification and decarbonization of the built environment. BIPV windows have the full functionality of fenestration and

enable glazing areas to become energy generators where still provide the primary function of a window of daylight utilization and views to the outdoor.

Olivieri et al. [9] in an experimental study analyzed daylighting and glare of both BIPV window and conventional window and showed the use of an active a-Si based BIPV window with visible transparency of 32% and electrical efficiency of 6.8% can provide sufficient daylight and prevent glare while offsetting building electricity consumption by up to 25%. The analysis was performed for window-to-wall-ratios (WWR) of 33% to 88%.

2.1.1 BIPV window technologies and applications

In terms of photovoltaic categorization, BIPV windows are commonly grouped under two main categories of i) spaced silicon cells and ii) thin film modules. The former group contains opaque (Mono- or multi-) crystalline silicon cells that partly obstruct the view, and laminated between two layers of glass, similar to a safety glass assembly. The latter category refers to transparent thin films BIPV windows (e.g., CdTe, micromorphous), with various possibilities for visual appearance and degree of transparency. The thin film is an intrinsic part of the Transparent Conductive Oxide (TCO) glass substrate while a second layer of glass is laminated on the rare side to protect the thin film from damage and deterioration [10](Figure 3).
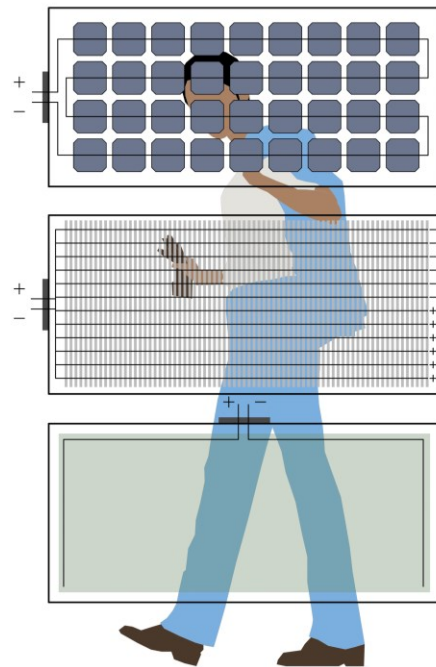
Figure 3 top: Mono-Si module; middle: a-Si module bottom: CdTe Module (Created by the author)

While spaced Si cells create nonhomogeneous semi-transparent surface due to opaque PV cells and the clear space between them, thin film BIPV modules tend to provide relatively uniform daylighting and luminance distribution. Figure 4 shows simplified schematic of the two main types of BIPV window categories, compared to opaque BIPV module (in this example installed on the curtain wall spandrel). Note

6

that in both cases, the laminated glass-glass photovoltaic layer will be the outermost glass pane of an Insulated Glass Unit (IGU).
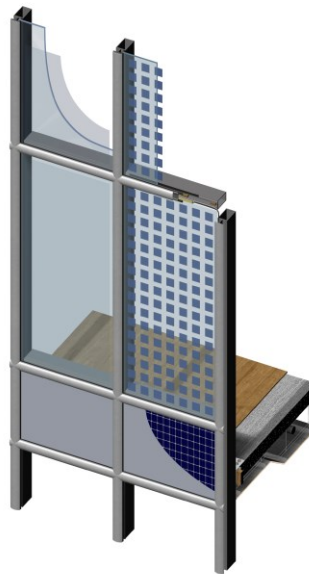
Figure 4. Semi-transparent BIPV, "see through" module in the left side and "spaced solar cells" on the right panel side of the curtain wall system and opaque BIPV panel on spandrel (Created by the author).

Thin film BIPV modules can incorporate different thin film technologies like amorphous silicon tandem (a-Si), cadmium telluride (CdTe), or cooper indium gallium (di)selenide (CIGS) deposited on a TCO. In most thin film BIPV modules the deposited photovoltaic layer is laser etched to achieve higher visible light transmittance (20% or higher). The active layer in thin film modules is between 3-5 µm thick, while the thickness of Crystalline silicon wafers used in c-Si based BIPV windows is between 150-200 µm [11].

Even though thin film technologies tend to have a higher degradation rate and lower efficiency compared to c-Si, they can be preferred dure to their homogeneous appearance [12].

There are various upcoming thin film photovoltaic technologies under research and development. Whereas these new generation of technologies might have higher efficiency and might provide the ability of tunable optical (i.e., transparency and colour) properties – an attribute that is key to building applications – the biggest limitation that currently prohibits their integration in buildings is their short life span of less than 25 years. Organic or dye-sensitized tandem films, quantum dots and perovskites are some examples of emerging 3rd generation photovoltaic that can potentially be used in BIPV windows in the near future [12]. Liu and Wu [13] have conducted an in-depth review on advanced architectural glazing technologies including Dielectric based Compound Parabolic Concentrators (DICPCs), where energy savings, and daylighting behavior of existing and advanced new BIPV technologies are extensively reviewed.

In terms of optical categorization, BIPV windows can also be categorized based on optical transparency as semi-transparent or translucent products [14]. While semi-transparent modules allow direct light to be transmitted through the module, the transmission of light in translucent modules takes place by diffuse transmission (scattering).

Figure 5 illustrates the PV systems with various degree of transmission, encapsulated into a substrate with average visible transmittance (AVT) of between 0-90% [15].
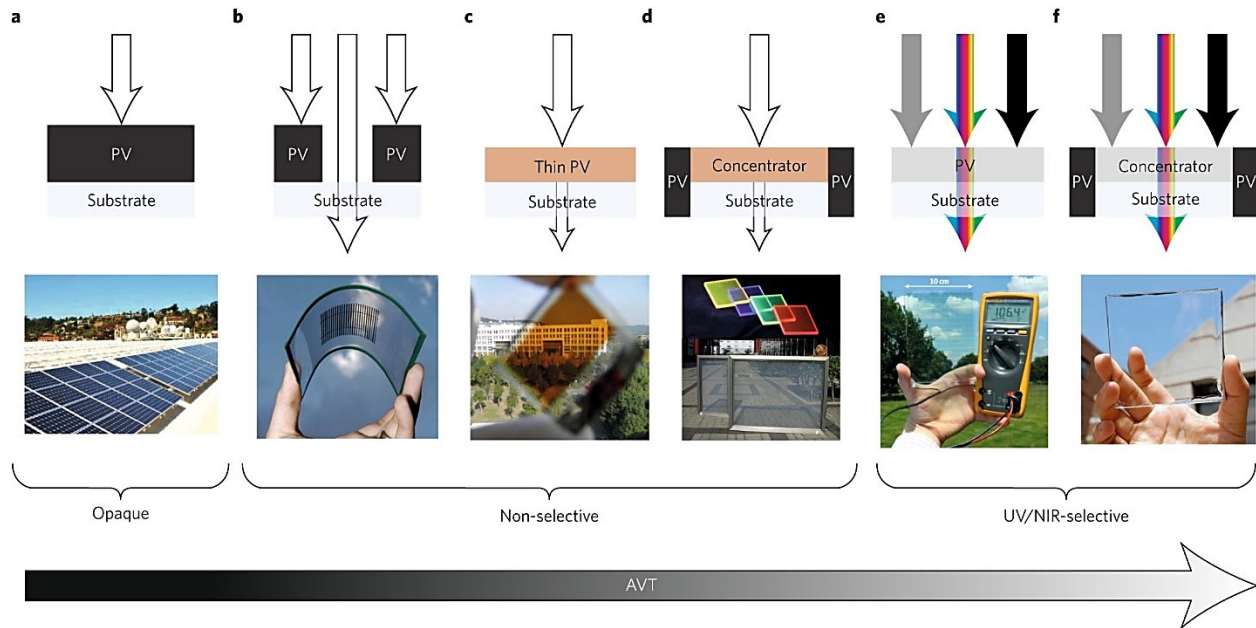
Figure 5. PV systems with various degrees of Visible transmission. a, opaque PV. b, semitransparent PV. c,d,e & f, translucent PV. Resource: Christopher et al. 2017 [15].

In terms of application categorization, IEC 63092-1 standard classifies BIPV application in the building skin in 5 different categories. A comprehensive report [14] provided by IEA describes these five class in detail, while taking into account the main features of each category such as function, performance, morphology, structure, and energy related aspects. According to IEC 63092, BIPV windows and fenestration lies under category B and D, (Table 1) which are both integrated into the building and accessible from within the building. In the former category (B) the products are installed at a tilt angle between 0 and 75 from the horizontal plane like atriums or skylights and in the latter category (D), the modules are installed at tilt angle between 75 and 90, such as windows, curtainwalls, or double skin facades. Figure shows example application of silicon based solar cells and thin film solar cells in curtain wall and skylight from category D and B, respectively.

Table 1- Application categories, Resource IEC 63092-1, 2020 [16]

Application categories		
Category A	Sloping, roof-integrated, not accessible from within the building	
Category B	Sloping, roof-integrated, accessible from withing the building	
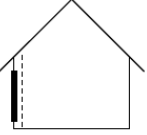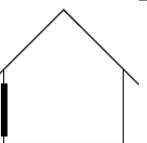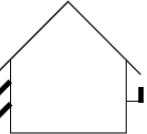
Category C	Non-sloping (vertically), envelope-integrated, not accessible from within the building	
Category D	Non-sloping (vertically), envelope-integrated, accessible from within the building	
Category E	Externally integrated, accessible or not accessible from within the building	

Figure 6 c-Si based BIPV curtain wall (left, Source: Ertex Solar); a-Si thin film BIPV (Right, Source: Onyx Solar)

Figure 7 illustrates the design of interconnected solar cells that are encapsulated into laminated glass-glass units to form the BIPV module, protecting the PV layer from mechanical damage, outdoor environment, and metal grid corrosion (e.g., busbars) [3]. The top illustration shows semi-transparent BIPV glass with partial view obstruction due to the use of opaque wafers being connected in series by electrical contacts. The bottom illustration represents the typical thin film material which is deposited on a layer of glass and etched by laser, creating a series of thin strips. Thin film BIPV windows require transparent conducting electrode to maintain the transparency and aesthetic of the glass for both front and rear side, however in some cases the regular electrical contacts are used (one conduct encapsulated in front side and the other on the back side of the deposited thin film).
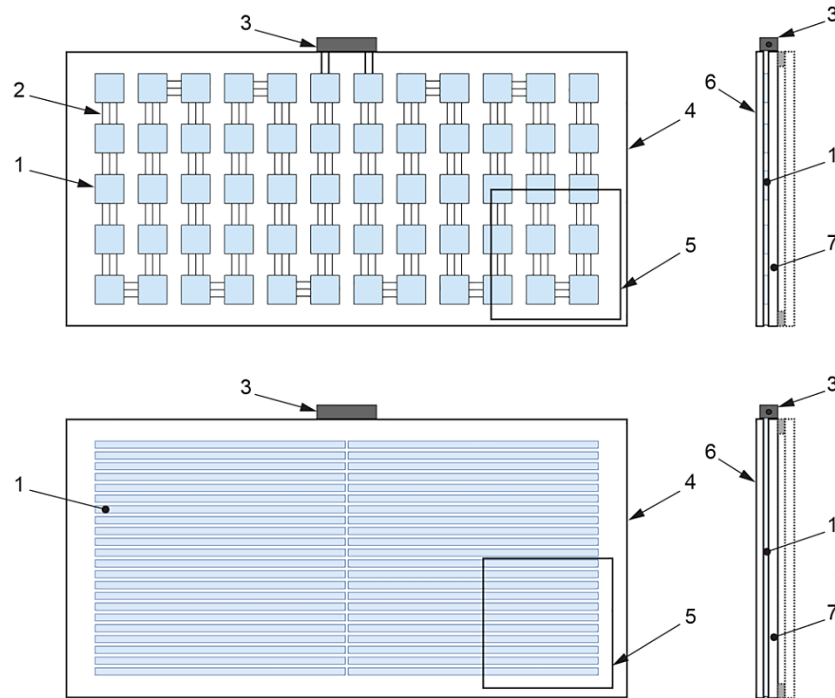
Key:

1 Photovoltaic cell (up) or thin film (down)	5 Optically representative area of module
2 Interconnection	6 Front sheet
3 Junction box	7 Back sheet
4 Perimeter of total module area	

Note: the same principles apply to modules consisting of other types of solar cell

Figure 7 Top: Schematic of typical c-Si glass-based PV module- Bottom: Schematic of laser grooved thin-film glass-based PV module [16]

2.1.2 Electrical performance

The electrical efficiency of a BIPV window is proportional to the packing factor and inversely proportional to temperature and transparency of the BIPV module. BIPV windows are expected to replace the conventional glazing areas where opaque PV modules are unlikely to be applied. In general, the higher the light transmittance of BIPV window either due to lower packing factor (the total area of opaque cells to total area of BIPV window) or smaller thickness of the absorbing layer leads to decreased power conversion efficiency and less opacity to human eye. Figure 8 highlights the highest and lowest electrical efficiency of three different BIPV module technologies (i.e., mono crystalline, amorphous silicon and Cadmium Telluride) under STC[2] as a function of module's visible transmittance [17].

---

[2] Standard test conditions (irradiance 1 kW/m2, ambient temperature 25 °C, AM 1.5G solar spectrum)
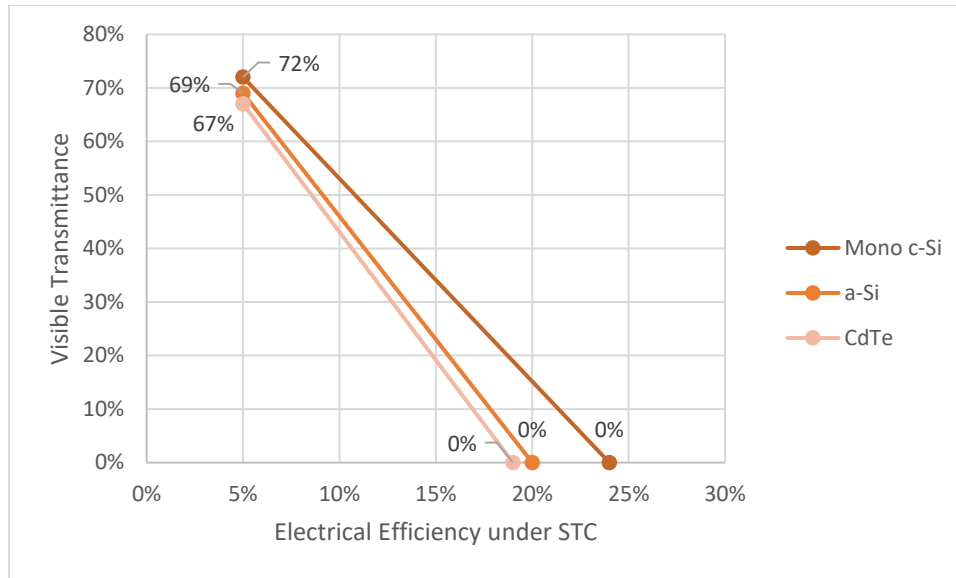
Figure 8 Electrical efficiency of BIPV window products with different visible transmittance. Data source: Mono c-Si, a-Si, and CdTe manufacturer companies' product datasheets

In this graph (Figure 8) the data from three types of commercially available semitransparent modules and the relations between modules transparency and energy conversion efficiency are presented. In c-Si based BIPV windows the transparency is achieved by the empty space between opaque solar cells in which the partial light could pass through, which is a function of packing factor. Hisashi et al. [18] performed an experimental study on transparent BIPV module with different packing factors, and observed that the area occupied by the solar cells affects module power output and operating temperature.

The electrical efficiency of a BIPV window is inversely proportional to transparency of the BIPV module. The data from the following chart are gathered from several experimental studies on different BIPV window configurations done by Kapsis et al. (Poly-Si) [19], Chinazzo et al. (CdTe) [20], Olivieri et al. (a-Si) [21], and Chae et al. (a-Si) [22]. The results indicate that the electrical efficiency of a BIPV transparent module is inversely proportional to the BIPV module visible light transparency.
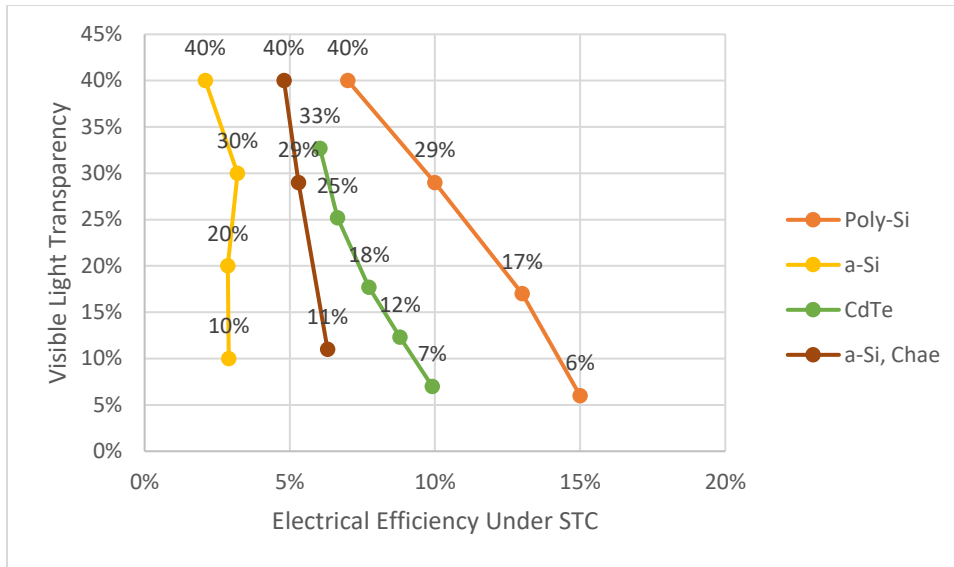
Figure 9 Electrical efficiency of different BIPV transparent modules adopted from different experimental studies.

Lee et al. [23] presented the IV[3] curves of BIPV modules with different transparency level in the following graph (Figure 10). The IV curve provides valuable insight into each of BIPV windows' performance. Higher light absorptance (less transparent) results in higher current flowing through the transparent active material, and simultaneously exhibits greater power conversion efficiency.
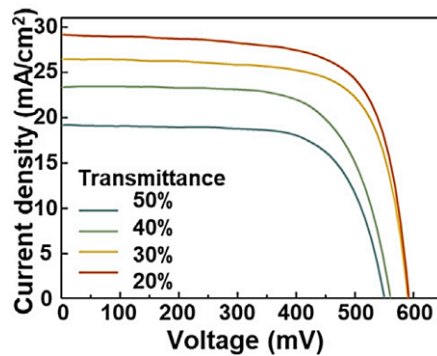
Figure 10 I-V characteristics of transparent BIPV with visible light transmittance of 20%-50% [23]

Additionally, Miyazaki et al. [24] conducted a standard simulation study on different BIPV window transmittance and WWR with EnergyPlus, in which they modeled an entire office floor to conduct annual energy analysis. The results showed that the annual energy production for a WWR of 50% is inversely proportional to the solar cells transmittance. As depicted in Figure 11, the difference between solar radiation of southern and northern zone is calculated to be about 33% at any solar cell transmittance.

---

[3] IV curve, or current-voltage curve, depicts the relationship between voltage (V) and current (I) in a circuit, offering insights into its electrical behavior.
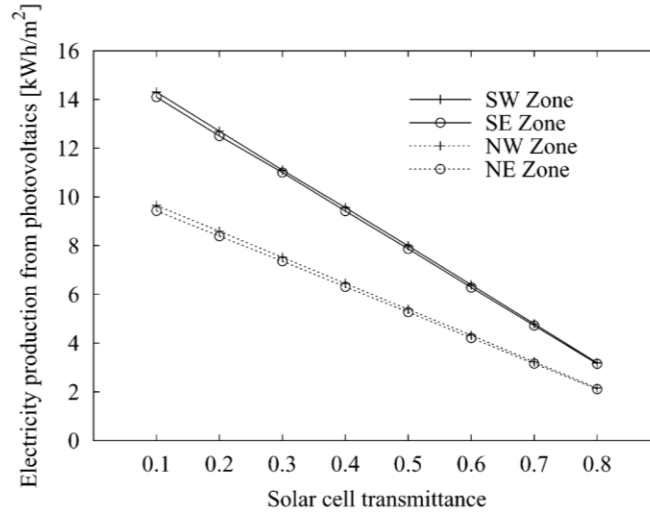
Figure 11 EnergyPlus simulation of electricity production as a function of solar cell transmittance and the orientation [24]

The efficiency of the BIPV windows is dependent to the module's temperature and its configuration since the module configuration affects the temperature. Figure 12 depicts the experimental and simulation results of the inner surface temperature of semitransparent BIPV window [25].
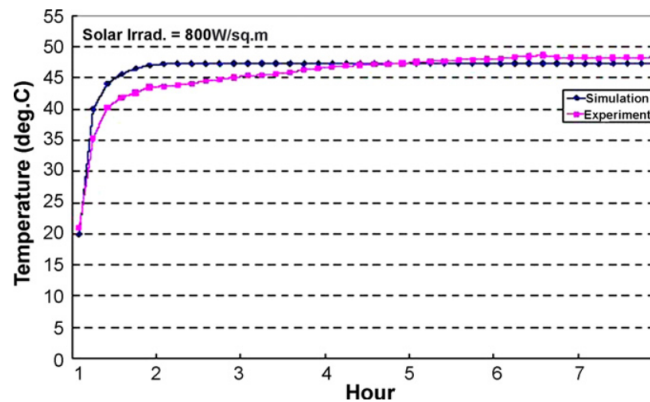
Figure 12 Inner temperature of semitransparent BIPV window [25]

2.1.3 Optical performance and daylight

Similar to conventional glazing systems, BIPV windows significantly affect buildings thermal and daylight performance, hence, impacting the building cooling, heating and lighting loads. Beyond energy, BIPV window optical properties such as the visible light transmittance (VLT), colour rendering and uniformity impact occupant's visual comfort [26]. Opaque silicon cells in c-Si based BIPV window create nonhomogeneous light distribution that could affect occupant's visual comfort due to luminance contrast.

Daylight simulation or experimental outdoor tests can guide design to mitigate glare, potentially finding an optimal balance between daylight use and solar electricity generation [27]. Chinazzo et al., through annual building energy performance simulations, found that the optical characteristics of BIPV windows have strong impact on occupant's comfort and building energy consumption [20]. The parametric analysis

13

showed that high (i.e., VLT=50%) visible transmittance of BIPV windows is preferred for office buildings located in high latitudes (i.e., the study investigated Geneva and Helsinki with latitudes of 46° and 60°, respectively), while in the case of low latitudes (i.e., Casablanca at 34°), VLT = 20% yielded optimal results between building energy consumption and occupant comfort. Note that increasing the packing factor in c-Si based BIPV windows or decreasing transparency in thin (transparent of translucent) solar films leads to higher electricity generation. In a similar parametric study for an office building in Toronto (latitude of 43°), Kapsis et al. [19] found that VLT= 30% provided sufficient daylight availability.

Further, Barman et al. [28] conducted an experimental study on five CdTe based BIPV modules with different visible light transparency (e.g., 7%, 12% 17%, 25%, 32%) and analyzed data regarding different window orientation, and WWR of between 20 % to 60%. They concluded that the module's transparency is the most sensitive factor compared to window to wall ratio and has the biggest effect on artificial light energy consumption. However, achieving higher transparency via Perovskite solar technology enables the VLT of above 70% without showing major decrease in energy efficiency and consequently less lighting energy consumption [29].

Regarding special applications of BIPV window technologies, Sun et al. [30] explored the indoor luminous effect of BIPV window by applying 4 different PV technologies (shown in Figure 13) in a south facing office setting. The study concluded that although all the tested windows reduce the glare probability compared to a clear double-glazed (DG) window, c-Si based double glazing embedded in Crossed Compound Parabolic Concentrator (CCPC) has the best performance in terms of daylight annual performance.

(a) DG   (b) 10%_CdTe PVG (c) 50%_CdTe PVG   (d) flat_si PVG   (e) CCPC+si PVG
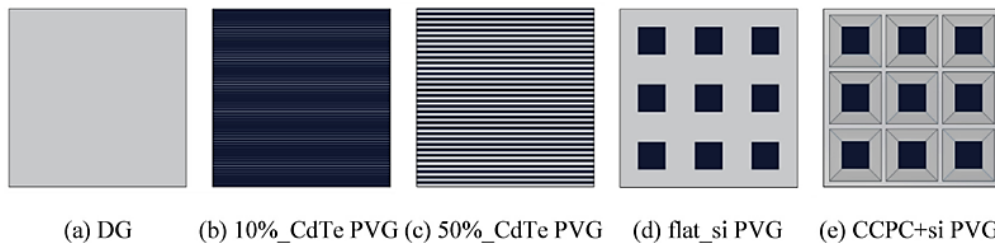
Figure 13 Schematic diagram of window systems in Sun et al. daylighting research [30]

Note that regarding BIPV window patterns, Markvart et al. [31] performed a comprehensive experimental study on indoor daylight availability and visual comfort for BIPV windows and concluded that the horizontal striped patterns in thin-film based windows are preferred over square patterns. Based on their evaluations (on both user experience and illumination measurement), the horizontal pattern and undisturbed view to the outside seems to be preferred over squared patterns (Figure 14) as the view through the stripped pattern is maintained, and the daylight in the room become more present.
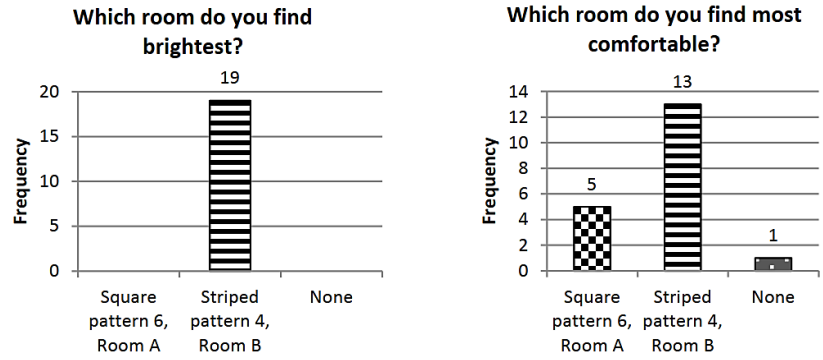
Figure 14. Comparing two test rooms with different CdTe patterns conducted by Markvart [31].

Moreover, Musameh et al. [32] in an building energy analysis compared the optical aspects of c-Si and a-Si based BIPV windows. The c-Si based module reduces the glare by 22% however the a-Si provides the better daylighting and glare reduction of 27%.

Chinazzo et al. [20] in their simulation based study provided results on the relationship between energy and comfort in BIPV windows with different transparencies of 20%, 30%, 40% and 50% in different climates, using 1)a uniform, 2)a two-section and 3) a three-section façade design. In their research, the optimal design in terms of daylighting was the combination of a two section façade with 50% on the upper section and 30% on the lower section of the BIPV facade which allowed for 19.5% energy saving (Figure 15). Their study can be helpful for the installation of BIPV windows with different transparencies.
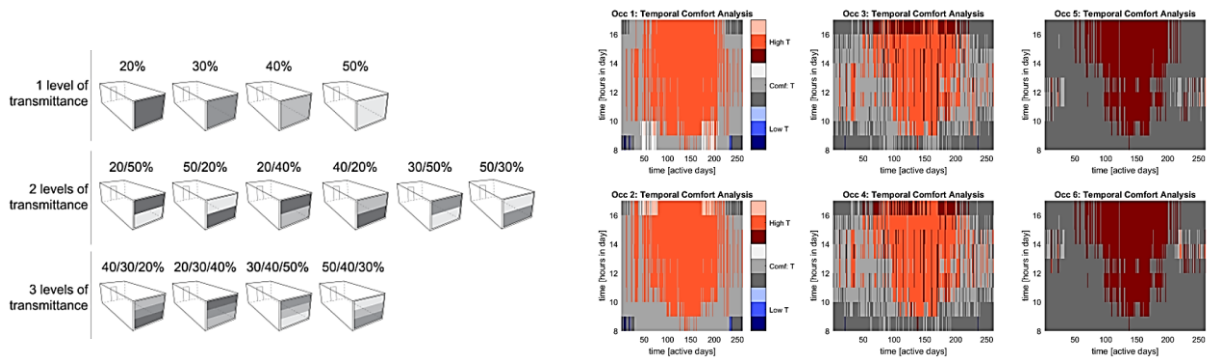
Figure 15 Transparency design variation and temporal comfort analysis by Chinazzo et al.[20]

Thin film BIPV windows are more homogeneous compared to semitransparent BIPV windows. Spaced silicon cells create nonhomogeneous daylighting due to opaque PV cells and the clear space between them. Figure 16 shows simplified sketch of 10%-60% transparency degrees created by spaces between opaque crystalline silicon cells. The greater the light transmittance (Wider inner cell distance), the better the lighting and the view to outside.

Thin film BIPV windows would not cast shadows in rooms. Additionally, these type of BIPV windows are better compared to semi-transparent BIPV windows, in terms of aesthetics, due to their uniform appearance [33]. Semitransparent BIPV windows with spaced crystalline silicon cells, however, have better efficiencies in most cases and can modify the view to outdoor where the view is not pleasing. Transparency of these technologies is the ratio of transparent surface (not covered with opaque wafers) to the total area of the glazing. Figure 16 shows different transparency ratios in semitransparent modules.

15
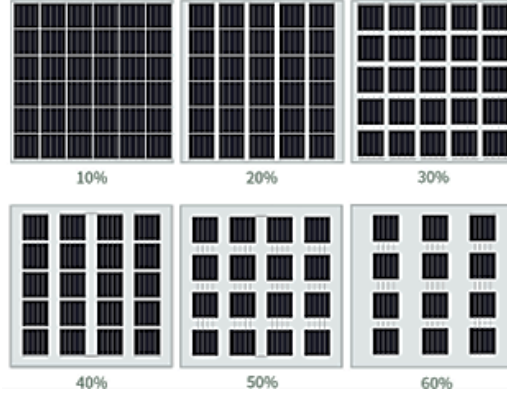
Figure 16 Different transparency degrees of crystalline silicon based BIPV modules [34]

2.1.4 Solar and thermal behaviour

Similar to a conventional window, the thermal performance of a BIPV window can be described using i) U-value and ii) the total solar energy transmittance (TSET). Simply put, the energy flow through a window is the sum of Q_i (temperature driven heat transfer), and Q_{ii} (solar driven heat transfer) (Equation 1). The U-value refers to the window's thermal transmittance driven by temperature difference only, under darkness (Equation 2)[35], while TSET describes the total amount of solar energy gain through the window (Equation 3) when exposed to sunlight.

$$Q_{total} = Q_i + Q_{ii} \tag{1}$$

$$Q_i = UA_{win}(t_o - t_i) \quad ; \quad U = \frac{1}{R} = \frac{1}{\frac{1}{h_i} + \Sigma_{i=2}^n R_i + \Sigma_{i=1}^n R_{gv,i} + \frac{1}{h_o}} ; \quad R_i = \frac{\delta_i}{\lambda_i} \tag{2}$$

$$Q_{ii} = \text{TSET} \cdot A_{win} \cdot E_{POA} \tag{3}$$

Note: in the above simplified equations (from ISO 15099[35]), energy transfer due to air leakage is neglected

where
Q_i is the conductive and convective energy exchange due to temperature difference (temperature of the sky, ground, and surrounding objects);
U is thermal transmittance [W/m^2K];
A_{win} is the area of the window [m^2];
$(t_o - t_i)$ is the temperature difference between outdoors and indoors;
R is thermal resistance [m^2K/W];
λ is thermal conductivity [$W/m.K$];
δ is the thickness [m] of each layer;
h_o is exterior surface coefficient of heat transfer [W/m^2K];
h_i is interior surface coefficient of heat transfer [W/m^2K];
Q_{ii} is the solar heat gain; TSET, is Total Solar Energy Transmittance [%]; and

16

E_{POA} is the incident irradiance on the plane of array [W/m^2].

John Wright [36] in an extensive study, summarizes and compares different methods to calculate solar heat gain of windows (including center of the glass, edge of the glass, and the frame). VISION and WINDOW are the widely used programs that calculate the TSET of windows with their wide inventory of glazing system product parameters (excluding BIPV windows).

For the BIPV windows, U-value can be assumed to be equivalent to a conventional window using a laminated safety glass as the outermost window pane, since the thermal conductivity (λ) of the PV cells is high (Table 2) with negligible thickness (200 and 500 μm).

Table 2 Thermal transmittance of a BIPV window, and outline of U-value

Layers	λ [W/m.K]	Thickness, δ [mm]
Front glass	1	2-9
EVA or PVB	0.35	0.2-0.5
PV cell	150	0.002-0.005
EVA or PVB	0.35	0.2-0.5
Rear glass	1	2-19
Note: The thickness of the rear glass is dependent on the size of the BIPV window.		

As shown in Equation 2, U-value determination is dependent on the indoor and outdoor surface air film values and temperatures. ISO 10292 [37], and ISO 15099 [35] include U-value calculation method, however, there are other glazing standards and rating systems (i.e., ASHRAE, NFRC, Passive house) that use different surface film coefficients and boundary conditions which consequently result in different results. Hanam et al. [38] compared different rating systems for a triple pane insulated glazing unit and showed that the U-value can vary up to 25% for a same window configurations complying with different standard's environmental conditions (Figure 17). Bae et al. [39] discussed the discrepancies between different ISO standards in U-value calculation in more details. Overall, it is important to specify environmental conditions while comparing U-value from different standards.
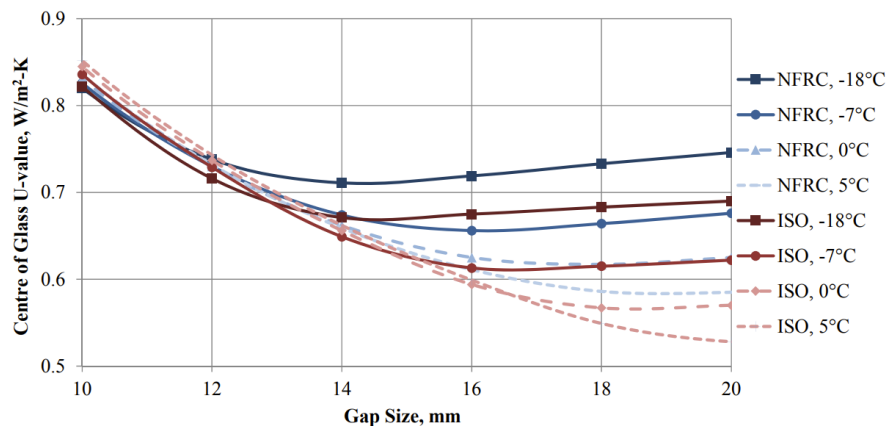
Figure 17 U-value in relation to gap size for different standards procedure using different surface temperature for similar glazing unit [38]

Unlike the U-value, solar gain of BIPV windows is noticeably different than regular windows, which is mainly due to the electricity generation of PV layer under solar irradiance. According to Yang et al. [40], in the thermal performance analysis, it was emphasized that TSET has the most significant impact on the thermal performance of BIPV windows. Lu and Law [41] simulated a generic office room in Hong Kong, and compared the annual total heat gain (both solar and thermal) of semitransparent BIPV window and clear glass for five different orientations (Figure 18). They concluded that the best electrical benefit can be gained from a BIPV window installed on South-East side which demonstrated 65% energy conservation compared to clear glass. PV cells absorb part of the sun radiation striking the window and transform it into electricity, whereas in clear glass sample, that energy is transmitted directly indoors. Figure 18 illustrates their simulation results.
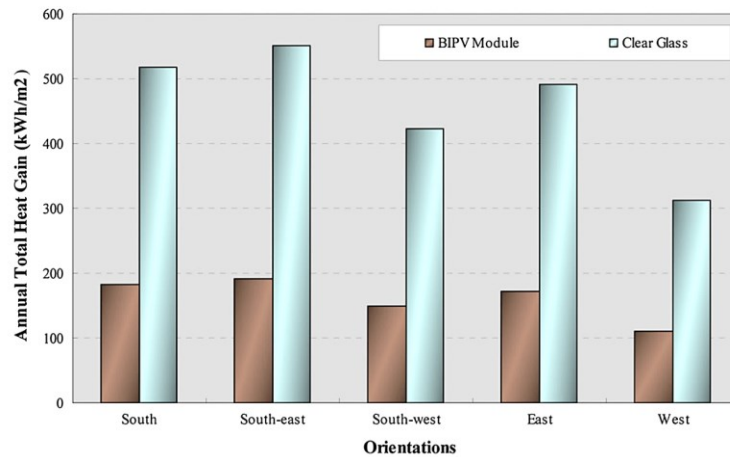
Figure 18. Comparison of annual total heat gain through BIPV window and clear glass window by Lu and Law [41]

While a BIPV product has almost the same U-value, its total solar energy transmittance is noticeably lower compared with other common double pane windows. Fung et al. [25] evaluated the TSET of a BIPV window using a Semi-transparent Photovoltaic Module Heat Gain (SPVHG) numerical model. They studied the impacts of different parameters and found out that the major component in total heat gain of BIPV windows is the electrical efficiency of the BIPV window, and the area of solar cells and/or the transparency of the active layer.

The key parameters of the vacuum PV glazing, and vacuum glazing adopted in the energy simulation by Qiu and Yang [42] are displayed in the Table 3. In a simulation study using EnergyPlus, they demonstrated that the a-Si based vacuum PV glazing can improve the energy performance by 66.0% (dependent to the climate backgrounds). Accordingly, it can be translated that the thermal performance of BIPV window, is mainly dependent on TSET.

Table 3 Vacuum PV glazing and Vacuum glazing key parameters [42]

Glazing Type	Thickness (mm)	Visible Transmittance	U-value	SHGC
Vacuum PV glazing	20.8	0.120	0.557	0.143
Vacuum glazing (low-e)	11.5	0.693	0.648	0.391

When solar radiation strikes a window surface, it is transmitted (τ), reflected (ρ), and absorbed (α) (Figure 19). Equation 4 shows the fractions of incident flux on a regular window. Their sum equals unity.

$$\rho + \alpha + \tau = 1 \tag{4}$$
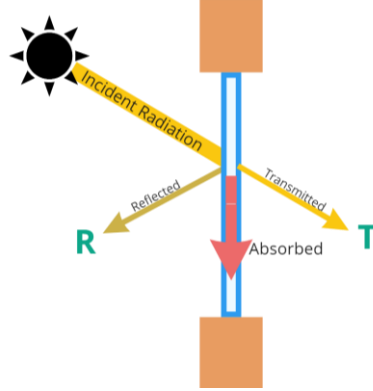
Figure 19 schematic of solar incident radiation within regular window (Illustration by author)

The absorbed part of solar energy subsequently is either reemitted inward (q_i) or outward (q_e)(Equation 5.). Each of these optical properties namely solar transmittance (τ), reflectance (ρ), and absorptance (α), of a regular or BIPV window under open circuit conditions can be calculated using ISO 9050 [43].

$$\alpha = q_e + q_i \tag{5}$$

However, when a BIPV window is connected to an electric load (i.e., closed circuit) part of absorbed solar incident energy is converted into electricity (Figure 20). Equation 6 shows the absorbed solar incident in a BIPV modules.

where
q_e is the fraction of absorbed solar energy re-radiated outwards;
q_i is the part of solar incident reemitted inwards;
η_{el} is the power conversion efficiency of the BIPV window which is the quotient of usable generated electricity as a portion of the solar incident radiation striking the BIPV window.

$$\alpha = q_e + q_i + \eta_{el}\,\alpha \tag{6}$$
$$\rho + (q_e + q_i + \eta_{el}) + \tau = 1 \tag{7}$$
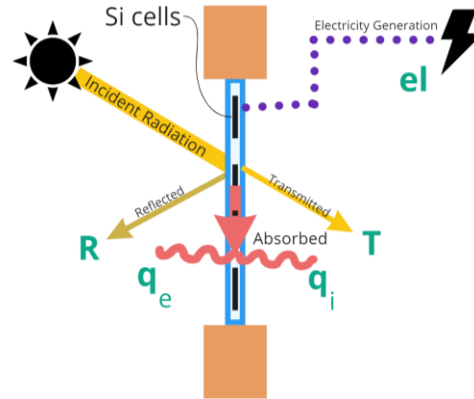
Figure 20 Schematic of solar incident radiation within BIPV window

Solar Heat Gain Coefficient (SHGC), Total Solar Energy Transmittance (TSET), and g-value, all refer to the fraction of incident solar radiation admitted through a window or BIPV window.

Packing Factor (PF) is the ratio of total area of PV cells to total area of PV module. IEC 63092 part 3 [44] demonstrated the dependency of TSET on PF (Figure 21). It is shown that the total solar energy transmittance is inversely proportional to the number of crystalline silicon cells.
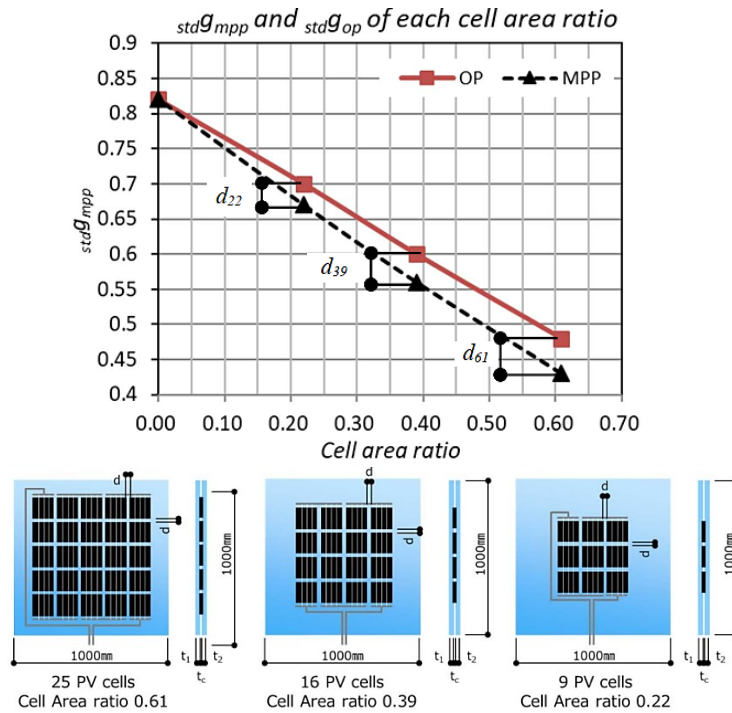
Figure 21 Cell area dependance of TSET under MPP, and operating condition [7]

The opto-thermal performance of CdTe-based BIPV window with 5 different transparencies were investigated by WINDOW7.3 software [28]. The results showed that as the a-Si layer's transparency increases, proportionally the total solar energy transmittance increases (Table 4).

Table 4. Simulation study by Barman et al. results for window systems and their properties [28]

Window systems	Construction	Efficiency	U-value	SHGC	VLT
CdTe-based BIPV WIN 1	PV1/airgap/low-e glass	9.91%	1.812	0.129	7.0%
CdTe-based BIPV WIN 2	PV2/airgap/low-e glass	8.8%	1.812	0.158	12.3%
CdTe-based BIPV WIN 3	PV3/airgap/low-e glass	7.73%	1.812	0.186	17.7%
CdTe-based BIPV WIN 4	PV4/airgap/low-e glass	6.64%	1.812	0.228	25.2%
CdTe-based BIPV WIN 5	PV5/airgap/low-e glass	6.04%	1.812	0.271	32.7%

Fung and Yang [25] conducted a laboratory test on semitransparent solar cells and concluded that the area of solar cells and/or the transparency of the active layer has significant effect on total heat gain, however, the influence of the modules' thickness and solar cells efficiency is little. Hisashi et al. [45] in an experimental study ascertained that that the thermal transmittance in BIPV modules is almost equivalent to the U-Value of the conventional glass regardless of the cell distances. They performed an experiment and concluded that U-value does not depend on PF and cell distance in c-Si based BIPV window. Table 5 shows the experimental results of their test.

Glass Types		Laminated		IGU		Low-E coated IGU			
		Not Low-E		Not Low-E		Summer ver.		Winter ver.	
Aperture Ratio (%)		(W/m²·K)		(W/m²·K)		(W/m²·K)		(W/m²·K)	
100	BM	①	5.12	②	3.11	⑦	2.26	⑧	2.37
20	BIPV	③	5.09	④	3.15	⑨	2.28	⑩	2.31
30	BIPV	③	5.08	④	2.96	⑨	2.30	⑩	2.31
40	BIPV	③	5.14	④	2.99	⑨	2.33	⑩	2.33
30 Wide	BIPV	⑤	5.08	⑥	3.06	⑪	2.29	⑫	2.27
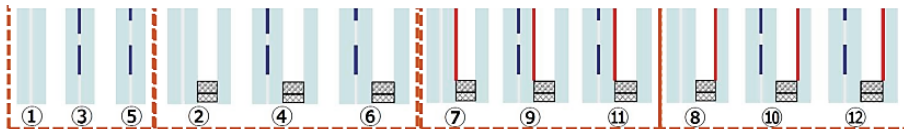
Table 5 Experimental result of U-value in different BIPV configuration comparing to the regular benchmarks [45]

BIPV windows can be constructed simply with the same configuration as glazing systems, where the outer pane of the glazing system is replaced with laminated PV module, creating a multi-glazed IGU. The construction schematic of Low-e reference IGU and a BIPV IGU can be seen in Figure 22. Different layers in CdTe based double glazed photovoltaic window with low-e coating are presented in Figure 23.
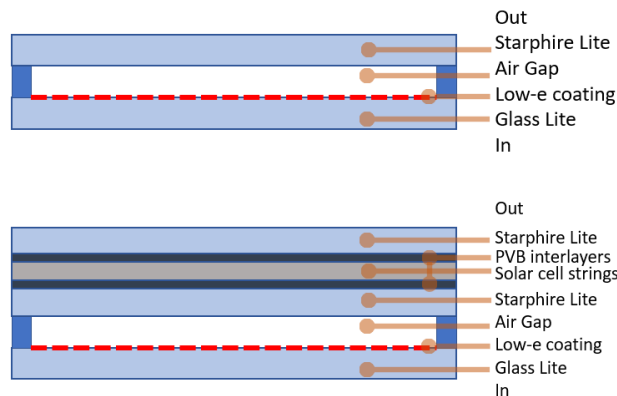
Figure 22 top: regular low-e IGU; bottom: BIPV IGU
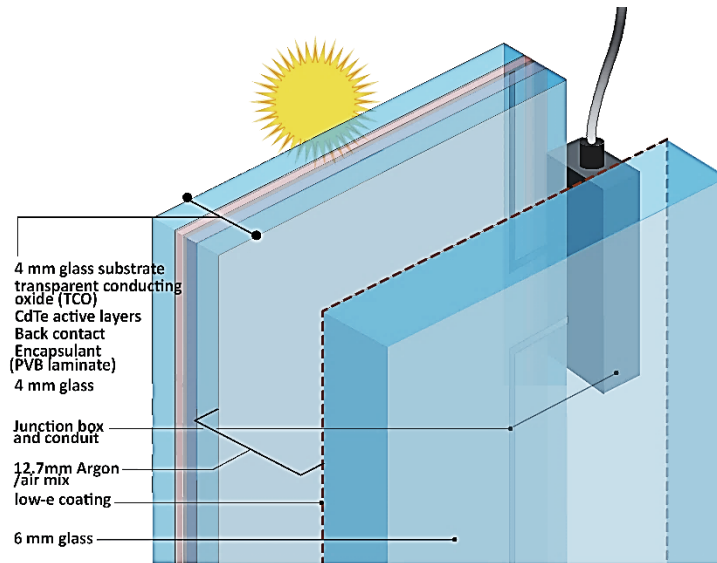
Figure 23 schematic of CdTe BIPV window

Semitransparent BIPV assemblies as part of a building envelope should provide thermal insulation during winter and regulate solar energy gain during the summer. For example, insulated glazing BIPV windows can be designed and built in such a way that offer optimal solar and thermal performance, as well as contributing to energy saving approaches like recovering heat in a double-glazed PV curtainwall or ventilated BIPV facades. At the same time, the electrical efficiency of BIPV module changes linearly with surface temperature. However, the temperature coefficient depends on the PV technology.

When it comes to ventilated façade configurations, experimental results have shown that an air gap of between 400-600 mm in a ventilated BIPV façade (at least 200 mm ventilation gap [46]) can reduce the solar heat gain coefficient up to 0.15 and substantially improve the module efficiency. Figure 24 shows four BIPV facade systems which were compared by numerical models. The change of U-value and indoor thermal comfort in these four façade systems were compared: (1) single skin facade, (2) Non ventilated BIPV double skin facade, (3) naturally ventilated BIPV double skin facades, (4) fan assisted BIPV double skin façade. Yang et al. declared that fan-assisted BIPV double skin façade (Figure 24, 4) can drastically improve the year round energy output by 35 % compared to nonventilated façades [40]. In similar experimental study He et al. [47] compared the PV double glazed window and PV single window, in which they indicated that the dominant source of heat gain through the BIPV window is the secondary heat gain (absorbed solar energy that is reemitted inwards). In PV double glazed window, the openings at the top and bottom contributed to the lower solar heat gain transmittance.
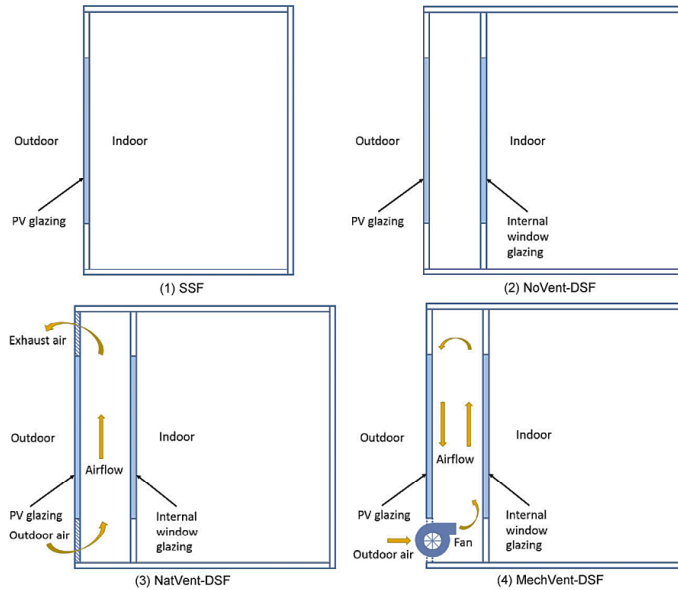
Figure 24 Four types of BIPV/T facade systems by Yang et al. 2018 [40]

Peng et al. [46] investigated ventilated a-Si based PV double-skin façade (PV-DSF) with a 400mm airflow cavity. Based on their experimental results, the ventilated PV-DSF provides lower TSET, and better energy conversion efficiency compared to non-ventilated PV-DSF due to its much lower operating temperature.

Wang et al. [48] compared the energy performance between PV double skin facades (PV-DSF) and PV insulating glass units (PV-IGU) (Figure 25). They found that the average TSET of the PV-DSF has lower rate compared to PV-IGU, with average saving potential of 28.4% and 30%, respectively.
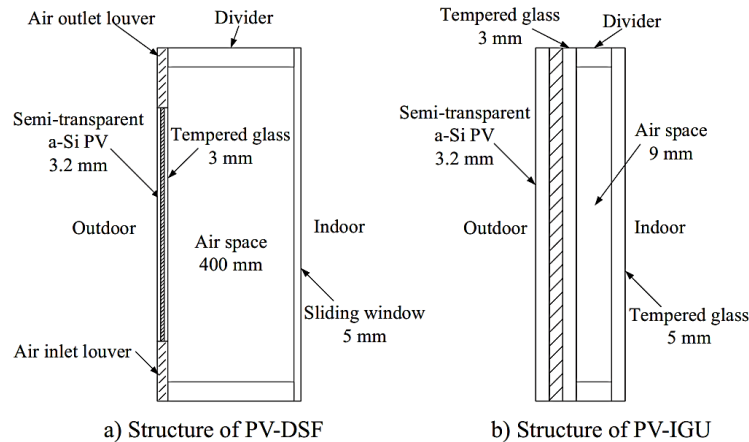
Figure 25 Schematic diagrams of the a)PV double skin facade and b) PV insulating glass unit [48]

BIPV thermal behavior affects system's output. Higher operating temperature at BIPV window installations with no proper ventilation on the rear side of the glazing system can affect the efficiency of the system as well as resulting in higher degradation rate. Gok et al. [49] in an experimental research with two different mounting setups (with same c-Si based BIPV module) showed that the thermal insulation and U-value of

the BIPV window influences the performance of the system, whereas the ventilated system had remarkedly lower performance loss rate than the insulated system.

Wang et al. [48] measured the energy conversion efficiency of ventilated PV-DSF and compared the data with PV-IGU with similar a-Si PV module properties (VLT of 205 and Efficiency of 6.3%). They showed that with lower module temperature PV-DSF has 1.8% higher efficiency than PV-IGU. In an experimental test in Hong Kong, they measured the SHGC of the PV-DSF and PV-IGU for 0.15 and 0.23, respectively. The PV-DSF demonstrated less SHGC and slightly higher U-value.

2.2 Total Solar Energy Transmittance (TSET) or g-value of windows

Total solar energy transmittance (TSET), SHGC or g-value mainly describes the fraction of the energy of the sun that passes through the glazing. SHGC and g-value, and TSET are all metrics used to quantify the performance of windows and glazing systems with regard to solar energy transmission, but they are typically associated with different standards and regions[4]. ISO 9050 [43], defines total solar energy transmittance as the sum of the solar direct transmittance (τ) and the secondary heat transfer factor towards the inside (q_i), the latter resulting from heat transfer by convection and longwave IR radiation of that part of the incident solar radiation which has been absorbed by the glazing (Equation 8, Figure 26).
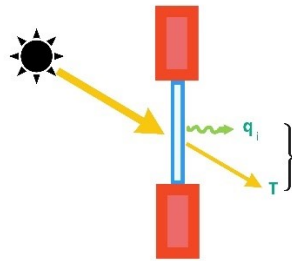
Figure 26 Schematic of total solar energy transmittance through window

$$TSET = \tau + q_i \tag{8}$$

where τ is the total solar transmittance, and q_i is inward flowing fraction of absorbed incident solar radiation. TSET of windows account for not only transmitted energy by direct light, but also the hemispherical (diffuse) light. TSET is highly dependent on angle of incidence, ISO 15099 and ASHRAE provide detailed numerical calculations, including the effects of angular and spectral dependence. Calculation of total solar energy transmittance based on direct and indirect transmittance, including angular properties can be presented in the following equation:

$$TSET\ (\theta) = \tau(\theta)_{direct\ 0.35-2.5\ \mu m} + \tau_{hemispherical\ 0.35-2.5\ \mu m} + q_{i\ 8-15\mu m} \tag{9}$$

---

[4] SHGC Is primarily used in North America, and it is defined by ASHRAE, however, g-value is more commonly used in Europe and Internationally, especially in ISO. TSET on the other hand, is often used in the context of BIPV windows and windows that generate electricity.

Where θ is the angle of incidence (AOI), $\tau(\theta)_{direct\,0.35-2.5\,\mu m}$ is the direct transmitted portion of solar incidence from the wavelength of 350 nm to 2500 nm, and $\tau_{hemispherical\,0.35-2.5\,\mu m}$ is the hemispherical transmittance, and $q_{i\,8-15\mu m}$ is the reemitted absorbed solar thermal energy towards the inside.

As demonstrated in equation 9. the TSET is the summation of transmitted solar energy (both direct and indirect) and the inward flowing heat that has been absorbed by fenestration[5]. Thus, the energy balance for regular and BIPV windows can be rewritten as follows:

$$\text{Regular Window (or BIPV window in open circuit): } \boldsymbol{\rho} + \boldsymbol{q}_e + \textbf{TSET}\,(\boldsymbol{\tau} + \boldsymbol{q}_i) = \textbf{1} \qquad (10)$$
$$\text{BIPV window in closed circuit: } \boldsymbol{\rho} + \boldsymbol{q}_e + \boldsymbol{\eta}_{el} + \textbf{TSET}\,(\boldsymbol{\tau} + \boldsymbol{q}_i) = \textbf{1} \qquad (11)$$

where
q_i is the absorbed part of solar energy that is reemitted inward;
q_e is the absorbed part of solar energy that is reemitted outward;

With this in mind, in BIPV windows, the electricity generation and visible transmittance are inversely proportional. Figure 27 shows the data gathered from EnergyPlus simulations by Miyazaki et al. [24] in respect to the effect of transmittance, WWR and electrical efficiency of semi-transparent solar cells on TSET.
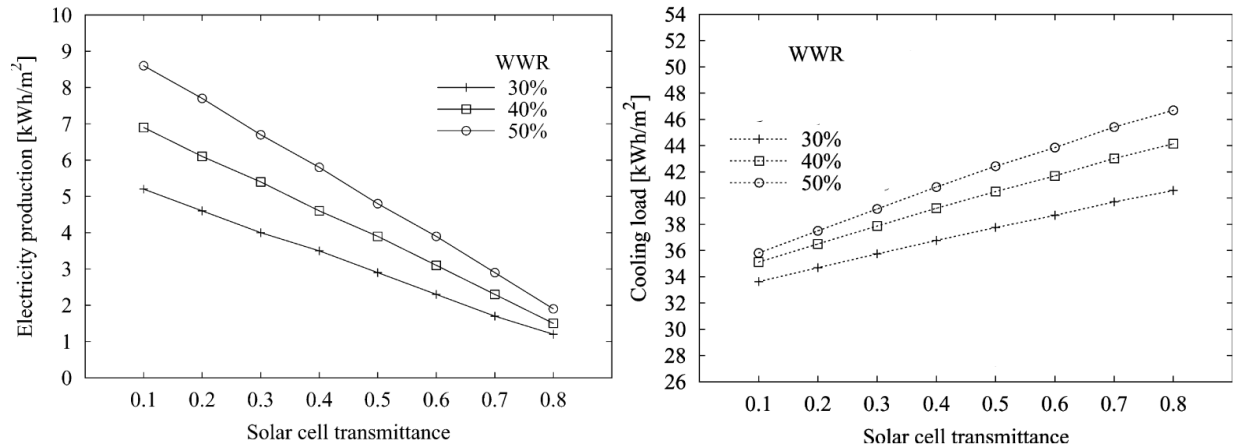
Figure 27 Annual electricity generation (Left) and annual cooling load (right) as a function of solar cell transmittance with different WWR by Miyazaki et al.[24]

Similar to conventional windows, BIPV also use low-emissivity coatings to reduce radiative heat exchange between the window multi-layers. As it is seen in Figure 28 coatings can selectively reduce radiant heat exchange while transmitting more than 75% of the visible portion of solar irradiance. As a result, the use of low-e coatings can reduce the inward flowing fraction of TSET.

---

[5] As it was described previously in Equation 5, The absorbed part of solar energy is either reemitted inward (q_i) or outward (q_e).
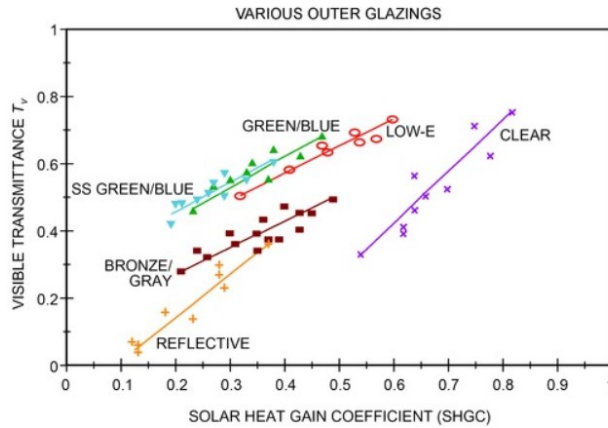
Figure 28 Visible transmittance versus SHGC for different glazing systems [50]

The primary purpose of a window is to provide daylighting and a view of the outdoors; however, the windows' energy aspect plays an important role in building energy consumption. Glazing optical properties like transmittance, absorptance and reflectance as well as TSET are provided in most window products or can be accurately calculated using simulation programs like LBNL WINDOW. McCluney [50] compared the visible transmittance of different glazing systems as a function of TSET (Figure 28).

TSET mainly depends on the transparency of BIPV module (or the PV cells coverage in semitransparent modules) and the energy that can pass through the system, instead of being reflected. Xu et al. [51] conducted an EnergyPlus simulation study for China, comparing different WWR and packing factors. They concluded that 80% reduction in yearly energy consumption can be achieved by applying BIPV window to south facing fenestration with WWR of 0.83 and cell coverage of 0.87, compared to regular double-glazed window (Figure 29).
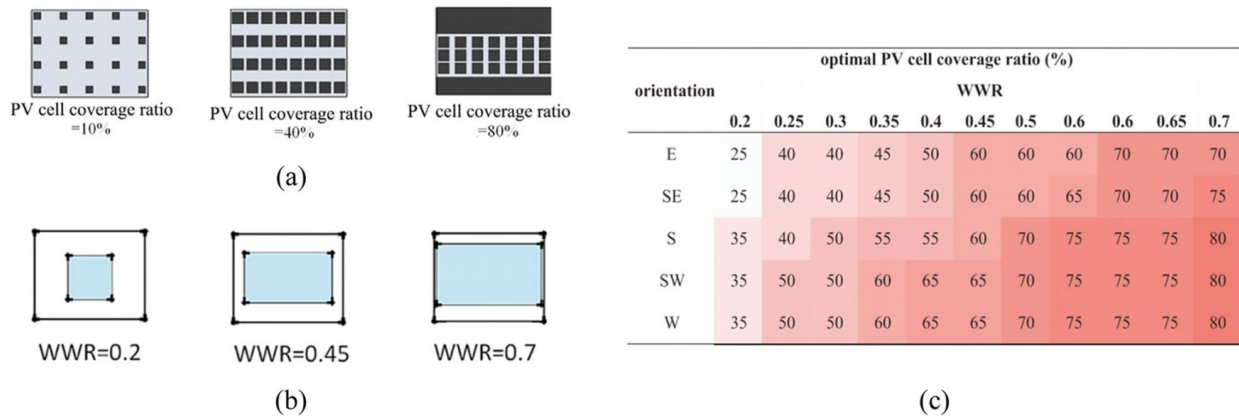
Figure 29 (a) PV cell coverage ratios with different inner cell difference and cells number, (b) different Window to Wall ratios applied to the research, (c) optimal PV cell coverage for different BIPV orientation [51]

Inward flowing secondary heat transfer, q_i, in a conventional glazing unity depends on glazing's position, and inside and outside boundary conditions like wind velocity, natural convection, emissivity of the surfaces, and vented/ unvented air spaces (Equation 12, 13).

Secondary heat transfer factor towards inside, q_i	Single glazing	$$q_i = \alpha_e \frac{h_i}{h_i + h_e}$$	(12)
	Double glazing	$$q_i = \frac{\dfrac{\alpha_{e1} + \alpha_{e2}}{h_e} + \dfrac{\alpha_{e2}}{U}}{\dfrac{1}{h_i} + \dfrac{1}{h_e} + \dfrac{1}{U}}$$	(13)

where

q_i is the net density of heat flow rate through the window to the indoor [W/m^2];

α_e is portion of absorbed solar energy by the single glazing pane (%);

$\alpha_{e1}, and\ \alpha_{e2}$ are the portion of absorbed solar energy by the first and second glazing layers respectively.

The absorbed heat transfer coefficient of the glazing towards the inside, h_i, and outward flowing energy coefficient towards outside, h_e, have been stated for simplicity by ISO 9050 in the conventional conditions where the glazing is vertical, wind velocity 4 m/s and inside surface is under natural convection:

$$h_e = 23\ ^W/_{m^2 \cdot K} \tag{14}$$

$$h_i = \left(3.6 + \frac{4.4\ \varepsilon_i}{0.837}\right) ^W/_{m^2 \cdot K} \tag{15}$$

Hanam et al. [38] in a literature review and simulation study compares the center of glass SHGC with both NFRC and ISO standards using THERM software. In their study, different calculated SHGC results complying with different standards are presented, and the differences between North American, European, and Passive House window thermal performance are studied (Figure 30).
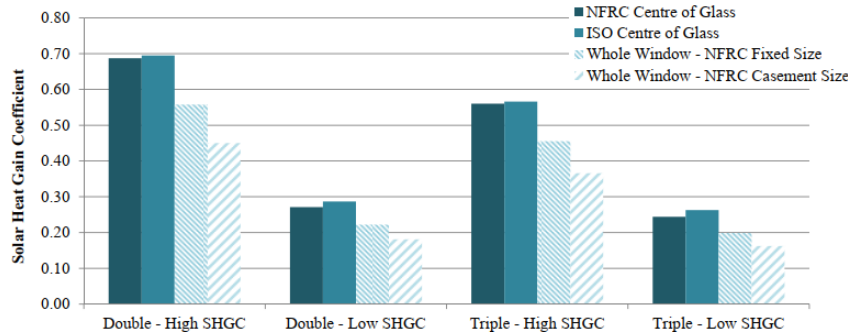
Figure 30. SHGC for various window configurations using NFRC and ISO standards [38]

Klems [52] developed a method for TSET determination of products with shading. His computational method can be used for TSET and performance determination of geometrically complex fenestration systems containing those with shades, venetian blinds, or translucent glazing. In another research Klems et al. [53] compared the calculated and measured TSET, and demonstrated that their TSET calculation method agrees with the gathered experimental data for the most optically complex fenestration elements such as venetian blinds.

Overall, TSET depends on various parameters that are determined by environmental conditions, and façade properties, in addition to the thermal and optical properties of the glazing system (like solar reflectance, solar transmittance, emissivity of the surface and thermal conductivities) [54]. Glazing units with a low TSET rating are preferred for hot and sunny climates, where the solar gains are undesired, while glazing units with high TSET rating might be more effective for heating dominated climate. The optimal solar heat gain through a glazing unit strongly depends on climate, building type and window to wall ratio.

2.2.1 Shading Coefficient (SC)

Unlike modern alternatives such as TSET, which provides more comprehensive evaluation of window performance, Shading Coefficient (SC) refers to the total solar energy transmitted through the subject window relative to the total solar energy transmitted through a 3 mm (1/8-inch) clear reference glass (Equation 16). At normal incidence [55].

$$SC = \frac{(\tau + q_i) \textbf{ of subject window}}{(\tau + q_i) \textbf{ of clear glass}} \tag{16}$$

While SC is occasionally used within the architectural community, manufacturers are now moving towards the use of Solar Heat Gain Coefficient (SHGC) and TSET rather than SC.

2.2.2 Solar Heat Gain Coefficient (SHGC)

Solar heat gain coefficient (SHGC), Total Solar Energy Transmittance (TSET), Solar factor or g-value all determine the ability of a fenestration in transmitting total solar energy. All these coefficients are often used synonymously in the literature, despite the fact that there are some differences in their definition.

SHGC represents the solar heat gain through the fenestration relative to the incident solar radiation. SHGC is a dimensionless number between 0 and 1, where higher number indicates the high heat gain through solar energy. SHGC can be determined for any angle of incidence, for the portion of solar incident that either transmits through the window or reradiates inward after being absorbed by fenestration. The angle-dependent and Wavelength-dependent calculation method for SHGC is expressed by ASHRAE [56] in Equation 17.

$$SHGC(\theta, \lambda) = \boldsymbol{\tau}(\theta, \lambda) + N\boldsymbol{\alpha}(\theta, \lambda) \tag{17}$$

where
θ is solar incidence angle;
λ is the wavelength; τ is the portion of incident solar irradiance that is transmitted through the glazing (direct and diffuse);
N is inward flowing fraction of absorbed incident solar radiation;
$\boldsymbol{\alpha}$ is the total spectral absorptance of the glazing system ($\frac{W}{m^2}$).
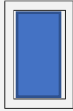
While TSET (also known as g-value, under European standards and industry) specifies the solar energy transmittance of the glass only, SHGC may include the frame as well: SHGC values can be presented for

center of glass or for the entire product. In the following chart, individual components from two commonly used standards are compared (Table 6).

Table 6 Comparison of TSET and SHGC calculation

Standard	Window Area		Solar Heat Gain
ISO 9050 and EN 410	A_g Total Glass Area		$TSET\ (or\ g-value) = \dfrac{Measured\ Solar\ Gain\ Through\ Glass}{Incident\ Solar\ Energy\ (@\ A_g)}$
NFRC200	A_g Total Glass Area A_f Frame Area		$SHGC = \dfrac{Measured\ Solar\ Gain\ Through\ Glass}{Incident\ Solar\ Energy\ (@\ A_f + A_g)}$

Solar heat gain values using ISO standards are greater than solar heat gain resulted from NFRC ratings, as the solar energy transmittance through the framing is up to 50% less compared to the total sun energy that would pass through the glass. Hence, it is important to be aware of different standards and not compare solar heat gain values from North American products with European ones, as they are based on different calculation procedures [57].

In addition, the boundary conditions for TSET determination such as Interior temperature, exterior temperature, solar radiation, inside surface film coefficient (h_i), and outside surface film coefficient (h_e) are different from the ones used for SHGC, as presented in Table 7.

Table 7 boundary and environmental conditions for SHGC calculation, vertical glazing.

	Exterior Temperature	Interior Temperature	Solar Irradiance	Exterior Surface film coefficient	Interior Surface film coefficient	Notes
	°C	°C	W/m^2	W/m^2K	W/m^2K	
NFRC 100 & 200, SHGC	32	24	783	26	3.29(Interior Aluminum Frame) 3.00(Interior Thermally Broken Frame) 3.12(Interior Thermally Improved Frame) 2.44(Interior wood/vinyl Frame)	Interior coefficients are convection only
ISO 15099, g-value	30	25	500	20	3.6	Convective heat transfer coefficient
Passive House Certification Criteria	30	25	500	25	7.7	Combined convection and radiation coefficient, increased surface resistance modeled at corners to account for reduced radiation/convection heat transfer

Overall, the discrepancies between TSET (g-value) and SHGC values are due to different calculation procedures and different boundary conditions corresponding to each standard. Whereas the calculation methodologies are the same, it is important to reference the values with their testing condition values.

Wang et al. [48] experimentally compared the TSET of a PV double skin façade (PV-DSF) and a PV insulating glass unit (PV-IGU), with the use of optical instruments and calculated the total solar energy transmittance by Equation 18.

$$SHGC \simeq \frac{(G_1 + G_2 + G_3)}{G_4} \tag{18}$$

where
G_1 is the direct transmitted solar radiation;
G_2 is the inward radiated absorbed energy from the inside window to the room;
G_3 is the convective heat transfer from the inside window to the indoor room;
G_4 is the incident solar radiation striking the window's outer surface.

Their comparative study lasted for 7 months, and it was conducted to validate the simulation model for predicting the energy performance of PV double skin façade and PV insulating glass unit. In a numerical simulation model validation study, Peng et al. [46] evaluated the overall energy performance of a ventilated double skin façade, also using Equation 18. In order to conduct the overall energy performance of a double skin PV façade in EnergyPlus, Peng et al. [33] validated their model via long-term outdoor experimental setup with optical measurement. They concluded that the simulation results agree well with the measured data. Similarly, the objective of their outdoor optical measurement was to validate a simulation model and consider overall performance and the accuracy of the simulation software or models available to measure the performance of BIPV windows (i.e., Sandia Array Performance Model (SAPM), EnergyPlus or Optic).

2.2.3. Existing testing standards

Traditional fenestration systems are experimentally tested for TSET depending on the specific requirements and available resources. Calorimeter hot box is the existing method to determine TSET experimentally that is designed and built to perform the test under steady state condition. Calorimetric approach using a solar simulator is described in ISO 19467.

The TSET testing standards for traditional fenestration can also be utilized for BIPV windows. It is important to test the BIPV windows under maximum power point (MPP) and closed circuit (CC) condition due to the integration of photovoltaic elements. Even though researchers have performed experiments on BIPV windows under open circuit condition (OC) to better understand the impact of electrical efficiency on TSET, it is unrealistic to report the TSET under OC as in practice the BIPV windows are rarely disconnected (open circuit). In summary, testing TSET of BIPV windows under MPP allows comprehensive and realistic assessment of their performance. Table 8 outlines the existing standards for TSET determination of BIPV windows. These existing standards ensure accurate and consistent total solar energy transmittance measurement.

Table 8 Existing standards for TSET determination

Testing Standard	Description
ISO 19467	Thermal performance of windows and doors —Determination of solar heat gain coefficient using solar simulator
ISO 15099	Thermal performance of windows, doors and shading devices — Detailed calculations,
ISO 9050	Glass in building – Determination of light transmittance, solar direct transmittance, total solar energy transmittance, ultraviolet transmittance, and related glazing factors
IEC 60904-8-1	Photovoltaic devices- Part 8-1: Measurement of spectral responsivity of a photovoltaic (PV) device
EN410	Glass in building- Determination of luminous and solar characteristics of glazing
ASTM E424	Standard test methods for solar energy transmittance and reflectance measurement of transparent materials
NFRC 200	Procedure for determining fenestration product solar heat gain coefficient and visible transmittance at normal incidence.
NFRC 201	Procedure for interim standard test method for measuring the solar heat gain coefficient of fenestration systems using calorimetry hot box methods
ASTM C1363	Standard test methods for the thermal performance of building materials and envelope assemblies by means of a hot box apparatus.

2.3 Experimental determination of TSET for BIPV windows

TSET of conventional windows is experimentally measured in an indoor environment that is kept under steady state conditions using a solar simulator as a light source. The amount of energy used to keep the environment in steady state yields the TSET. Future, complex systems like BIPV windows with embedded PV cells or non-homogeneous surfaces can be tested in calorimeters. However, literature indicates that the experiment is more challenging and new methodologies are needed.

Experimental determination of TSET for BIPV windows is grouped under two categories of i) solar calorimetric method, and ii) solar optical method that are presented in this section with their advantages and limitations. The solar calorimetric method primarily relies on the measurement of heat transfer through BIPV window under steady state standard test conditions, which is the current experimental process used for both regular windows and BIPV windows. On the other hand, the solar optical method employs radiometric instruments to measure TSET by analysing the direct and diffuse transmittance of solar energy through BIPV windows.

The experimental determination of TSET for both solar calorimetric method and solar optical method then can be categorized into two groups: 1) indoor test facility using a solar simulator and 2) outdoor test facility, using sunlight. Overall, in all experimental test setups determining the fenestration total solar energy transmittance can be with different methods, sensors, or different boundary conditions. The TSET results are based on various test parameters and conditions:

- Indoor or outdoor (Sun or solar simulator, wavelength and the value or incident solar irradiance)
- Angle of incidence (normal or variable)
- Boundary conditions (e.g., ISO, ASHRAE, Passive House or real)

- Tested area (Center of glass or whole window)
- Module test conditions (e.g., BIPV window under MPP or OC)
- Test condition (STC or real test condition)

Many studies were conducted on the solar thermal method in TSET determination of BIPV windows, however, there has been limited focus on solar optical methods. Mazzali et al. [58] conducted an indoor experimental test using Hot Plate and Solar Calorimeter, and showed that the use of laminated BIPV system improves energy performance and modifies the energy balance of the building system both in winter and summer. Peng et al. [65] in an experimental comparative study between conventional IGU and the BIPV IGU, indicated that the discomfort glare is reduced in BIPV IGU, and their analysis showed that these technologies save approximately about 17% of total electricity use of the room.

Hisashi et al. (2016) conducted an indoor experimental test in accordance with ISO 19467 (International Standard about thermal performance of windows and doors and determination of solar heat gain coefficient using solar simulator) and demonstrated the decrease in SHGC by 1.6 to 2.9 times.

Kapsis et al. [2] focused on the experimental measurement of SHGC under operational conditions. It was observed that the solar heat gain coefficient of a 40% VT photovoltaic window and nominal conversion efficiency of 7%, reduces by 2% when it is at the maximum power point rather than when it is not generating electricity and it is under open circuit conditions. In addition, BIPV windows with less Visible transmittance (VT 6% and nominal conversion efficiency of 15%) showed 23% reduction in SHGC. Feng and Wang [59] designed and developed instruments to measure the glazing parameters in an inexpensive and easy-to-use procedure.

2.3.1 Solar calorimetric methods

Hotbox calorimeters are commonly deployed for measuring the U-value and TSET of building components. This section focuses on hotbox calorimetric methods used for the determination of TSET. A hotbox calorimeter is a well-insulated airtight chamber equipped with a cooling system (Figure 31). The glazing unit under testing is placed at the aperture of the calorimeter facing a solar simulator of known spectrum and collimation. Alternatively, the calorimeter box is exposed to the sun and the test is conducted in an outdoor setup.

Figure 31 General view of SERIS chamber system when it is under test and the inside view from left to right respectively [60]

There are distinct differences and challenges between indoor and outdoor calorimetric methods. While TSET is angle-dependent, for indoor testing, the solar simulator is mostly maintained at near normal to the plane of the window, for instance, ISO 19467 and NFRC 201 specify the tilt angle less than 5°. On the other hand, most outdoor calorimetric tests are conducted under real irradiance conditions. These outdoor calorimeters are either tilted towards the sun or are placed vertically and at a greater angle of incidence.

Indoor testing provides controllable conditions and test repeatability under both steady-state or dynamic conditions. Kapsis et al. [19] used 8 metal halide lamps emulating the sunlight with test bench positioned from 0° to 90° to simulate the results for both vertical façade and a flat roof, respectively (Figure 33). To achieve homogenous and uniform light, Chen et al. [5] positioned the lamps at 10 m distance from the specimen and applied a correction factor to minimize the spectral mismatch (Figure 32). While indoor calorimeters provide test repeatability, outdoor tests are effective on the angular characterization of TSET with most sunlight being collimated. Outdoor calorimetric methods have also been used to test advanced fenestration systems like BIPV windows or advanced shading devices under realistic and dynamic climate conditions, where angular dependency of the TSET is important.
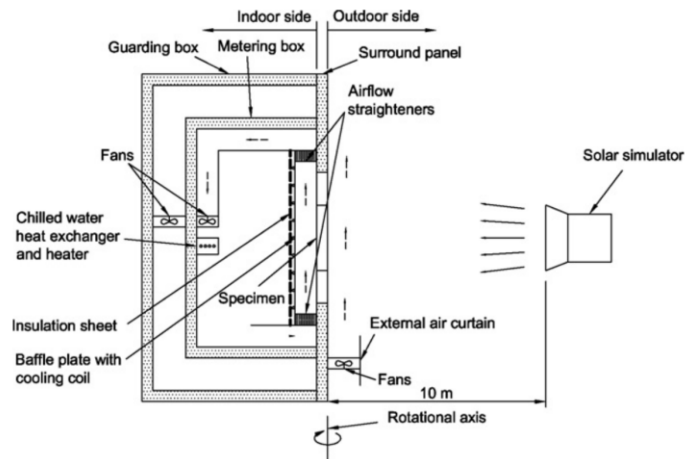
Figure 32 SERIS CHB schematic diagram with a rotational axis to create different angle of incident [5]
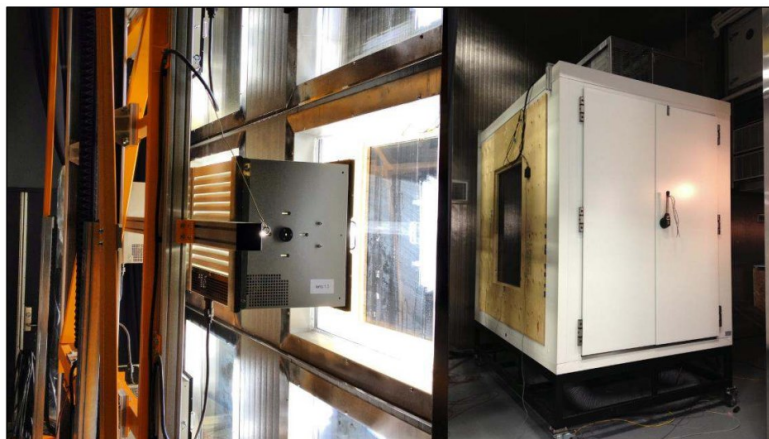
Figure 33 TSET experimental determination at Concordia University, Left: Solar simulator, Right: Environmental chamber [61]

Solar calorimeters could be very different in terms of configuration. The calorimeters' chamber size, aperture size, solar spectrum, and the system used to condition within the calorimeter are some of the key configurations that can vary between different facilities and methods (Figure 33). The following sections discuss the technical difference, challenges and solutions for the two main categories of solar calorimeters: 1) indoor, and 2) outdoor TSET testing.

Using a thermally guarded calorimeter, the TSET can be determined under steady state conditions, using linear regression analysis.

$$Q_{net} = Q_{TSET} + Q_{cond} = (TSET \cdot E_{POA}) + (U \cdot \Delta T) \qquad [W/m^2] \text{ (19)}$$

$$TSET = \frac{Q_{net} - U\Delta T}{E_{POA}} \qquad \text{(20)}$$

where
Q_{net} is the total energy transfer through the window [W/m^2];
Q_{TSET} is transmitted solar irradiance to the plane-of-array [W/m^2];
Q_{cond} is the conductive energy transmission through test window [W/m^2];
$TSET$ is the total solar energy transmitted through BIPV window [W/m^2];
E_{POA} is total solar irradiance to the plane-of-array (POA) [W/m^2];
U is the thermal transmittance characteristics of tested BIPV window [W/$m^2 \cdot °C$]; and
ΔT is the temperature difference between inside and outside [$°C$].

2.3.1.1 Correction of U-value Adjusting for Surface Film Coefficient

As temperature differences and ambient conditions affect the measured thermal transmittance, it is necessary to provide reliable information about the boundary conditions during measurements. In order to check the quality of the measurement, the heat flux meter (HFM) method can also be implemented, following the ISO 10293 [62], using a window specimen of known U-value. Wright [63] indicated that using fixed surface film coefficient in overall U-value calculation can result in measurement inaccuracies.

There are many different predictive models for convective and radiative film coefficients, in this section one of the method is presented as one of the commonly used models for surface film coefficient determination.

The indoor surface coefficients can be estimated including both convective and radiative film coefficient (Equation 21) [64].

$$h_{in} = h_{conv} + h_{rad} = \qquad \text{(21)}$$
$$1.77(T_{surface-4} - T_{in})^{1/4} + \varepsilon_{surface-4}\sigma(T_{surface-4}{}^4 - T_{in}{}^4)/(T_{surface-4} - T_{in})$$

where
h_{in} is indoor surface air film;
h_{conv} is the convective and gas convective heat transfer coefficient;
h_{conv} is the convective surface film coefficient;
$T_{surface-4}$ is the temperature of innermost surface; and

σ is the Stefan-Boltzmann constant.

Similarly, the outdoor film coefficient (h_{out}) can be calculated by including both convective and radiative film coefficients. The Equation 22. can be used [65].

$$h_{out} = h_{conv} + h_{rad} = h_{conv} + \varepsilon_{surface-1}\sigma(T_{surface-1}{}^4 - T_{sky}{}^4)/(T_{surface-1} - T_{sky}) \quad (22)$$

where

h_{out} is outdoor surface air film ($^W/_{m^2 \cdot K}$);

h_{conv} is the convective and gas convective heat transfer coefficient ($^W/_{m^2 \cdot K}$);

h_{rad} is the radiative surface film coefficient ($^W/_{m^2 \cdot K}$);

ε is the emissivity of the outermost surface;

$T_{surface-1}$ is the temperature of outermost surface;

T_{sky} is the effective sky temperature or radiative temperature and can be estimated by Equation 23. And clear sky model from Clark & Allen Equation 24.

$$T_{sky} = (\frac{IR_H}{\sigma})^{0.25} - 273.15 \quad [°C] \quad (23)$$

$$T_{clear\ sky} = 0.787 + 0.764\ ln\ (T_{dp}/273)^2 \quad [K] \quad (24)$$

where

IR_H is the infrared radiation rate emitted from the sky on an upward-facing horizontal surface ($^W/_{m^2}$);

T_{dp} is dewpoint temperature in Kelvin;

σ is the Stefan-Boltzmann constant.

The exterior convection coefficient in h_{conv} can be estimated by Sparrow, Ramsey, and Mass (1979) model (Equation 25). The total convection coefficient in their model is split into forced and natural components.

$$h_{conv} = h_f + h_n \quad (25)$$

$$h_f = 2.537 W_f R_f (PV_z/A)^{1/2} \quad (26)$$

$$h_n = 1.31|\Delta T|^{1/3} \quad (27)$$

where

W_f is the wind direction modifier;

R_f is the surface roughness multiplier (where in this experiment is 1.00 for glass as a very smooth surface);

P is the perimeter of surface [m];

V_z is the local wind speed at altitude z (z is altitude, height above ground) [m/s];

A is the surface area (m^2); and

h_n is the natural convective heat transfer coefficient ($^W/_{m^2 \cdot K}$). For standard film coefficients, see Appendix.

2.3.1.2 Indoor testing

In indoor TSET testing, measurements are conducted in a controlled environment under steady state solar simulator as described in ISO 19467. Indoor calorimeters have different configurations based on the calorimetric box size, measurement, and control systems. Olivieri et al. [66] assessed the accuracy of an indoor calorimeter under controlled and quasi-steady conditions. The main components of their indoor test facility were 1) calorimeter box, 2) chiller with integrated pump 3) and chilled water buffer tank as represented in following schematic diagram (Figure 34). The simplified thermal model used in the Olivieri et al. [66] calorimetric testing facility is presented in Equation 28. In general, the energy balance of the calorimeter box yields the normal TSET value for the BIPV window under test.
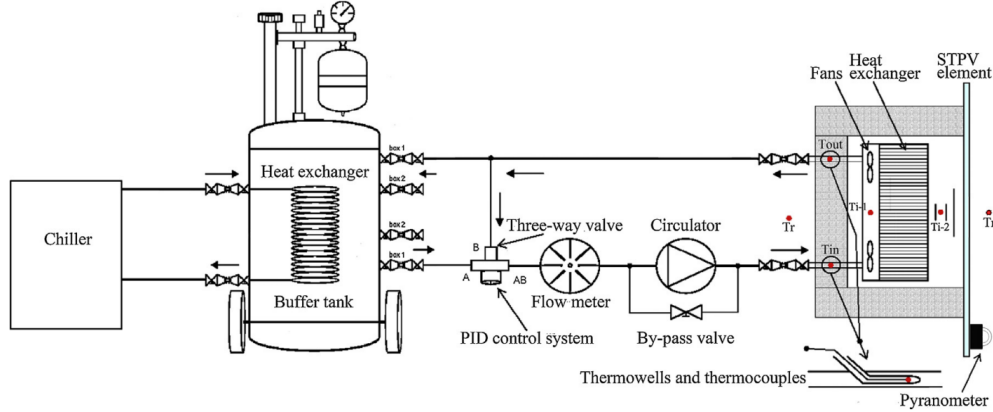
Figure 34 schematic diagram of indoor calorimeter testing facility with a chiller [66]

$$q_{solargain} + q_{Fan} = q_{Water} + q_{Glass} + q_{Box} + q_{Glass} + q_{C-Water} + q_{C-Box} \qquad (28)$$

where

$q_{solargain}$ is the solar gain [W],

q_{Fan} is the internal gains due to the fans [W],

q_{Water} is the thermal power extracted by the water heat exchanger [W],

q_{Glass} is the thermal loss through the glass,

q_{Box} is the thermal loss through the calorimeter walls [W],

$q_{C-Water} \ and \ q_{C-Box}$

are the thermal power stored in the water and in the box, respectively [W]. Guarded airtight calorimeters with well insulated cooling systems reduces measurement uncertainty.

To prevent uncertainty in data acquisition, at least 30 measurements are typically used to minimize the variations like the heat flow between the box and the ambient environment. Since the tests are performed under quasi-state condition to determine the net flow passing through the test specimen, the existing test methodology requires enough time to stabilize depending on thermal properties of the specimen, the storage of the apparatus and mechanical equipment controls that can result to cycling or drifting. Long run periods are a necessary to achieve accuracy of the conducted tests, and ranges from few hours to more than a day to maintained the temperature difference and indoor and outdoor film coefficients prescribed by existing standards [67].

Apart from thermal energy exchange between the two environments (i.e., inside the calorimeter that emulated indoor building conditions, and outside the calorimeter that emulate outdoor conditions) for indoor solar calorimeters, the TSET indoor experimental determination also requires the use of a steady state solar simulator. Full scale solar simulators need to comply with ISO 19467 regarding the light spectrum distribution and collimation. Chen et al. [60] introduced a linear correction factor to account for the spectrum of the solar simulator and reflection properties of the absorber plate. Kuhn [68] presented a thorough TSET experimental determination under quasi-state laboratory conditions, using different transparent and translucent materials including BIPV modules.

The advantages and limitations of indoor calorimetric measurements using a solar simulator can be summarized as follows:

Advantages

Controlled and Reproducible Environment: Indoor setups provide a controlled testing environment, allowing for consistent testing conditions and reduced external variables, facilitating consistent and repeatable measurements.

Versatility: Tests can be conducted regardless of weather conditions or time of day, ensuring year-round availability.

Limitations

Spectral Accuracy: Even advanced solar simulators might not perfectly replicate the full spectral complexity of natural sunlight, potentially affecting accuracy for certain materials.

Non-Uniformity: Achieving uniform irradiance across large test samples might be challenging, leading to non-uniform heating effects and thus, potentially unreliable TSET measurements.

Long Measurement Periods: Literature has indicated that calorimetric measurements require long conditioning periods to achieve quasi-steady or steady state conditions [69].

2.3.1.3 Outdoor testing

The main difference between outdoor and indoor tests is the light source, where in indoor test apparatus, a solar simulator is used instead of natural sunlight. Outdoor calorimeter test facilities are preferred for TSET determination of BIPV windows due to high light collimation and solar spectrum, assuming clear sunny sky conditions.

Harrison and Collins [70] fabricated an outdoor solar calorimeter that was able to test both thermal and optical performance of a test specimen. They proposed a smaller calorimeter chamber along with solar tracking capabilities rapidly and accurately perform TSET measurements. For optical measurement, they positioned two pyranometers to the mask wall, for direct and diffuse radiation, along with a pyrgeometer for long wave measurement (figure 37). The researchers noted that it was challenging to determine the indoor and outdoor film coefficients due to the tilt angle and fluctuation of wind speed.
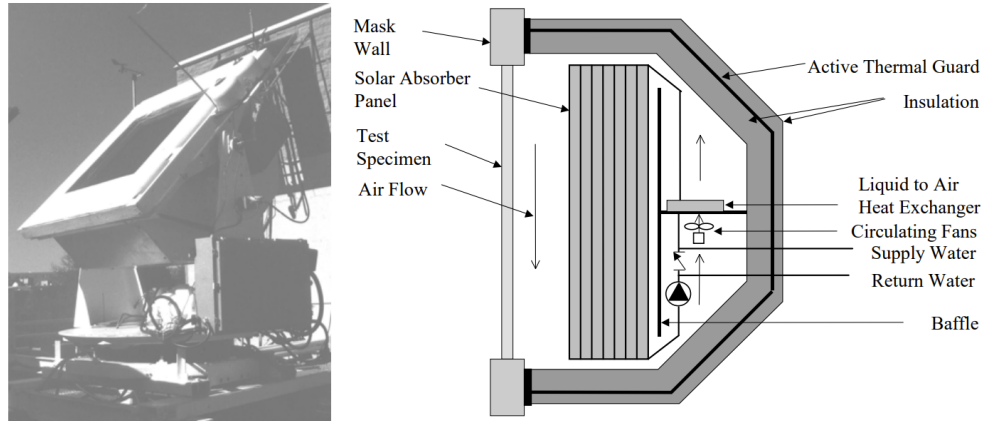
Figure 35 Outdoor solar calorimeter for TSET measurement at Queen's University [70]

Bloem et al. [71] in a comparative analysis, developed an outdoor calorimeter to test thermal and electrical performance of BIPV windows under real climatic conditions. In Figure 36 their calorimetric setup with external dimensions of 2 m x 2 m x 0.46 m is shown. Their set-up allowed full size PV modules to be tested with dimensions of 1.2 m x 1.2 m, and 30 mm thick.

Figure 36 front and rear view of outdoor experimental setup for BIPV window TSET determination [71]

TSET experimental tests are subject to climate condition uncertainties and variations. While for conventional glazing systems the effective TSET at oblique angle of incidence can be extrapolated from experimental measurements at normal, the method is not viable for optically-complex fenestration systems [72].

Paud et al. [73] in an experimental study, developed, and evaluated a portable calorimeter which can be mounted on existing glazing units and measure the TSET under real operating conditions (figure 39). The portable nature of their calorimeter (with dimensions of 500 mm x 500 mm x 500 mm), allows fast TSET assessment. However, the study showed that the apparatus tends to overestimate TSET when compared to normal standard values.

Figure 37 transportable calorimeter for in-situ measure of TSET [73]

Backer and Van Dijk [74] conducted research on the outdoor PASLINK test facility and developed a procedure which aimed to achieve accurate test results under real dynamic outdoor conditions. The researchers found that employing multiple shorter tests within dynamic outdoor testing conditions, as opposed to measurements within longer intervals under quasi-state conditions, lead to more accurate TSET measurements.

The advantages and limitations of outdoor calorimetric measurements can be summarized as follows:

Advantages

Realistic Conditions: TSET measurements are conducted under actual solar and environmental conditions, providing the most accurate representation of real-world performance.

Solar Spectrum and Uniformity: Natural sunlight contains the entire solar spectrum, fully collimated and uniform across test specimens, capturing all spectral interactions with window materials, including PV cells.

Angular Measurements: Outdoor measurements have been proven effective when it comes to developing a better understanding on the performance of advanced window systems under various incidence angles.

Limitations

Weather Dependence: Measurements are influenced by weather conditions, including cloud cover and time of day, potentially limiting test availability.

Variability: Natural sunlight is dynamic, leading to variations in solar angle, intensity, and spectral composition.

Complexity: Outdoor setups are subject to external variables that might be difficult to repeat or measure accurately.

2.3.2. Solar optical methods

To tackle the various challenges and limitations associated to calorimetric measurements, researchers have proposed optical methods for the experimental determination of TSET. Optical measurements can bring more accurate results compared to calorimetric methods due to i) effective spectral resolution, ii) ability

to measure under dynamic conditions and iii) ability to capture the performance of complex, inhomogeneous and active window technologies, like BIPV windows.

Spectral Resolution: Many glazing systems and materials selectively absorb or reflect specific portion of the solar spectrum. Optical measurements can analyze solar radiation across a wide range of wavelengths, allowing them to capture the varying response of materials to different parts of the solar spectrum. Calorimetric methods often do not account for these spectral variations. Optical measurements can precisely quantify this behavior, while calorimetric methods might overlook the selective nature of energy absorption.

Dynamic Conditions: Optical measurements can be conducted under dynamic conditions that closely mimic real-world scenarios, considering changing solar angles, cloud cover, and shading. Calorimetric methods are often conducted under controlled steady-state (or quasi-steady) conditions, which might not replicate real-life variability. TSET is influenced by properties like transmittance, reflectance, and absorptance, all of which are better characterized through optical measurements. Calorimetric methods primarily focus on overall heat transfer.

Inhomogeneous Materials: Optical measurements can account for variations in optical properties across a single material, such as coatings with different layers or dyes. Calorimetric methods might struggle to differentiate these nuances. In addition, TSET involves intricate interactions between incident solar radiation, transmitted radiation, absorbed radiation, and re-radiated heat. Optical measurements directly capture these interactions, providing a more comprehensive understanding of the system's behavior.

As previously discussed, Olivieri et al. [9] used UV/VIS/NIR spectrophotometer to obtain optical characterization of different elements coupled with EnergyPlus simulation to obtain TSET of BIPV windows with different transmittances, while Klems et al [53] utilized a scanning photometer, to determine TSET for complex fenestration systems. Klems et al. [75] carried outdoor measurement with two calorimeter chambers to compare the TSET of selective glazing with clear double glazing. In which they used an electric heater, and a liquid-to-air heat exchanger to obtain an accurate heat balance on 10 minutes interval measurements. A sun tracking pyrheliometer and horizontally mounted pyranometer was also used outside the chambers to measure the beam solar intensity and total horizontal solar intensity, respectively, in addition to a vertically mounted pyrgeometer that measured the total long-wave incident radiation reemitted by the sky and ground. As thermal sensors are much less sensitive than the photometric sensors, they demonstrated that solar-optical measurements appear to be the most agreeable with the characterization (including TSET) of complex fenestration systems (like BIPV windows)[76].

The following equipment can be used in the optical determination of window TEST and other optical properties:

Pyranometers: Total Plan of Array (POA) irradiance and transmitted was measured using two pyranometers: one placed outdoors or the POA and one indoors behind the window, respectively. The ratio of the two was used to determine the direct solar transmittance, τ, from around 200 to 4000 nm.

Pyrgeometer: A pyrgeometer was used to determine the inward flowing fraction of absorbed incident solar radiation, q_i, from around 4400 to 50000 nm.

Pyrheliometer: A pyrheliometer attached to a solar tracking weather station was used to determine the ratio of direct-to-diffuse irradiance, from around 200 to 4000 nm.

2.3.2.1 Indoor testing

The primary advantages of indoor optical testing are: i) fully controlled environment and ii) repeatability. Generally, optical tests tend to be faster and more accurate as they do not require steady-steady conditions However, the solar simulator uniformity and collimation might create measurement discrepancies. ISO 9060 addresses the specification and classification of instruments for measuring direct and hemispherical irradiance. Employing class-A optical measurement instruments (i.e., pyranometers and pyrgeometers) can minimize the error with uncertainty of less than 2%.

Chen et al. [5] in an indoor calorimetric setup with solar simulator, used a pyranometer on the outside surface of the calorimetric box to measure solar irradiance distribution. It was estimated that the dominant uncertainty in the TSET determination of BIPV window is about 3%, and is mainly due to the measurement of solar irradiance, where solar simulator lamp aging, irradiance grid density distribution, and position of the pyranometer are all contributors to the measured uncertainty. Figure 38 illustrates the contours of solar irradiance and its distribution on a 1 m x 1 m specimen plane, which shows a bright spot in the center that cannot be avoided. Consequently, a correction factor was developed to take into account the uncertainties related to the mean irradiance and its variation in the 3h test interval.
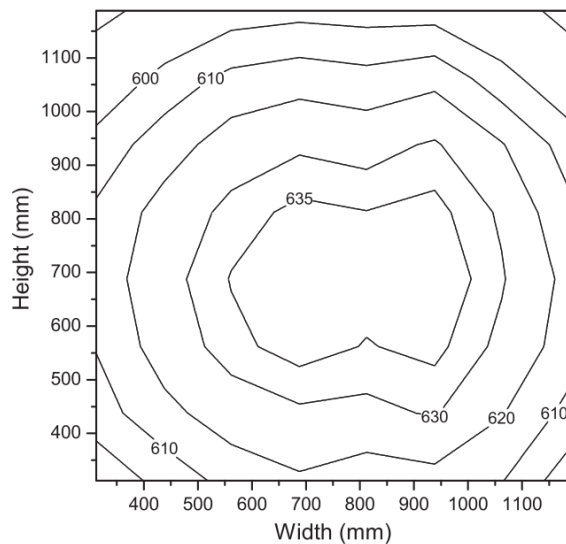
Figure 38 Solar irradiance distribution contours for a solar simulator used in Chen et al. indoor experiment.[5]

Feng and Wang [59] designed, developed, and validated a low-cost measurement system. They employed optical sensors to test glazing characteristics under quasi-steady conditions. Their goal was to develop an inexpensive easy-to-use home window measurement, where they used 3D printer to fabricate the main instrument casing and support, enabling the selected sensors be well-embedded.

2.3.2.2 Outdoor testing

The biggest challenge in experimental determination of TSET in photovoltaic windows is determining the electricity generation of the modules which is angle-dependent and varies significantly under real condition as it is highly dependent on solar spectrum and angle of incidence. Outdoor TSET determination using optical methods can be more effective as it is performed under dynamic and real environmental conditions.

Wang et al. [77] conducted outdoor optical measurements to assess the energy performance of a BIPV window (a-Si based insulating glass unit with 9mm air gap, PV-IGU) (Figure 39). The purpose of their field experiment using optical measurement was to validate the results obtained by developed comprehensive simulation model within EnergyPlus. Two pyranometer were adopted in the experiment that are shown in the Figure 39. Horizontal pyranometer and vertical pyranometer were used for measuring the total solar radiation (global and diffuse), and incident solar radiation on the window plane, respectively. The environmental parameters with optical sensors were measured and inputted into the simulation model and it was found out that the annual overall energy performance of PV IGU determined by simulation result was reliable. However, the simulated heat gain through the PV-IGU was slightly overestimated compared with the data measured with heat flux meter (Figure 40). Overall, the purpose of their optical method was to evaluate the numerical simulation model which was more reliable and accurate compared with their previous study [48], and the influence of air gap depth on overall energy performance of PV IGU.
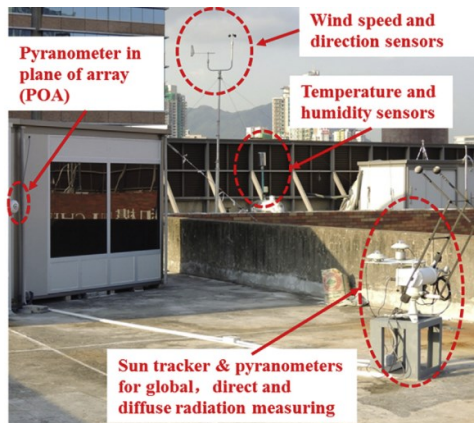
Figure 39 outdoor optical measurement instruments [77]
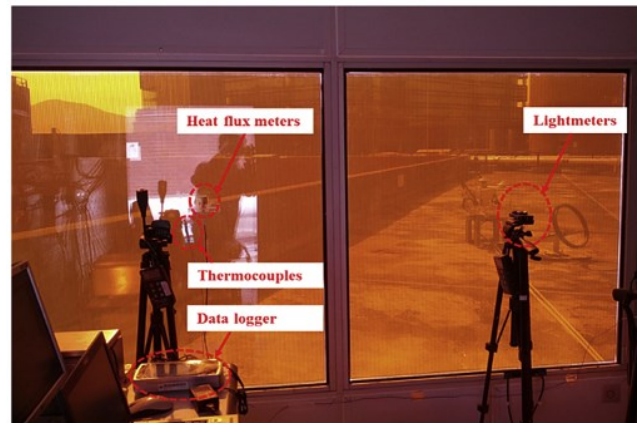
Figure 40 Measurement instruments inside the room [77]

Peng et al. [33] studied various simulation models developed for double-skin façade and their thermal and power performance and simultaneously, took into account the daylighting and dynamic power output performance of the full system. The continuous optical measurement was carried out to validate the various sub-models such as SAPM[6] and the measured data was compared with previous outdoor tests in Hong Kong [77].

Similarly, Xu et al. [51] conducted an experimental test under outdoor conditions and used optical sensors to better address environmental impact and weather conditions. The test bed was constructed on the roof

---

[6] Sandia PV power model (SAPM) considers several power performance factors for predicting PV system power under variable irradiance.

of a building in Wuhan, China (Figure 41). The test was conducted for over a year to validate the model for calculation of optimal PV cell coverage and electricity consumption for different window to wall ratios. The purpose of the study was to establish techniques for optimal PV cell coverage ratio determination and consequently incorporating them into EnergyPlus for overall energy performance of the room, including cooling, heating, and lighting.

Figure 41 Experimental setup for BIPV module TSET determination [51]

Wang et al. [48] compared the overall energy performance of PV double skin façade (PV-DSF) and PV insulating glazing units (PV-IGU) via a simulation model that was developed in EnergyPlus. Both PV modules were a-Si with similar properties. Long term outdoor optical experiment was also conducted to validate the simulation results. Figure 40 shows their measurement setup, where they have used three pyranometers for incident and transmitted POA irradiance, RTDs and heat flux meters to measure the temperature and thermal performance respectively. With their optical instruments, they verified the results gained from simulation, concluding that the performance of PV-IGU and PV-DSF are 28.4% and 30%, respectively, better than regular insulating glazing units.
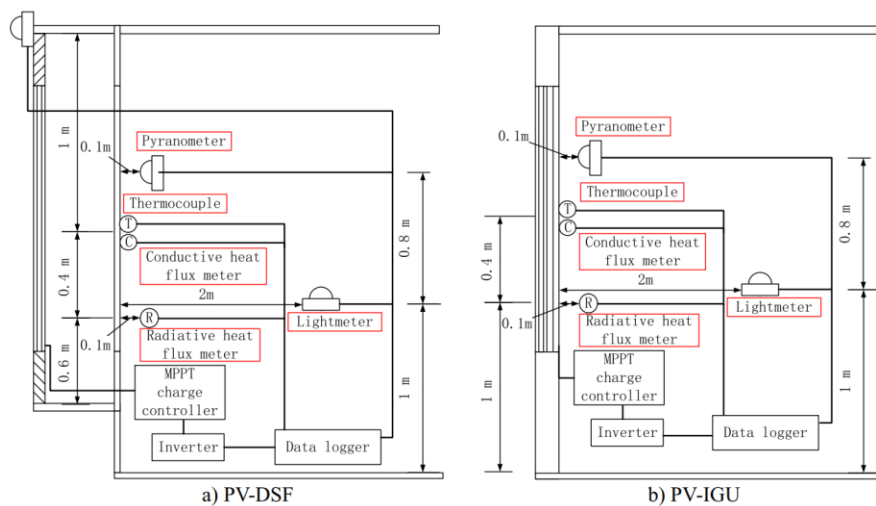
Figure 42 schematic diagram of the measurement setup by Wang et al in a comparative study between two different glazing systems [48]

This outdoor optical experiment was conducted for about 7 months on the south side of the site office building in Hong Kong (Figure 43), and the performance comparison of the PV-DSF and PV-IGU was performed in January (mostly sunny in Hong Kong). The purpose of the outdoor optical test was to validate the developed simulation model and calculate the TSET and U-Values of the PV-DSF and PV-IGU. The TSET was approximately measured using Equation 18 as previously described in 2.2.2 Solar Heat Gain Coefficient (SHGC). In their TSET optical experiment was only conducted when the solar irradiance was higher than 200 W/m^2 to minimize the calculation error.

Figure 43 Test bed on the south facing facade in Hong Kong for the PV-DSF and the PV-IGU various performance comparison [48].

Overall, reviewed literature presents various optical measurement methods in an outdoor experimental test setup. However, none of the reviewed methods were developed to measure accurate TSET of BIPV windows. Equipment and testbeds were mostly conducted to compare energy performance of complex fenestration systems like Photovoltaic window double skin façade with ventilation, that highly rely on outdoor test conditions.

2.3.3 Numerical modelling

An in-depth thermal study of BIPV windows, and several numerical models for TSET determination are proposed. These models are taking into account the energy balance between and across IGU layers (Figure 44).
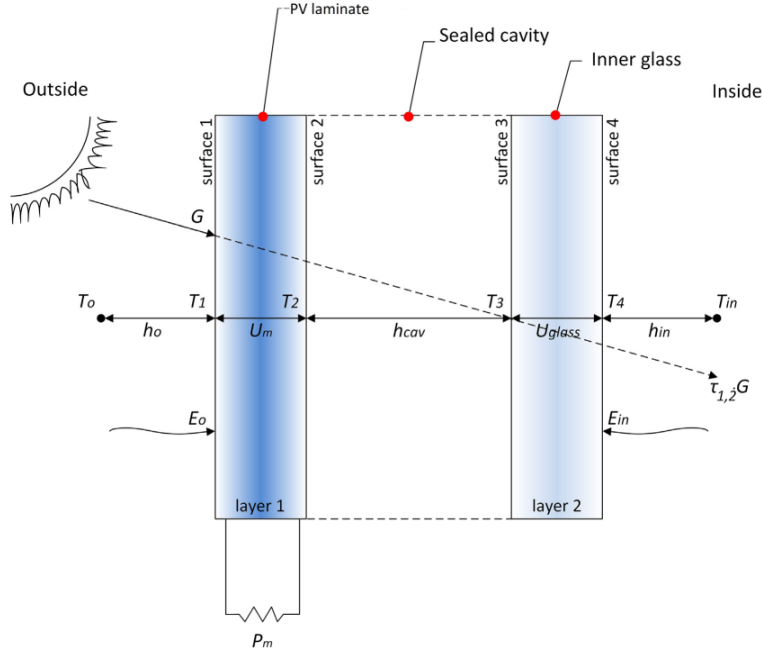
Figure 44 energy balance for BIPV double glazing [26]

There are different numerical models for TSET calculation, simplified [26] and more complex [78] models, which have been proven reliable for regular windows, however experimental measurement is recommended for complex fenestration systems (Including BIPV windows) [76]. A simplified numerical model that assumes homogenous properties for each surface is presented below, inspired by ISO 15099. Energy transfer within a double glazing BIPV window is modeled in Equation 29 to 32 where can be applied to any type of multi-glazed BIPV window configuration, analogously. In this numerical model, one-direction heat conduction is assumed, and since the glass panes including the BIPV glass are thin enough, the model ignores any thermal capacity. Furthermore, distribution of solar irradiance absorbed is equally distributed within each pane, including the BIPV module.

For energy transfer between the outermost surface (i.e., surface-1) and the outdoor environment and the surface-2 of BIPV window:

$$(E_0 \varepsilon_1 - \varepsilon_1 \sigma T_1^4) + h_0 (T_0 - T_1) + [\frac{\alpha_1 G}{2} - \frac{P_m}{2 A_m}] = U_m (T_1 - T_2) \tag{29}$$

BIPV window between surface-2 and surface-3:

$$U_m (T_1 - T_2) + [\frac{\alpha_1 G}{2} - \frac{P_m}{2 A_m}] = [\sigma \frac{\varepsilon_2 \varepsilon_3}{1 - (1 - \varepsilon_2)(1 - \varepsilon_3)} (T_2^4 - T_3^4)] + h_{cav} (T_2 - T_3) \tag{30}$$

BIPV window between surface-3 and surface-4:

$$[\sigma \frac{\varepsilon_2 \varepsilon_3}{1 - (1 - \varepsilon_2)(1 - \varepsilon_3)} (T_2^4 - T_3^4)] + h_{cav} (T_2 - T_3) + \frac{\alpha_2 G}{2} = U_{glass} (T_3 - T_4) \tag{31}$$

45

The energy exchange between the innermost surface (i.e., surface-4) and indoor can be calculated with following equation:

$$U_{glass}(T_3 - T_4) + \frac{\alpha_2 E}{2} = [\varepsilon_4 \sigma T_4^4 - E_{in}\varepsilon_4] + h_{in}(T_4 - T_{in}) \tag{32}$$

where
E (W/m^2): Solar POA irradiance;
E_{in}, E_{out} (W/m^2): Thermal radiation incident on window outer surfaces;
P_m (W): The output of BIPV window under MPP;
U_{pv}, U_{glass} $(W/m^2 K)$: Thermal transmittance of the PV module and thermal transmittance of inner glass respectively;
σ [5.6703·10-8 $W/m^2 k^4$]: Stefan-Boltzmann constant;
T_i(K): Average temperature of each surface (i=1 outermost surface and i=4 innermost surface);
T_{in}, T_o (K): Indoor and outdoor air temperature;
T_c(K): BIPV window cell temperature the outermost surface temperature (Tc = T1);
ε is Emissivity of each surface;
h_{cav} (W/m^2K): Convective heat transfer combined with gas-conductive heat transfer coefficient of the sealed cavity; and
h_{in}, h_o(W/m^2K): Indoor and outdoor air film convective heat transfer coefficient respectively.

Beanas and Machado [78] presented a more complex numerical model accounting for the thermal capacity of each window layer and any inhomogeneous properties such as opaque and transparent parts of the BIPV module. The model was validated performing field measurement on a case study. The model also accounted for the spectral sensitivity of the PV layer. The relative spectral distribution of the solar radiation in the model is given by the following equation:

$$\eta_{ec} = \eta_{bare} \int_{\lambda_1}^{\lambda_2} S(\lambda) \frac{A_{cell}(\lambda)}{1 - r_{cell}(\lambda)} d\lambda \tag{33}$$

Finally, Fung and Yang [25] evaluated the TSET of a BIPV window using the Semi-transparent Photovoltaic Module Heat Gain (SPVHG) model. They studied the impacts of different parameters and found that the design parameter that has the biggest impact on TSET for BIPV windows is the area of solar cells and/or the transparency of the active layer. Their model was also validated by using an indoor calorimeter and a solar simulator.

2.4 Summary

With population rise, rapid growth in global building floor area and rise of buildings' glazing area in new architecture styles, the impact of the optical and thermal characteristics of glazing on annual energy consumption for buildings become prominent in every climate. As Building-Integrated Photovoltaic (BIPV) windows are expected to become more popular, especially in office building applications, the can assist with climate change mitigation through the generation of onsite sustainable solar energy. These windows not only let in light while moderating unwanted solar gains but also generate electricity from the sun.

BIPV windows are commonly categorized under two main categories of i) spaced silicon cells and ii) thin film modules. Spaced silicon cells are comprised of opaque crystalline silicon cells that partly obstruct the view. On the other hand, thin film modules are comprised of transparent layer deposited onto glass, allowing for a clearer view. The properties of BIPV window depend on several factors, including the embedded solar cell technology, transparency, PV cell coverage, and the window assembly configuration. Achieving the right balance between daylighting, thermal performance, and electricity generation is essential to maximize the benefits of BIPV technologies.

Total solar energy transmittance (TSET) of BIPV windows plays a crucial role in determining their impact on the building's energy performance, ensuring the right balance between daylighting, solar heat gains, and electricity generation is achieved. Measuring TSET for BIPV windows is a challenge especially when electricity production is considered, as part of the energy that is converted into the electricity.

Currently, TSET for regular windows is typically calculated using established methods like LBNL Window simulation software, or for more complex glazing configurations, it is experimentally measured, as simulation software has limitations in such cases. Similarly, when it comes to BIPV windows, simulation software does not take into account the electricity production, and hence the need to develop a specialized experimental method to accurately assess their overall energy performance and balance becomes apparent.

TSET of regular windows is currently measured thermally with calorimetric hot box and a solar simulator. Inside the calorimeter, "indoor building" conditions are replicated, and outside the calorimeter standard "outdoor conditions" are emulated. This calorimeter is designed and built to perform the test under steady state condition. The amount of energy used to keep the "indoor environment" in steady state yields the TSET.

However, existing standard methods often fall short when it comes to BIPV windows because they rely on indoor tests with normal angle of incidence and fixed conditions, which may not fully account for the dynamic interplay between energy generation and thermal performance in real-world applications.

Researchers have investigated the reduction of the TSET in BIPV windows in relation to PV cell coverage, transparency, angle of incidence, and transient outdoor test conditions. The literature on BIPV window shows the need to develop a measurement method that considers the dependencies of the on angle of incident, spectral properties of the solar irradiance and the boundary conditions on TSET.

Developing a reliable experimental test for determining TSET of BIPV window, using outdoor and optical measurement has not been investigated in literature. In Chapter 3, a new methodology that is angle-dependent and fits well into new generation of active window technologies like BIPV is proposed. In this

first effort, the theoretical background and methodology are presented, including a critical review of existing procedures for the determination of the TSET. The challenges and limitations associated to experimental procedure and effectiveness of the proposed methodology are discussed under Chapter 4. Discussion.

Chapter 3. Methodology

This section introduces a new experimental methodology for the determination of the total solar energy transmittance (TSET) of BIPV windows. Unlike existing calorimetric standards, the proposed method employs optical measurements instead of thermal measurements.

The methodology is versatile and can be applied in both outdoor and indoor testing facilities. Although specifically designed for BIPV windows, it has the potential to be utilized for other window technologies, such as coated, reflective, and electrochromic windows.

The proposed methodology consists of three distinct steps: 1)BIPV window pre-characterization, 2) Test setup, and 3) Experimental determination of TSET. Determining TSET of BIPV windows under Maximum Power Point (MPP) operation accounts for that part of the absorbed solar radiation that becomes electricity and not just heat.

3.1 BIPV Window Pre-Characterization

Prior to the experimental determination of TSET, mechanical, thermal, and electrical characteristics of the module should be measured, calculated, and reported. The following section describes the steps that proceed the experimental determination of TSET for BIPV windows, refered to as "pre-characterization". Note that some of these values are used as inputs in the calculations associated to the determination of TSET.

3.1.1 Mechanical Characteristics

The pre-characterization is performed for the IGU, excluding window frame. The following mechanical characteristics of the BIPV window should be reported:

- Integrated photovoltaic technology (e.g., CdTe, mono-Si, a-Si)
- Dimensions: width, height and thickness of area exposed to the sun (frameless), A (mm)
- Packing factor, when applicable, PF (%)
- Weight, W (kg)
- Number of panes, including the outermost laminated PV glass layer
- Type of junction box
- Description of each IGU layer, including composition of gas cavity, when available

For an example, see "Theoretical Study" under Chapter 4.

3.1.2 Thermal Characteristics

The following thermal characteristics of the BIPV window should be reported:

- Steady state thermal transmittance, U-value (W/m^2K)
- Innermost and outermost surface emissivity, ε (%)

The steady state thermal transmittance of the BIPV window can be determined using one of the following standard procedures, under open circuit[7] (OC):

- The guarded hot plate method based on ISO 10291 [79] or ASTM C177 [80]
- The heat flow meter method according to ISO 10293 [62], or ASTM C209 [81]
- The calculation method, following the ISO 10292 [37]

Note that the boundary conditions under steady state standard testing conditions may differ from the ones under the proposed TSET procedure, effectively resulting in a different U-value. For more information on how to tackle this challenge, see "Correction of U-value", under Chapter 4.

As temperature differences and ambient conditions affect the measured thermal transmittance, it is necessary to provide reliable information about the boundary conditions during measurements. The heat flux meter (HFM) method can also be implemented, following the ISO 10293 [62]. To experimentally measure the steady-state thermal transmittance with a HFM, long-term tests should be implemented in locations with less regular climatic conditions (e.g., locations with irregular or fluctuating climate conditions such as cold climates where it is hard to have the steady outdoor temperature). The measurement frequency can be set to 20 seconds to provide reasonable accuracy and track small effects. Furthermore, the temperature sensors should be attached at least 25 cm away from the edges to prevent the edge-of-glass temperature difference [82].

In order to calculate the longwave radiation heat exchange between the BIPV window and the surrounding environment, the emissivity of the innermost and outermost surfaces can be measured with the calibrated emissometer complying with ASTM C1371-15 [83] standard. The emissometer is calibrated prior to each measurement using a reference specimen of known surface emissivity. To get a reliable emissivity measurement of the innermost and outermost IGU surfaces, at least five measurement locations for each surface are recommended as shown in Figure 45. The final surface emissivity for each surface is the statistical average value of the five (or more) measurements.
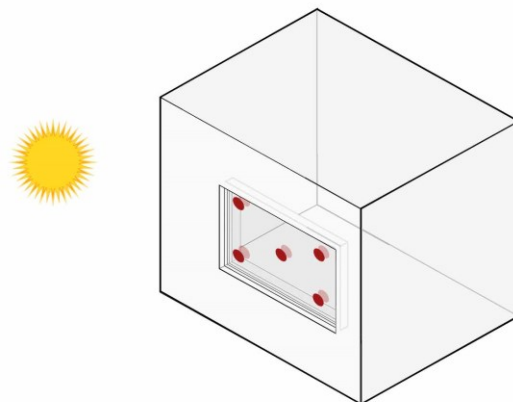
Figure 45 Minimum recommended measurements to determine surface emissivity values for innermost and outermost surfaces of the BIPV window.

---

[7] State with no electricity production

3.1.3 Electrical Characteristics

The following electrical characteristics of the BIPV window should be measured and reported under Standard Test Conditions (STC, irradiance of 1000 W/m^2, air mass of 1.5, and module temperature of 25 °C), as described under IEC 61215[84].

- Module electrical efficiency, η (%)
- Maximum power at MPP (W)
- Voltage at MPP, V_{mp} (V)
- Current at MPP, I_{mp} (A)
- Open Circuit Voltage, V_{oc} (V)
- Short Circuit Current, I_{sc} (A)
- Power temperature coefficient, β (%/K)

When applicable, the electrical and TSET characterization should take place after the window is light-soaked. Light-induced degradation (LID) is a phenomenon that depletes efficiency or causes a power drop in the solar modules when exposed to light. E.g., CdTe photovoltaic technologies should be light-soaked in compliance with the light induced stabilization procedures under IEC 61215-2 [85], to ensure stable performance upon exposure to light during testing.

CdTe based PV degradation rate is higher under OC compared to MPP conditions [86]. Transient effects on thin film module performance over periods of hundreds of hours have been observed by Gostein and Dunn [87].

3.2 Test Setup

This section gives an overview of the most important aspects to be considered for the mounting of the BIPV window, as well as how to install and configure any optical measurement systems. The descriptions below primarily address outdoor TSET testing of a BIPV window. However, these practices can also apply to indoor testing with a continuous solar simulator. The methodology involves installing the BIPV window for characterization and a non-photovoltaic "Reference window" with a known standard TSET (Figure 46).

51
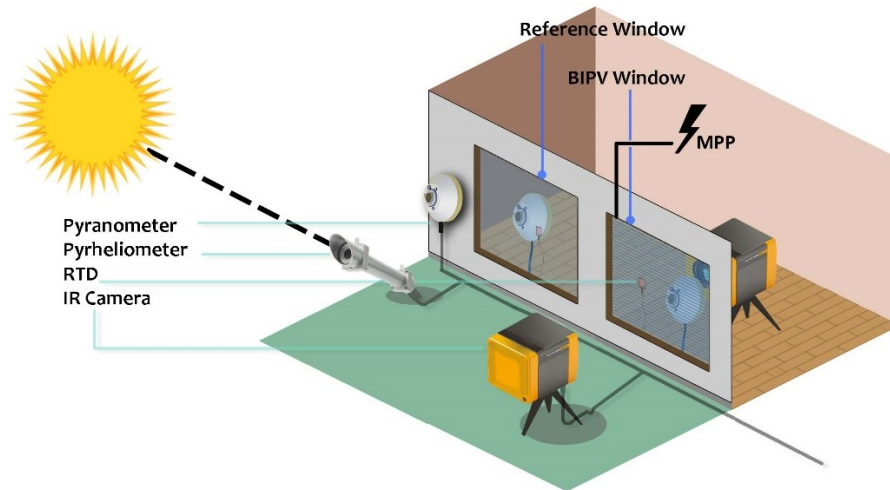
Figure 46 Schematic of the Reference (left) and BIPV (right) window, and test instrumentation.

3.2.1 Window preparation and Installation

Prior to any steps, the BIPV window and Reference window must be carefully inspected under an illumination of no less than 1000 lux to ensure that there are no cracks, bubbles, delamination, internal condensation or any evidence of visual defects [84].

For optimal measurements, the BIPV window and Reference window should be installed on the same façade of an outdoor facility, facing near-south (i.e., South ± 45°, assuming a location on the northern hemisphere). The two windows should be installed at least 0.8 m above the ground[8] and next to each other. The mounting location should be selected to ensure no shading during testing periods. The use of a thermally broken stick curtain wall system is recommended. The use of pressure plates that are fastened to the outside of the mullions to retain the IGUs in place, allow easy mounting and dismounting of the test specimens (Figure 47). The mullions should cast minimal shading on the BIPV window while enabling wire management without compromising the continuity of the control layers (i.e., water, air, vapor and thermal)[9]. The indoor room surfaces should minimize solar reflections and be maintained at spatially uniform and steady-state conditions.

The BIPV window requires to be connected to an electric load operating under maximum power point (MPP). Monitoring of the performance with an IV tracker can ensure that the window operates at peak efficiency and possibly detect any failed or malfunctioning components or shading (Figure 46).

The Reference window should be a clear double-glazed insulated unit of known TSET that does not incorporate any angular-selective films or coatings.

---

[8] The height of 0.8 is chosen to simulate real-world conditions where most windows are typically installed at certain height above the ground. In addition, influence of the ground reflection is reduced and the risk of window obstructions by people or objects passing by the area is minimized.

[9] Note that the photovoltaic layer dimensions should be less than the frameless IGU dimensions to allow mounting while minimizing shading effects due to window frame.
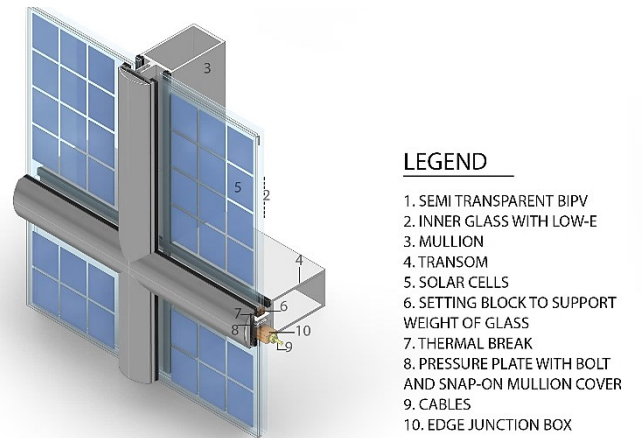
Figure 47 Pressure plates fastened to the outside of the mullions, retaining the IGUs in place.

3.2.2 Equipment Selection and Setup

A series of actinometers is deployed to perform quick (i.e., in the order of minutes) and reliable measurements that can be used to determine the TSET of a BIPV window. As discussed earlier, a Reference window is used to correct the optical measurements for the termination of the TSET of the BIPV window. Care must be taken that all outdoor instruments do not shade the BIPV and Reference windows during the test periods.

Pyranometers

As shown in Figure 46, three pyranometers, one pyrheliometer, an IR camera and several RTDs are deployed to perform the window characterization. An outdoor pyranometer is installed at the height of window centroid, normal to the window, to capture the total solar irradiance to the plane-of-array (E_{POA}).

A second pyranometer should be installed indoors, behind the BIPV window, facing outwards, normal to the window to measure the transmitted solar irradiance incident to the plane-of-array for the BIPV window (Q_{BIPV_sol}). The distance between the indoor pyranometer and the BIPV window depends on the specimen technology (e.g., Si, a-Si, thin film, CdTe, etc.) and should represent the overall performance of the IGU. E.g., For a CdTe-based window, due to homogenous nature of the PV film, the pyranometer behind the window should be within less than 200mm from the innermost window surface.

Similarly, a third pyranometer should be installed indoors, behind the Reference window, facing outwards, normal to the window, to measure the transmitted solar irradiance to the plane-of-array for the Reference window (Q_{REF_sol}).

Pyrheliometer

An outdoor pyrheliometer is used to measure direct normal irradiance (DNI). It is recommended that the pyrheliometer is installed on a sun tracker to constantly face normal to the sun [88]. The direct solar irradiance incident to the plane-of-array (E_b) can be determined by Equation 34. [88]:

$$E_b = DNI \cdot \cos(AOI) \tag{34}$$

where AOI refers to the solar angle of incidence.

Weather Station

A weather station located in proximity to the testing site should monitor the following climatic conditions:

- Outdoor dry bulb temperature measured at approximately 1.5 m above ground (T_{out})
- Wind speed measured at 10 m above ground (WS).

Infrared Camera

An IR camera should be installed indoors, facing the window, to measure the average indoor surface temperatures for the BIPV (T_{BIPV_in}) and Reference window (T_{REF_in}). Similarly, an IR camera should be installed outdoor, facing the window, to measure the average indoor surface temperatures for the BIPV (T_{BIPV_out}) and Reference window (T_{REF_out}).

The distance between the camera and the window surface depends on the specifications of the device, where cameras with wider field view can be installed further away to capture the surface temperatures for both BIPV and Reference window. The IR cameras should be oriented so to minimize thermal reflections. RTD surface sensors can be used to achieve a measurement accuracy of ±2°C or 2% of the measurement[10] (whichever is larger).

RTD Sensors

Solar-shielded RTDs can be installed on the surface of the window frames to measure surface temperatures that can be used to calibrate the IR camera surface window measurements. The RTD surface sensors should not obstruct the view of any actinometers and should not cast shadow on the windows. In addition, the indoor average temperature should be measured, accounting for both air and surface temperatures (T_{in}).

As indicated in ISO 19467 Annex E [89], the surface temperature should be measured preferably at nine locations on the internal and external sides and at least 25 cm away from the window frame. The RTD sensors are better able to eliminate the impacts of casting shadow on the active layer part of BIPV window as much as possible (Figure 48).

---

[10] The RTD sensors used for measuring surface temperature can be used to calibrate the IR camera.
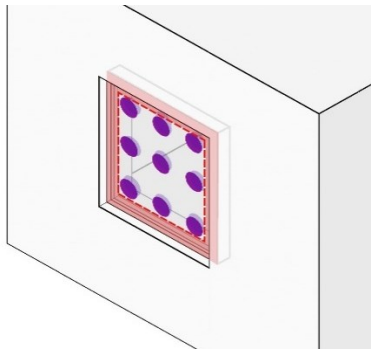
Figure 48 schematic illustration of RTD sensors placement, to prevent edge of window temperature difference. Note : the sensors are thin to prevent shadow casting and are not shown to scale in the illustration.

Data Acquisition System

A data acquisition system should be connected to actinometers and RTDs and collect synchronized measurements. The frequency of the measurements is recommended to be 20 seconds or more to meet instruments' response time and reduce transient spikes and sudden changes caused by e.g., passing birds, planes, or small cloud movement.

Table 9 summarizes the instruments placement and the frequency of the measurements needed. Figure 49 schematically shows the location, and direction of each instrument[11].
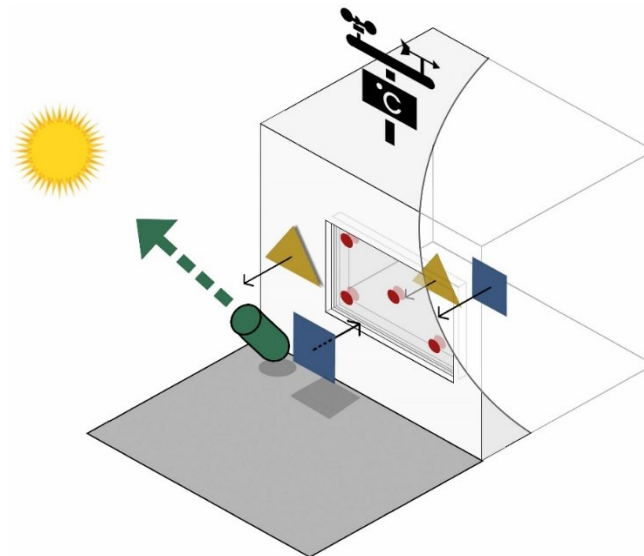
Figure 49 Instruments setup location and orientation. Note that instrument installation must not obstruct BIPV window surface from direct or diffuse light.

---

[11] The accuracy and uncertainty of the instruments are indicated in Table 17

Table 9 Summary of the location, direction and frequency of measurements taken of all instruments.

Instrument	Setup locations	Direction	Measurement input	Measurement location	Frequency of measurements	Measurement period
Pyranometer, Spectrally Flat Class A	Outdoors	Facing window, outwards, along with the window normal	E_{POA}	At height of window centroid	At 20 seconds intervals or longer based on device's highest response time	Average out to 5 min
	Indoors	Facing window, outwards, along with the window normal.	Q_{BIPV_sol}, Q_{REF_sol}	20 cm away from the window		
Pyrheliometer, Spectrally Flat Class A	outside	Normal to sunrays (i.e., installed on sun tracker)	E_{Direct}	At height of 1.5 m from the ground	At 20 seconds intervals or longer based on device's highest response time	Average out to 5 min
IR cameras	Outdoors	Facing window, inwards	T_{BIPV_out}, T_{REF_out}	At height of 1.5 m from the ground	At 20 seconds intervals	Average out to 5 min
	Indoors	Facing window, outwards	T_{BIPV_in}, T_{REF_in}			
RTDs	Outdoors	N/A	TS_{BIPV_out}, TS_{REF_out}, TS_{BIPV_in}, TS_{REF_in}, T_{in}	Window frame surface of BIPV and Reference window	At 20 seconds intervals	Average out to 5 min
	Indoors					
Weather Station	Outdoors	N/A	T_{out}	1.5 m above ground	At 5 seconds intervals	Average out to 5 min
			WS	10 m above ground		

3.3 Experimental Determination of TSET

3.3.1 Test conditions and period

In order to achieve repeatable and reproducible results, the experiment is recommended to be conducted on a sunny day with limited cloud cover and under solar angle of incidence (AOI) of no more than 60 degrees. The E_{POA} should not vary more than 50 W/m^2 or 5% (whichever is smaller) during the test period.

The indoor and outdoor air and surface (i.e., window, frame and indoor surfaces) temperatures should be constant with a variation of less than ±2°C during the test period.

The test period should be for 5 minutes. The measurement frequency for the various equipment is presented under. The statistical average and standard deviation should be calculated for all measurement inputs as follows:

Statistical average for input X (Equation 35):

$$\bar{X} = \frac{1}{n} \sum_{i=1}^{n} X_i \tag{35}$$

Standard deviation for input X (Equation 36):

$$s = \sqrt{\frac{1}{n-1} \sum_{i=1}^{n} (X_i - \bar{X})^2} \tag{36}$$

3.3.2 Determination of the TSET for the BIPV window

The perceived TSET for the BIPV window under the specific test conditions is calculated as follows:

$$TSET = \frac{Q_{BIPV\_sol} + Q_i}{E_{POA}} \tag{37}$$

where Q_{BIPV_sol} is measured by indoor pyranometer and the Q_i is calculated as follows:

$$Q_i = \varepsilon_{BIPV\_in} \cdot \sigma \cdot \left(T_{BIPV\,in}^4 - T_{in}^4\right) \tag{38}$$

Similarly, the perceived TSET for the Reference window under the specific test conditions is calculated as follows:

$$TSET_{REF} = \frac{Q_{REF\_sol} + Q_{iREF}}{E_{POA}} \tag{39}$$

Where

$$Q_{iREF} = \varepsilon_{REF\_in} \cdot \sigma \cdot \left(T_{REF\_in}^4 - T_{in}^4\right) \tag{40}$$

The equipment responsible for measuring the variables in the above equations is detailed in the following table (Table 10):

Table 10 Measured variables and corresponding equipment.

Parameter	Description of Measured Variable	Unit	Equipment
Q_{BIPV_sol}	Direct and diffuse solar irradiance transmitted through BIPV window	W/m^2	Indoor pyranometer (facing the BIPV window)
Q_{REF_sol}	Direct and diffuse transmitted solar irradiance through reference window	W/m^2	Indoor pyranometer (facing the REF window)
E_{POA}	Solar global irradiance	W/m^2	Outdoor pyranometer (mounted outside on the façade plane)
ε_{BIPV_in}	Emissivity of the innermost surface of the BIPV window	%	Emissometer
$T_{BIPV\,in}, T_{REF\,in}$	Average indoor surface temperatures for the BIPV and REF window	K	IR camera

Note: the accuracy and measurement intervals of the equipment is further discussed in Table 17.

Note that the perceived TSET for both the BIPV and reference window are under a specific AOI, solar spectrum and specific ratio of direct to diffuse irradiance. The placement of the sensors is shown in the following schematic (Figure 50), with the corresponding measured data indicated.
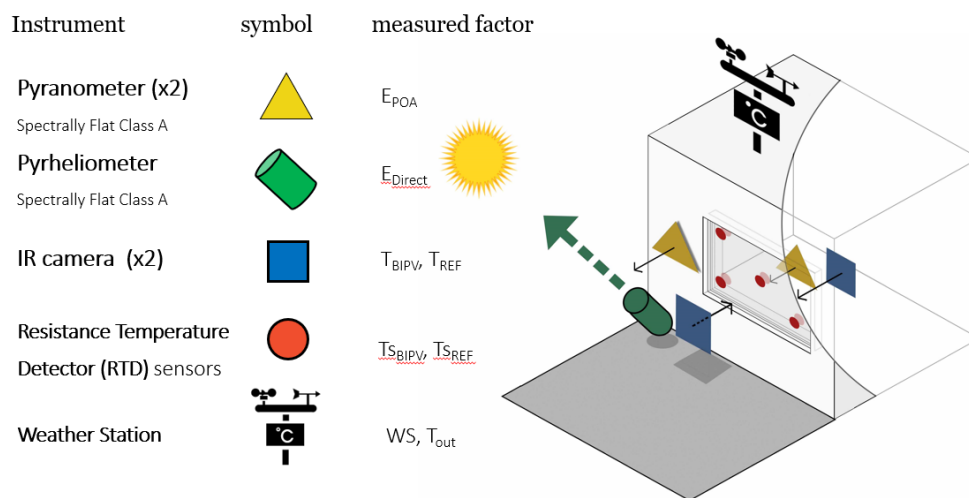
Figure 50 The location of sensors, and corresponding measured data

3.3.3 Measurement result correction using the Reference window

The perceived TSET for both the BIPV and Reference windows ($TSET_{BIPV}$ and $TSET_{REF}$, respectively) are under a specific AOI, solar spectrum and direct-to-diffuse irradiance ratio.

The corrected direct $TSET_{BIPV}$ can be calculated for any AOI using the following empirical equation:

For double glazed IGU with no angular selective properties

$$TSET_{BIPV}(AOI) = \frac{\widehat{TSET}_{REF}}{TSET_{REF}} \cdot TSET_{BIPV} \cdot [a \cdot AOI^4 + b \cdot AOI^3 + c \cdot AOI^2 + d \cdot AOI + e] \quad (41)$$

where $\widehat{TSET}_{REF}$ refers to known normal direct TSET of the Reference window, and the coefficients are:

$a = -1.03 \cdot 10^{-8}$

$b = -1.26 \cdot 10^{-6}$

$c = 0.0009$

$d = -0.00166$

$e = 1.00491$

Note that the empirical coefficients of the Equation 41 were statistically developed using polynomial regression analysis with 70 double glazed IGUs of known angular TSET properties as inputs (Refer to Appendix), generated using LBNL Window 7.8. The TSET prediction error for AOI < 60deg was estimated to be less than 5% for a double glazed IGU with no angular selective properties.

Chapter 4. Discussion

This section discusses the challenges, solutions and limitations of the limitations of the experimental determination of the TSET of BIPV windows using optical measurements. A CdTe based BIPV window is used as an example to discuss the methodology in further details. The following section provides a theoretical example of the proposed methodology applied, followed by a discussion on challenges, limitations and potential steps to overcome them.

It is important to note that the study aims to provide the theoretical foundation for the TSET optical characterization of TSET, using i) fundamental principles of heat transfer and ii) existing literature. However, the proposed solutions to foreseen challenges need to be evaluated and potentially modifies through an experimental study. IEA PVPS Task 15 aims to evaluate and fine tune this proposed methodology through an international experimental round-robin and provide input to the development of a new international TSET standard applicable to BIPV windows and other window technologies.

The main key steps of the proposed methodology are i) module pre-characterization ii) TSET test setup, and iii) experimental determination of TSET. Prior to the experimental determination of TSET, mechanical, thermal, and electrical characteristics of the tested module are either measured or calculated. The optical measurement equipment is mounted and installed as discussed in Chapter3, subsequently the experiment is conducted and the TSET is calculated based on the gathered data.

For correcting the result, a reference window with known TSET is used and an empirical equation is developed to adjust the values accordingly. The fourth order empirical equation (Equation 41.) is statistically developed to take into account the specific AOI, solar spectrum and direct-to-diffuse irradiance ratio. Seventy different double glazed IGUs with known angular TSET properties are generated as inputs using LBNL Window 7.8 (Figure 51, Note: the inputted IGUs can be find in Appendix), to generate the correction equations. Subsequently, the error has been estimated to be less than 5% (Table **11**) for a double glazed IGU with no angular selective properties, and AOI < 60deg.

Figure 51 input IGU generated using LBNL Window to develop correction coefficient.

Table 11 Root Mean Square Error (RMSE) and R-squared of the generated polynomial regression model.

	a	b	c	d	e
Polynomial coeffients	-1.03199E-08	-1.2666E-06	9.09516E-05	-0.00166	1.00491
Standard error values for the coefficients	2.02288E-09	3.67102E-07	2.14121E-05	0.00044	0.00251
Coefficient of determination	0.996				
Standard error for the TSET estimate	0.022				

4.1 Limitations

As discussed in the literature review, the experimental determination of TSET under outdoor environment has the following intrinsic limitations.

4.1.1. Weather Dependence

Measurements are influenced by weather conditions, including cloud cover and time of day, potentially limiting test availability. To reduce error associated with weather variability, it is recommended that all outdoor measurements are conducted under the following conditions:

Table 12 Proposed experimental conditions based on literature.

Global horizontal irradiance	≥ 500 (W/m^2)
Temporal variation of global irradiance to the plane-of-array (E_{POA})	≤ 50 W/m^2 or $\leq 5\%$ (whichever is smaller), during the test period
Solar angle of incidence (AOI)	$< 60°$
Cloud cover	$\leq 25\%$ (clear sky)
Outdoor dry bulb air temperature	$\pm 2°C$ during the test period

4.1.2 Solar Spectrum Variability

Solar spectrum has daily and seasonal variations, but it can also vary between locations of different geographic latitude and elevation. To correct the outdoor measurements to standard condition measurements (i.e., 1.5 Air Mass), (ASTM G173 [90]) the Sandia or CREST empirical methods can be used, as described under Marion (2010)[91]. Both methods should be tested and evaluated for effectiveness prior to use. Alternatively, measurements can be conducted indoors, under a continuous solar simulator of a standard spectrum.

4.1.3 Angular Dependance

Considering that the TSET measurements take place outdoors, the AOI is expected to be different than normal. In section

3.3.3 Measurement result correction using the Reference window, an empirical equation is provided to correct the TSET measured under AOI < 60° to any AOI, including normal (perpendicular to the window). The following section describes the derivation of the empirical equation (32) for double glazed IGU with no angular selective properties. Similar equations can be developed and used for a triple or higher glazed IGU.

Step 1: Generated Data. Using LBNL Window 7.8, the angular variation of TSET for several (n = 70) double glazed IGUs were simulated, $TSET(AOI)$. All IGU models were developed using the following conditions:

- Two layers of glass
- 12.7 mm cavity, mix 5% air and 95% Argon
- A low-emissivity coating in surface-2 or -3
- No use of angular selective properties (e.g., films or coatings)

Step 2: Data Normalization. Considering that the angular TSET of each IGU can vastly differ due to the optical characteristics of each glass layer, the generated data was normalized as follows:

$$TSET_{norm}(AOI) = \frac{TSET(AOI)}{TSET(0°)}, \text{ where } TSET_{norm}(0°) = 1 \text{ and } TSET_{norm}(90°) = 0$$

Step 3: Polynomial Regression Analysis. Using the normalized data as input, an empirical TSET equation was developed using polynomial (4th order) regression analysis:

$$TSET(AOI) = TSET(0°) \cdot [a \cdot AOI^4 + b \cdot AOI^3 + c \cdot AOI^2 + d \cdot AOI + e]$$

where $\widehat{TSET_{REF}}$ refers to known normal direct TSET of the Reference window, and the coefficients are (Table **13**):

$a = -1.03 \cdot 10^{-8}$

$b = -1.26 \cdot 10^{-6}$

$c = 0.0009$

$d = -0.00166$

$e = 1.00491$

Note that the empirical coefficients of the Equation 41 were statistically developed using polynomial regression analysis with 70 double glazed IGUs of known angular TSET properties as inputs (Refer to Appendix), generated using LBNL Window 7.8. The TSET prediction error for AOI < 60deg was estimated to be less than 5% for a double glazed IGU with no angular selective properties.
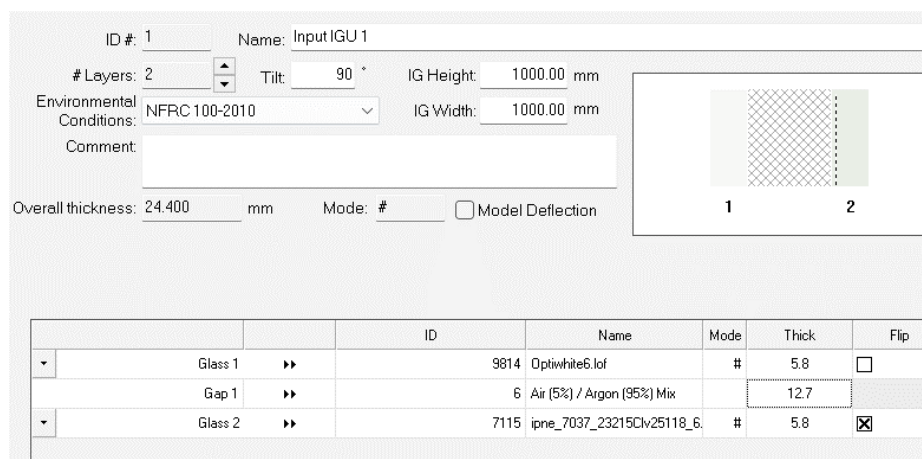
	a	b	c	d	e
Polynomial coeffients	-1.03199E-08	-1.2666E-06	9.09516E-05	-0.00166	1.00491
Standard error values for the coefficients	2.02288E-09	3.67102E-07	2.14121E-05	0.00044	0.00251
Coefficient of determination	0.996				
Standard error for the TSET estimate	0.022				

4.2 Measurement of indoor and outdoor combined

Literature has indicated that measuring combined indoor and outdoor window film coefficients accurately may require a combination of various methods (e.g., surface heat flux measurements, thermal imaging, comparative analysis using a reference specimen), careful experimental design, and data analysis to account for the complex interactions involved. Prior to TSET testing, it is essential to experimentally investigate and evaluated the effectiveness of the applied methods, document all experimental conditions and sources of potential error to ensure the validity of the experimental results.

4.3 Window installation

Prior to outdoor experimental tests, The BIPV window should be visually examined for defects or damage, and preconditioned to two cycles of light and dark exposure of 24-100 hours each [86]. The pre-conditioning allows the BIPV window to achieve some level of stabilization before performing the test.

The edges of the BIPV frameless window should allow for the unit to be mounted into a window frame while avoiding any shading effects (Figure 52).
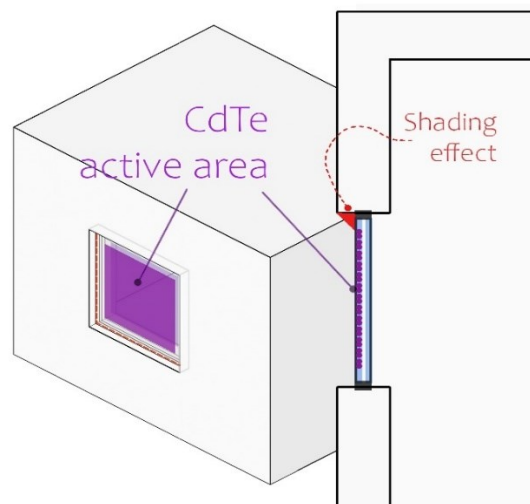
Figure 52 Schematic of BIPV window installation without overhangs or shading effect on CdTe active area

BIPV window and the reference window should be installed to prevent air and water leakage, while minimizing the thermal effects of the mounting frame. ASTM E2112 covers the installation process required for BIPV and reference window in new and existing construction [92]. A gasket should be applied on the frameless module's edges to eliminate water and air leakage, complying with standard practice for installation of exterior window.

4.4 Theoretical Characterization of a CdTe BIPV Window

For this theoretical study, a BIPV CdTe-based double IGU is assumed (Figure 53). The proposed steps are common across BIPV technologies (e.g., Si, a-Si, CIGS) and IGUs (e.g., double, triple), unless otherwise specified. The following properties should be measured/simulated and reported as specified under Chapter 3. Methodology.
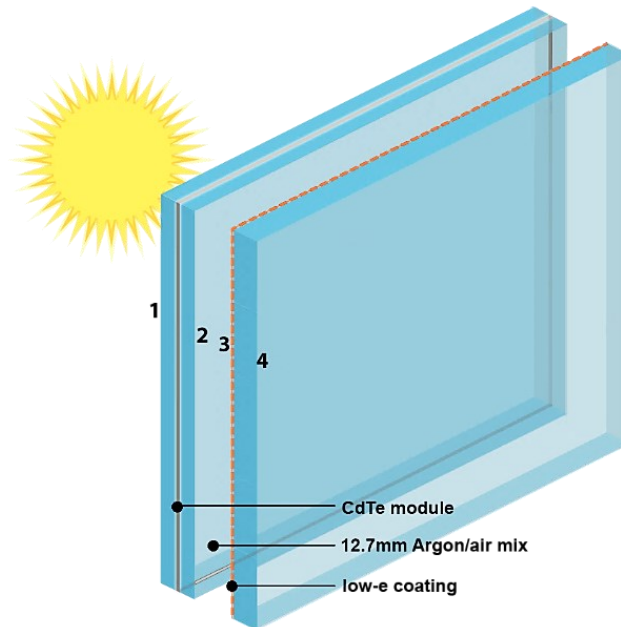
Figure 53Schematic of BIPV CdTe double glazed window

4.4.1 Mechanical Data Report

The BIPV window has dimensions of 1000 mm by 1000 mm and total thickness of 25 mm. The semi-transparent photovoltaic technology used is Cadmium Telluride (CdTe) thin film. The outer pane is a semi-transparent CdTe laminated glass module that consists of (outside to inside): 4 mm glass substrate with a transparent conducting oxide (TCO) which acts as a front contact for the CdTe thin film, the CdTe active layers, the back contact, the PVB laminate, and a 4 mm back sheet glass that protects the active layers from damage and deterioration. The inner pane of the IGU is a 6 mm glass with a low-emissivity coating on

surface-3. Between the outer and inner glass, there is a 12.7 mm sealed cavity with mixture of 5% air and 95% Argon. The BIPV mechanical data is summarized in Table 14.

Table 14 Mechanical Data of CdTe BIPV window

BIPV Window Specification	Data
Photovoltaic Technology	CdTe
Dimensions (excl. frame)	1000 mm x 1000 mm x 25 mm
Weight	~25 kg
Outer BIPV module	4 mm / 4 mm laminated; heat strengthened. safety glass *
Inner glass pane	6 mm, clear glass with low-e coating
Sealed Cavity	12.7 mm, mix 5% air and 95% Argon, thermally broken spacers
Junction box	Edge with T4 connectors

4.4.2 Thermal Data Report

Further, the thermal transmittance of the BIPV window should be determined and reported. In this theoretical study, the detailed calculation method is used through LBNL WINDOW7.8 software, following the ISO 10292 [37]. Note that WINDOW7.8 calculates the thermal transmittance of a window assembly under steady state standard testing conditions. However, the U-value does vary based on outdoor and indoor conditions (e.g., ambient temperature, wind).

Table 15 Thermal characteristics of the CdTe BIPV window

BIPV Window Specification	Data
Steady state thermal transmittance, U-value	1.603 W/m^{2}K
Emissivity, outermost surface	84%
Emissivity, innermost surface	84%

4.4.3 Electrical Data Report

Before running the test, the electrical characterization of BIPV window should be reported under STC. Table 16 summarizes the electrical characteristics of the CdTe based laminated window.

Table 16 Electrical characteristics of the CdTe BIPV window.

BIPV Window Specification	Data
Module efficiency, η	11.8%
Maximum Power Output, Pmax	117.8 Wdc
Voltage at MPP, Vmp	70.1 Vdc
Current at MPP, Imp	1.7 Adc
Open Circuit Voltage, Voc	88.1 Vdc
Short Circuit Current, Isc	1.8 Adc
Temperature coefficient, β	-0.311%/K at MPP

The current-voltage (IV) curve of the BIPV window is also provided, based on the manufacturer's spec sheet (Figure 54).
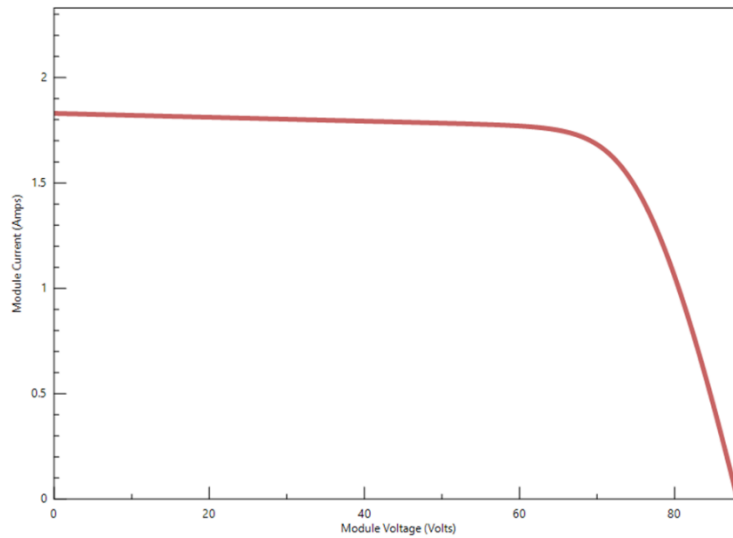
Figure 54 IV curve of the BIPV window

4.5 Uncertainty and Error Report

To illustrate the range of typical uncertainty for the proposed methodology using optical measurements, the accuracy and uncertainty of equipment should be reported. Table 17 provides an example from selected instruments' manufacturer specification sheets.

For optical equipment like pyranometer the performance is correlated to i) temperature, ii) level of irradiance, and iii) angle of incidence. Overall, for a high quality pyranometer the WMO [93] expects up to 3% uncecrtainty for the total hourly radiation, and 2% daily.

Table 17 The accuracy and uncertainty of the used equipment.

instrument	Setup locations	orientation	Measured Parameter	Instrument uncertainty/ Accuracy		Accuracy Notes	Non-Stability Non-linearity	Response time
Class A Pyranometer	Outside	Along with the window normal	E_{POA}	10 to 32 $\frac{\mu V}{W}/m^2$ Accuracy in terms of :	Tilt response <1%	CMP 6/ CMA 6 from kipp Zonen can be used	<1%	<18 s
					Temperature response <4% (-10 to 40 C interval of 50k)			
					Direct			
	Inside	Facing window	$G_{trans\,direct}$ $G_{trans\,diffuse}$ Q_{sol}	5 to 15 $\frac{\mu V}{W}/m^2$	Same as outside pyranometer	Pyrgeometer can be used inside to capture longer wave		18s
Pyrheliometer	outside	Facing sun (installed on sun tracker)	E_{direct} E_b	7 to 14 $\frac{\mu V}{W}/m^2$	Angle			5 s
					Diffuse			
					Direct			
RTD (More accurate) Or thermocouple	Inside and outside		$Temp_{out}$ $Temp_{in}$ $Temp_{surface}$	± 0.05 to ± 0.1 °C		Better accuracy compared to thermocouples(lowered accuracy around ± 0.2 to ± 0.5 °C)		1-7 s
IR camera	inside	Facing window	q_i	±2°C (±3.6°F) or ±2% of reading				About 10 minutes
Emissometer	NA Take 5 spot for both inside and outside	the measurement from surface-1 and surface-4 of window	ε	0.5% For high and low check https://inglas.org/tir100/downloads/				<5 second For each measurement

4.5.1 Equipment Calibration

The instruments used in the experiment should be calibrated in a regular basis, based on manufacturers' recommendations. The pyranometer used both outside and inside for total solar irradiance and transmitted solar irradiance respectively can be calibrated in accordance with ISO/TR 9901:1990, Solar energy-field pyranometers- recommended practice for use. Pyranometer calibration can be done either by comparison to a reference pyranometer (ISO 9847) or by using a pyrheliometer (ISO 9846). The sensitivity of this instrument is determined under well-defined reference operating conditions.

As a new methodology, it is necessary that the quality and accuracy of the result undergo some uncertainty and error evaluation/assessment. Reliability of the procedure and results therefore need to be assessed. The uncertainty of the result of this optical measurement may reflect the uncertainty of sensors which can be adjusted with correction factor. ISO/IEC Guide 98-3 presents uncertainty in measurement (GUM) and accepted procedure for characterizing the quality of a measurement.

Chapter 5. Conclusions and Future Steps

The global need to combat climate change has brought building sector and its need for significant reduction in energy consumption into focus. Achieving net-zero energy building performance requires a comprehensive approach, including energy conservation measures, improved building systems efficiency, and on-site renewable energy generation. Building Integrated Photovoltaic (BIPV) window plays a crucial role in this transition, as they generate renewable electricity while also reducing solar heat gains and enhancing visual and thermal comfort.

This thesis introduces a novel experimental methodology for determining the total solar energy transmittance (TSET) of BIPV windows using outdoor measurements, addressing the limitations of existing indoor calorimetric methods. By employing optical measurements under real-world conditions, this methodology aims to offer more accurate, faster, and practical approach to TSET testing. It is adaptable for various window technologies and is particularly suitable for BIPV windows. The proposed methodology also considers the angular dependency of TSET, providing a more comprehensive assessment of window performance.

The main difference between the proposed new methodology and current calorimetric measurement is the use of optical measurements instead of thermal measurements. While the calorimetric method requires controlled and steady state condition, the optical measurement simply can be applied under actual solar spectrum for different AOI and under real boundary conditions.

The main key steps of the proposed methodology are i) module pre-characterization ii) TSET test setup, and iii) experimental determination of TSET. Prior to the experimental determination of TSET, mechanical, thermal, and electrical characteristics of the tested module are either measured or calculated. The optical measurement equipment is mounted and installed as discussed in Chapter3, subsequently the experiment is conducted and the TSET is calculated based on the gathered data.

The experimental setup uses pyranometers (for solar transmittance measurements), pyrheliometer (for direct incident measurements), several Resistance Temperature Detector (RTD) sensors and infrared cameras (for surface temperature measurements), allowing the determination of TSET (and its angular dependency) based on a series of instantaneous outdoor measurements under sunny conditions that could result to reliable and repeatable TSET measurements. For the case of BIPV windows, a load at maximum power point (MPP) is connected to the window, allowing the maximum fraction of the absorbed solar energy to be extracted and converted into electricity.

A new approach is proposed for the conversion of measured TSET to TSET under standard test conditions, using a reference window of known TSET.

An empirical equation is developed to adjust the values accordingly. The fourth order polynomial (empirical) equation was statistically developed to take into account the specific AOI, solar spectrum and direct-to-diffuse irradiance ratio. Seventy double glazed IGUs with known angular TSET properties are generated as inputs using LBNL Window 7.8, to generate the empirical equation and the error has been estimated to be less than 5% for a double glazed IGU with no angular selective properties, and AOI < 60deg (The method is not applicable to products with angular selective coatings and AOI more than 60 degrees,

since the hemispherical transmittance value has larger discrepancies for the larger angle of incidence, namely 60°).

Furthermore, the methodology implication is not limited to BIPV windows, and can be applied for TSET determination of coated, reflective, and electrochromic windows, under test conditions beyond standard test condition, STC (irradiance of 1000 W/m^2, air mass of 1.5, and module temperature of 25 °C).

While this research presents a theoretical foundation for the TSET optical characterization of BIPV windows, further experimental validation and refinement are essential steps into future contribution.

Overall, the research presented in this thesis lays a strong foundation for advancing the assessment of Building Integrated Photovoltaic (BIPV) windows and other advanced window technologies. To further enhance the impact and applicability of this research, several future steps and areas of development can be considered:

1- Simulation of the TSET optical measurement:
Tools such as EnergyPlus, Ladybug, and Honeybee can be used to model the proposed optical measurement, where the simulated outcomes can be used to compare and validate the measured results.

2- Experimental Validation of the Proposed Methodology:
As mentioned, experimental validation is crucial to confirm the effectiveness and accuracy of the proposed methodology. Conducting a series of real-world experiments with various types of BIPV windows and also regular windows will help refine the methodology and ensure its robustness.

3 - Collaboration with international standardization and research organizations
The International Electrotechnical Commission (IEC) or the American Society for Testing and Materials (ASTM), can facilitate the development of standardized testing procedures for TSET measurement using optical methods. Collaboration with international research associations like IEA Task 15 helps exchange knowledge and refine the methodology.

4 – Applicability beyond BIPV windows
This methodology has the potential to be investigated for fenestration systems other than BIPV windows, and in different test setup (for example in a calorimetric box). Complex fenestration systems like electrochromic windows can be used to investigate the optical method in TSET determination.

5- Efficiency analysis
This methodology can be conducted to evaluated actual total solar energy transmittance in a faster and more realistic test. Energy analysis from gathered results can be conducted and the environmental benefits of BIPV windows can be assessed in future research.

By pursuing these future steps and areas of development, this research can play a pivotal role in advancing the adoption of BIPV windows and other energy-efficient building technologies, ultimately contributing to a more sustainable and environmentally friendly built environment.

Appendix

In order to correct the measured TSET, reference window with equivalent characteristics of BIPV window is assumed and the coefficients are generated using LBNL Window7.8.

SHGC for different angle of incidence generated with LBNL Window is shown in the following diagram for few generated reference windows (Table 18).

Table 18 SHGC of reference windows as a function of AOI, calculated by LBNL Window

IGU Layers		TSET(AOI)										
Outer glass NFRC#	Inner Glass NFRC#	0	10	20	30	40	50	60	70	80	90	Hemis
9814	7115F	0.437	0.44	0.44	0.437	0.43	0.415	0.382	0.309	0.172	0	0.39
11510	7115F	0.436	0.439	0.439	0.436	0.428	0.413	0.381	0.308	0.171	0	0.388
21514	7115F	0.433	0.436	0.436	0.433	0.425	0.41	0.377	0.305	0.17	0	0.385
11503	7115F	0.427	0.43	0.43	0.427	0.419	0.404	0.371	0.3	0.166	0	0.38
12266	7115F	0.424	0.428	0.427	0.424	0.416	0.401	0.369	0.298	0.164	0	0.377
2020	7115F	0.41	0.413	0.412	0.409	0.401	0.385	0.353	0.284	0.156	0	0.362
3191	7115F	0.253	0.254	0.251	0.246	0.238	0.224	0.202	0.161	0.09	0.001	0.214
2258	7115F	0.156	0.158	0.156	0.154	0.151	0.145	0.133	0.108	0.064	0	0.137
25532	7115F	0.146	0.148	0.147	0.144	0.141	0.136	0.124	0.1	0.058	0	0.128
8815	7115F	0.138	0.139	0.138	0.137	0.134	0.129	0.119	0.098	0.059	0	0.112
18810	7115F	0.127	0.128	0.127	0.126	0.123	0.119	0.11	0.092	0.056	0	0.113
14709	3303F	0.724	0.724	0.721	0.715	0.703	0.675	0.609	0.47	0.243	0	0.628
3073	3303F	0.675	0.675	0.671	0.665	0.653	0.626	0.564	0.436	0.226	0.001	0.583
2020	3303F	0.672	0.671	0.667	0.661	0.647	0.62	0.557	0.429	0.22	0	0.578
9874	3303F	0.464	0.463	0.458	0.45	0.436	0.413	0.368	0.284	0.149	0	0.389
14127	20712F	0.376	0.379	0.374	0.368	0.361	0.345	0.309	0.237	0.127	0	0.322
3068	11580	0.585	0.585	0.582	0.578	0.569	0.547	0.496	0.387	0.203	0.001	0.51
401	11580	0.393	0.393	0.389	0.382	0.371	0.351	0.313	0.242	0.126	0	0.331
20946	11580	0.38	0.383	0.378	0.372	0.364	0.348	0.311	0.238	0.126	0	0.325
5067	11580	0.414	0.413	0.408	0.401	0.389	0.367	0.326	0.25	0.128	0	0.346
4340	11580	0.648	0.649	0.647	0.644	0.635	0.614	0.559	0.439	0.235	0	0.571
120	11580	0.588	0.588	0.586	0.581	0.572	0.549	0.497	0.387	0.202	0	0.512
9994	11580	0.288	0.29	0.286	0.282	0.276	0.265	0.239	0.185	0.101	0	0.248
18177	11580	0.304	0.306	0.303	0.298	0.292	0.279	0.251	0.194	0.105	0	0.261
5004	11580	0.645	0.645	0.643	0.639	0.631	0.609	0.555	0.435	0.233	0	0.567
9816	11580	0.641	0.641	0.639	0.636	0.627	0.606	0.551	0.432	0.231	0	0.564

3005	9924	0.765	0.765	0.763	0.759	0.749	0.722	0.655	0.51	0.269	0	0.671
2988	9924	0.656	0.656	0.652	0.646	0.633	0.606	0.545	0.421	0.216	0	0.565
5434	5012	0.268	0.27	0.267	0.263	0.257	0.245	0.218	0.166	0.086	0	0.229
5385	5012	0.225	0.227	0.225	0.222	0.217	0.208	0.187	0.146	0.081	0	0.195
3116	5012	0.213	0.215	0.213	0.21	0.205	0.197	0.178	0.14	0.077	0	0.185
5316	5012	0.155	0.157	0.155	0.154	0.151	0.145	0.133	0.107	0.062	0	0.137
6229	5004	0.382	0.385	0.38	0.374	0.366	0.349	0.31	0.234	0.12	0	0.325
5284	103	0.387	0.389	0.385	0.379	0.37	0.353	0.314	0.239	0.124	0	0.33
6046	103	0.375	0.377	0.373	0.367	0.359	0.342	0.305	0.232	0.121	0	0.32
6261	103	0.282	0.284	0.281	0.277	0.27	0.258	0.23	0.175	0.091	0	0.241
3114	103	0.278	0.28	0.277	0.273	0.267	0.255	0.228	0.176	0.094	0	0.238
5439	103	0.269	0.271	0.268	0.264	0.258	0.246	0.219	0.167	0.087	0	0.23
6298	103	0.247	0.249	0.246	0.243	0.237	0.227	0.204	0.158	0.085	0	0.212
5393	103	0.246	0.247	0.245	0.241	0.236	0.226	0.203	0.158	0.085	0	0.212
2047	103	0.241	0.242	0.24	0.237	0.231	0.221	0.199	0.155	0.084	0	0.207
9834	19546F	0.257	0.258	0.255	0.249	0.24	0.226	0.203	0.161	0.088	0	0.216
9874	19546F	0.34	0.341	0.339	0.335	0.325	0.31	0.281	0.223	0.12	0	0.293
9884	19546F	0.277	0.278	0.275	0.27	0.261	0.247	0.223	0.177	0.096	0	0.235
21523	19546F	0.435	0.438	0.438	0.435	0.427	0.412	0.379	0.306	0.169	0.001	0.387
21523	20966	0.378	0.38	0.38	0.378	0.371	0.357	0.329	0.265	0.147	0.001	0.336
21547	20966	0.358	0.36	0.359	0.356	0.349	0.336	0.307	0.247	0.135	0	0.316
28176	20966	0.371	0.374	0.373	0.371	0.364	0.35	0.321	0.259	0.143	0.001	0.32
1624	10503	0.307	0.309	0.305	0.3	0.294	0.28	0.249	0.189	0.098	0	0.261
1646	10503	0.235	0.237	0.234	0.23	0.225	0.215	0.192	0.146	0.076	0	0.201
13536	10503	0.388	0.39	0.386	0.38	0.372	0.355	0.317	0.242	0.127	0	0.332
5071	14346	0.424	0.427	0.427	0.424	0.417	0.402	0.371	0.3	0.168	0	0.378
2179	14346	0.196	0.199	0.197	0.194	0.19	0.182	0.165	0.132	0.075	0	0.171
5052	21485	0.329	0.33	0.326	0.318	0.305	0.286	0.255	0.199	0.106	0	0.273
14145	21485	0.348	0.352	0.348	0.342	0.333	0.318	0.287	0.223	0.122	0	0.299
14145	9726F	0.421	0.426	0.422	0.414	0.403	0.384	0.345	0.268	0.144	0	0.362
28000	9726F	0.758	0.764	0.763	0.757	0.742	0.714	0.652	0.517	0.276	0	0.669
9814	1682F	0.346	0.349	0.349	0.347	0.341	0.33	0.305	0.25	0.142	0	0.31
5466	9721	0.216	0.217	0.215	0.211	0.206	0.197	0.178	0.138	0.076	0	0.185
5481	9721	0.228	0.23	0.227	0.224	0.219	0.21	0.19	0.15	0.084	0	0.197
14186	19552F	0.475	0.478	0.476	0.472	0.464	0.449	0.411	0.329	0.184	0	0.42
5004	19552F	0.502	0.506	0.505	0.502	0.494	0.477	0.441	0.359	0.202	0	0.448
5004	19554F	0.424	0.427	0.427	0.424	0.417	0.402	0.371	0.3	0.168	0	0.378
17605	19554F	0.407	0.41	0.41	0.407	0.399	0.385	0.354	0.286	0.158	0	0.362

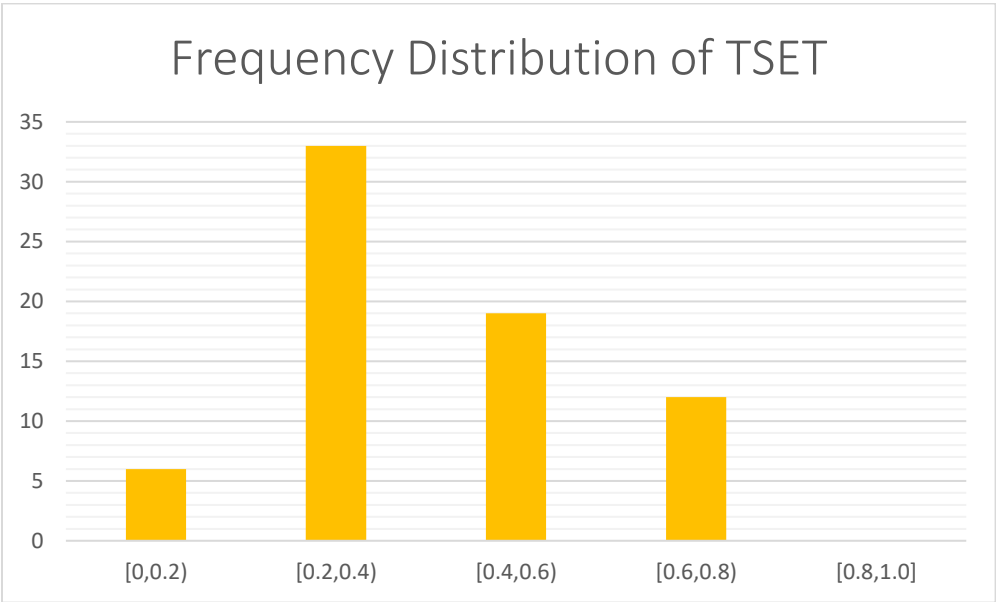|											
17605	3308F	0.693	0.693	0.689	0.683	0.671	0.643	0.58	0.447	0.23	0	0.599
17726	3308F	0.234	0.236	0.233	0.23	0.225	0.216	0.195	0.153	0.085	0	0.203
5004	3308F	0.773	0.773	0.771	0.767	0.756	0.729	0.66	0.512	0.268	0	0.677
5004	11571	0.636	0.641	0.64	0.635	0.624	0.601	0.551	0.442	0.241	0	0.564
5004	5368F	0.467	0.47	0.47	0.468	0.46	0.443	0.409	0.33	0.183	0	0.416
5005	5368F	0.465	0.468	0.468	0.466	0.458	0.441	0.407	0.328	0.182	0	0.414

Figure 55 Frequency distribution of TSET for 70 inputted IGUs
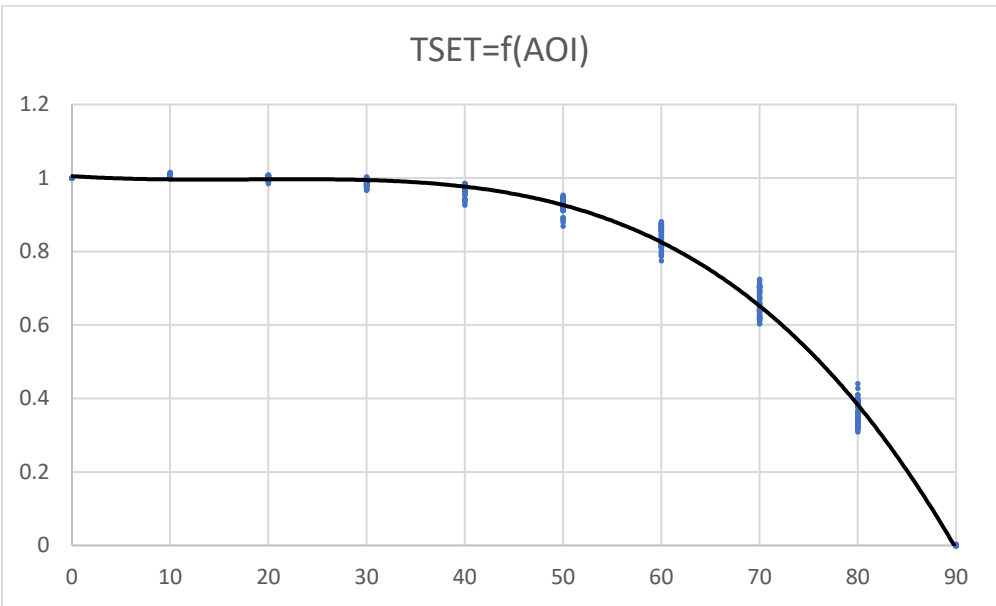

Figure 56 TSET trendline of 70 inputted IGUs as a function of AOI

Surface film coefficients in different standards:

For the purpose of comparing glazing U-values, ISO 10292 specifies surface film coefficients of indoor and outdoor surface film coefficients for 8 and 23 W/m^2k respectively. However, EN 673 [94], which is a standard based on ISO 10292[37], uses slightly different surface film coefficients (hi=7.7 W/m^2k and ho=25 W/m^2k).

The following table, comprehensively shows different surface film coefficients used for U-value calculation from different standards:

	Exterior (W/m^2k)	Interior (W/m^2k)	Notes
NFRC 100 - Interior Aluminum Frame - Interior Thermally Broken Frame - Interior Thermally Improved Frame - Interior Wood/ Vinyl frame (Frame and edge of glass simulations)	26.0	 3.29 3.00 3.12 2.44	
ISO 10077-1	25	7.7	
ISO 15099	20	3.6	
EN 673 (Center of glass simulation)	25	7.7	
ISO 10292 (Center of glass simulation)	23	8	
Passive House Institute Window Certification Criteria	25	7.7	

Unlike most standards that do not consider different surface film for TSET calculation, ISO 15099 specifies surface film coefficients of 2.5 and 8.0 for interior and exterior respectively ("for summer conditions").

References

[1] IEA, "Global energy use and energy-related CO2 emissions by sector," *IEA*, Paris, 2020. [Online]. Available: https://www.iea.org/data-and-statistics/charts/global-energy-use-and-energy-related-co2-emissions-by-sector-2020

[2] "ASHRAE Standard 90.1-2022—Energy Standard for Sites and Buildings Except Low-Rise Residential Buildings." [Online]. Available: https://www.ashrae.org/technical-resources/bookstore/standard-90-1

[3] "IEA-PVPS_Task_15_Report_C0_International_definitions_of_BIPV_hrw_180823.pdf." Accessed: Feb. 21, 2023. [Online]. Available: https://iea-pvps.org/wp-content/uploads/2020/02/IEA-PVPS_Task_15_Report_C0_International_definitions_of_BIPV_hrw_180823.pdf

[4] V. Delisle and C. Kapsis, "BIPV as a Distributed Energy Resource," in *2020 ASHRAE Winter Conference*, ASHRAE, 2020.

[5] F. Chen, S. K. Wittkopf, P. Khai Ng, and H. Du, "Solar heat gain coefficient measurement of semi-transparent photovoltaic modules with indoor calorimetric hot box and solar simulator," *Energy and Buildings*, vol. 53, pp. 74–84, Oct. 2012, doi: 10.1016/j.enbuild.2012.06.005.

[6] R. Mitchell, "WINDOW 6.2/THERM 6.2 research version user manual," 2008, Accessed: Nov. 06, 2023. [Online]. Available: https://escholarship.org/content/qt4rx784fq/qt4rx784fq.pdf

[7] "IEC 63092-1:2020 | IEC Webstore." Accessed: May 18, 2023. [Online]. Available: https://webstore.iec.ch/publication/32158

[8] "National Survey Report of PV Power Applications in Canada 2020".

[9] L. Olivieri, E. Caamaño-Martín, F. J. Moralejo-Vázquez, N. Martín-Chivelet, F. Olivieri, and F. J. Neila-Gonzalez, "Energy saving potential of semi-transparent photovoltaic elements for building integration," *Energy*, vol. 76, pp. 572–583, Nov. 2014, doi: 10.1016/j.energy.2014.08.054.

[10] "Solar Panel Construction," CLEAN ENERGY REVIEWS. Accessed: May 30, 2023. [Online]. Available: https://www.cleanenergyreviews.info/blog/solar-panel-components-construction

[11] S.-W. Choi *et al.*, "Flexible and transparent thin-film light-scattering photovoltaics about fabrication and optimization for bifacial operation," *npj Flex Electron*, vol. 7, no. 1, Art. no. 1, Mar. 2023, doi: 10.1038/s41528-023-00251-6.

[12] J. Romaní, A. Ramos, and J. Salom, "Review of Transparent and Semi-Transparent Building-Integrated Photovoltaics for Fenestration Application Modeling in Building Simulations," *Energies*, vol. 15, no. 9, Art. no. 9, Jan. 2022, doi: 10.3390/en15093286.

[13] X. Liu and Y. Wu, "A review of advanced architectural glazing technologies for solar energy conversion and intelligent daylighting control," *ARIN*, vol. 1, no. 1, p. 10, Aug. 2022, doi: 10.1007/s44223-022-00009-6.

[14] P. Bonomo *et al.*, "Categorization of BIPV applications," International Energy Agency IEA-PVPS Task 15, Report, 2021. Accessed: Feb. 21, 2023. [Online]. Available: https://iea-pvps.org/key-topics/categorization-of-bipv-applications/

[15] C. J. Traverse, R. Pandey, M. C. Barr, and R. R. Lunt, "Emergence of highly transparent photovoltaics for distributed applications," *Nat Energy*, vol. 2, no. 11, Art. no. 11, Nov. 2017, doi: 10.1038/s41560-017-0016-9.

[16] K. Kapsis, H. R. Wilson, G. Kelly, and T. Moran, "IEC 63092-1:2020 Requirements for building-integrated photovoltaic modules." Accessed: May 18, 2023. [Online]. Available: https://webstore.iec.ch/publication/32158

[17] "Best Research-Cell Efficiency Chart." Accessed: Jun. 07, 2023. [Online]. Available: https://www.nrel.gov/pv/cell-efficiency.html

[18] Hisashi Ishi, "The technical architectural issues toward establishment of international standardization for BIPV (Building Integrated Photovoltaics) module and systems as facade engineering field," *GBRC: General Building Research Corporation*, vol. 44, no. 2, pp. 13–23, 2019.

[19] K. Kapsis, A. Athienitis, and S. Harrison, "Determination of Solar Heat Gain Coefficients for Semitransparent Photovoltaic Windows: An Experimental Study," *ASHRAE Transactions*, vol. 123, pp. 82–94, 2017.

[20] G. Chinazzo, A. Legrain, G. Peronato, J. Wienold, and M. Andersen, "Energy Performance And Occupancy-Based Analysis Of Visual And Thermal Comfort For Transmittance Level And Layout Variations Of Semi-Transparent Photovoltaics," presented at the Building Simulation 2019, Rome, Italy, pp. 4385–4392. doi: 10.26868/25222708.2019.210262.

[21] L. Olivieri, E. Caamaño-Martin, F. .Olivieri, and J. Neila, "Integral energy performance characterization of semi-transparent photovoltaic elements for building integration under real operation conditions," *Energy and Buildings*, vol. 68, pp. 280–291, Jan. 2014, doi: 10.1016/j.enbuild.2013.09.035.

[22] Y. T. Chae, J. Kim, H. Park, and B. Shin, "Building energy performance evaluation of building integrated photovoltaic (BIPV) window with semi-transparent solar cells," *Applied Energy*, vol. 129, pp. 217–227, Sep. 2014, doi: 10.1016/j.apenergy.2014.04.106.

[23] K. Lee *et al.*, "The Development of Transparent Photovoltaics," *Cell Reports Physical Science*, vol. 1, no. 8, p. 100143, Aug. 2020, doi: 10.1016/j.xcrp.2020.100143.

[24] T. Miyazaki, A. Akisawa, and T. Kashiwagi, "Energy savings of office buildings by the use of semi-transparent solar cells for windows," *Renewable Energy*, vol. 30, no. 3, pp. 281–304, Mar. 2005, doi: 10.1016/j.renene.2004.05.010.

[25] T. Y. Y. Fung and H. Yang, "Study on thermal performance of semi-transparent building-integrated photovoltaic glazings," *Energy and Buildings*, vol. 40, no. 3, pp. 341–350, 2008, doi: 10.1016/j.enbuild.2007.03.002.

[26] N. Martín-Chivelet *et al.*, "Building-Integrated Photovoltaic (BIPV) products and systems: A review of energy-related behavior," *Energy and Buildings*, vol. 262, p. 111998, May 2022, doi: 10.1016/j.enbuild.2022.111998.

[27] K. Kapsis, V. Dermardiros, and A. K. Athienitis, "Daylight Performance of Perimeter Office Façades utilizing Semi-transparent Photovoltaic Windows: A Simulation Study," *Energy Procedia*, vol. 78, pp. 334–339, Nov. 2015, doi: 10.1016/j.egypro.2015.11.657.

[28] S. Barman, A. Chowdhury, S. Mathur, and J. Mathur, "Assessment of the efficiency of window integrated CdTe based semi-transparent photovoltaic module," *Sustainable cities and society*, vol. 37, pp. 250–262, 2018.

[29] D. Singh, R. Chaudhary, and A. Karthick, "Review on the progress of building-applied/integrated photovoltaic system," *Environ Sci Pollut Res*, vol. 28, no. 35, pp. 47689–47724, Sep. 2021, doi: 10.1007/s11356-021-15349-5.

[30] Y. Sun *et al.*, "Analysis of the daylight performance of window integrated photovoltaics systems," *Renewable Energy*, vol. 145, pp. 153–163, Jan. 2020, doi: 10.1016/j.renene.2019.05.061.

[31] J. Markvart, A. Iversen, A. Logadottir, and K. Johnsen, "Indoor light and visual comfort with solar cells in glass facades," Sep. 2012, Accessed: Feb. 27, 2023. [Online]. Available: https://www.osti.gov/etdeweb/biblio/22005453

[32] H. Musameh, H. Alrashidi, F. Al-Neami, and W. Issa, "Energy performance analytical review of semi-transparent photovoltaics glazing in the United Kingdom," *Journal of Building Engineering*, vol. 54, p. 104686, Aug. 2022, doi: 10.1016/j.jobe.2022.104686.

[33] J. Peng, D. C. Curcija, L. Lu, S. E. Selkowitz, H. Yang, and R. Mitchell, "Developing a method and simulation model for evaluating the overall energy performance of a ventilated semi-transparent photovoltaic double-skin facade," *Progress in Photovoltaics: Research and Applications*, vol. 24, no. 6, pp. 781–799, 2016, doi: 10.1002/pip.2727.

[34] "Jiaxing Botao Solartech Co., Ltd." Accessed: Mar. 02, 2023. [Online]. Available: https://fysolarpanel.en.alibaba.com/minisiteentrance.html?from=detail&productId=60362228280?spm=a2700.details.0.0.278010f9r79MF8&tracelog=product_detail_cp

[35] "ISO/CD 15099 Thermal performance of windows, doors and shading devices — Detailed calculations," ISO. [Online]. Available: https://www.iso.org/standard/84800.html

[36] J. L. Wright, "Summary and comparison of methods to calculate solar heat gain," 1995, Accessed: Nov. 05, 2023. [Online]. Available: https://uwspace.uwaterloo.ca/handle/10012/11575

[37] "ISO 10292:1994 Glass in building — Calculation of steady-state U values (thermal transmittance) of multiple glazing." [Online]. Available: https://www.iso.org/standard/18334.html

[38] B. Hanam and P. Eng, "ENERGY PERFORMANCE OF WINDOWS: NAVIGATING NORTH AMERICAN AND EUROPEAN WINDOW STANDARDS," 2014.

[39] M. Bae, Y. Lee, G. Choi, S. Kim, and J. Kang, "Analysis of the Calculation Method for the Thermal Transmittance of Double Windows Considering the Thermal Properties of the Air Cavity," *Sustainability*, vol. 12, no. 24, Art. no. 24, Jan. 2020, doi: 10.3390/su122410439.

[40] S. Yang, A. Cannavale, D. Prasad, A. Sproul, and F. Fiorito, "Numerical simulation study of BIPV/T double-skin facade for various climate zones in Australia: Effects on indoor thermal comfort," *Build. Simul.*, vol. 12, no. 1, pp. 51–67, Feb. 2019, doi: 10.1007/s12273-018-0489-x.

[41] L. Lu and K. M. Law, "Overall energy performance of semi-transparent single-glazed photovoltaic (PV) window for a typical office in Hong Kong," *Renewable Energy*, vol. 49, pp. 250–254, Jan. 2013, doi: 10.1016/j.renene.2012.01.021.

[42] C. Qiu and H. Yang, "Daylighting and overall energy performance of a novel semi-transparent photovoltaic vacuum glazing in different climate zones," *Applied Energy*, vol. 276, p. 115414, Oct. 2020, doi: 10.1016/j.apenergy.2020.115414.

[43] "ISO 9050:2003." [Online]. Available: https://www.iso.org/standard/35062.html

[44] "IEC 63092-3 Photovoltaics in buildings — Part 3: Evaluation methodology of SHGC for Building integrated photovoltaic modules with various designs." [Online]. Available: https://www.iso.org/standard/83518.html

[45] Hisashi ISHII, Michio KONDO, Masafumi SAITO,et., "Thermal Properties for BIPV in Glass Façade Experimental Results of Thermal Transmittance and Solar Heat Gain Coefficient for Crystal Silicon PV Module." Accessed: Feb. 28, 2023. [Online]. Available: https://jglobal.jst.go.jp/en/detail?JGLOBAL_ID=200901094510408210&e=publication%2Fpaper

[46] J. Peng, D. C. Curcija, L. Lu, S. E. Selkowitz, H. Yang, and W. Zhang, "Numerical investigation of the energy saving potential of a semi-transparent photovoltaic double-skin facade in a cool-summer Mediterranean climate," *Applied Energy*, vol. 165, pp. 345–356, Mar. 2016, doi: 10.1016/j.apenergy.2015.12.074.

[47] W. He, Y. X. Zhang, W. Sun, J. X. Hou, Q. Y. Jiang, and J. Ji, "Experimental and numerical investigation on the performance of amorphous silicon photovoltaics window in East China," *Building and Environment*, vol. 46, no. 2, pp. 363–369, 2011.

[48] M. Wang *et al.*, "Comparison of energy performance between PV double skin facades and PV insulating glass units," *Applied Energy*, vol. 194, pp. 148–160, May 2017, doi: 10.1016/j.apenergy.2017.03.019.

[49] A. Gok, E. Ozkalay, G. Friesen, and F. Frontini, "The Influence of Operating Temperature on the Performance of BIPV Modules," *IEEE Journal of Photovoltaics*, vol. 10, no. 5, pp. 1371–1378, Sep. 2020, doi: 10.1109/JPHOTOV.2020.3001181.

[50] W. R. McCluney, "Sensitivity of fenestration solar gain to source spectrum and angle of incidence," Art. no. CONF-960606-, Dec. 1996, Accessed: Jul. 04, 2023. [Online]. Available: https://www.osti.gov/biblio/433717

[51] S. Xu, W. Liao, J. Huang, and J. Kang, "Optimal PV cell coverage ratio for semi-transparent photovoltaics on office building façades in central China," *Energy and Buildings*, vol. 77, pp. 130–138, Jul. 2014, doi: 10.1016/j.enbuild.2014.03.052.

[52] J. H. Klems, "Solar Heat Gain Through Fenestration Systems Containing Shading: Procedures for Estimating Performace from Minimal Data".

[53] J. H. Klems, J. L. Warner, and G. O. Kelley, "A Comparison Between Calculated and Measured SHGC for Complex Fenestration Systems".

[54] H. Manz, "Total solar energy transmittance of glass double façades with free convection," *Energy and Buildings*, vol. 36, no. 2, pp. 127–136, Feb. 2004, doi: 10.1016/j.enbuild.2003.10.003.

[55] R. Mitchell, C. Kohler, D. Arasteh, J. Carmody, C. Huizenga, and D. Curcija, "THERM 5 / WINDOW 5 NFRC simulation manual," Lawrence Berkeley National Lab. (LBNL), Berkeley, CA (United States), LBNL-48255, Jun. 2003. doi: 10.2172/834262.

[56] "ASHRAE 2021 Handbook—Fundamentals: Chapter 15 FENESTRATION." [Online]. Available: https://handbook.ashrae.org/Print.html?file=https://handbook.ashrae.org/Handbooks/F21/IP/F21_Ch15/F21_Ch15_ip.aspx

[57] "International Window Standards," Apr. 2014. [Online]. Available: https://www.bchousing.org/publications/International-Window-Standards.pdf

[58] U. Mazzali, P. Ruggeri, M. Zinzi, F. Peron, P. Romagnoni, and A. Daneo, "Set-up and Calibration by Experimental Data of a Numerical Model for the Estimation of Solar Factor and Ug-value of Building Integrated Photovoltaic Systems," *Energy Procedia*, vol. 78, pp. 2202–2207, Nov. 2015, doi: 10.1016/j.egypro.2015.11.319.

[59] Y. Feng and J. Wang, "Design and development of a low-cost glazing measurement system," *MethodsX*, vol. 7, p. 101028, 2020, doi: 10.1016/j.mex.2020.101028.

[60] F. Chen and S. K. Wittkopf, "Summer condition thermal transmittance measurement of fenestration systems using calorimetric hot box," *Energy and Buildings*, vol. 53, pp. 47–56, Oct. 2012, doi: 10.1016/j.enbuild.2012.07.005.

[61] H. R. Wilson *et al.*, "Multifunctional Characterisation of BIPV-Proposed Topics for Future International Standardisation Activities," in *Multifunctional Characterisation of BIPV-Proposed Topics for Future International Standardisation Activities*, 2020.

[62] "ISO 10293: 1997 Glass in building — Determination of steady-state U values (thermal transmittance) of multiple glazing — Heat flow meter method."

[63] J. Wright, "A Simplified Analysis of Radiant Heat Loss Through Projecting Fenestration Products", [Online]. Available: https://core.ac.uk/reader/144150330

[64] S. J. Harrison and S. J. Van Wonderen, "Solar heat gain performance evaluation of commercial solar-control glazings and shading devices," 1996.

[65] "EnergyPlus Version 22.1 Documents." [Online]. Available: https://bigladdersoftware.com/epx/docs/22-1/

[66] L. Olivieri, F. Frontini, C. Polo-López, D. Pahud, and E. Caamaño-Martín, "G-value indoor characterization of semi-transparent photovoltaic elements for building integration: New equipment and methodology," *Energy and Buildings*, vol. 101, pp. 84–94, Aug. 2015, doi: 10.1016/j.enbuild.2015.04.056.

[67] J. Kosny, E. Kossecka, and E. Kossecka, "Hot-Box Testing of Building Envelope Assemblies—A Simplified Procedure for Estimation of Minimum Time of the Test," *Journal of Testing and Evaluation - J TEST EVAL*, vol. 36, May 2008, doi: 10.1520/JTE100795.

[68] T. E. Kuhn, "Calorimetric determination of the solar heat gain coefficient g with steady-state laboratory measurements," *Energy and Buildings*, vol. 84, pp. 388–402, Dec. 2014, doi: 10.1016/j.enbuild.2014.08.021.

[69] P. Loutzenhiser, H. Manz, and G. Maxwell, "Empirical validations of shading/daylighting/load interactions in building energy simulation tools," *A report for the international energy agency SHC task*, vol. 34, 2007.

[70] S. Harrison and M. Collins, *QUEEN'S UNIVERSITY SOLAR CALORIMETER–DESIGN, CALIBRATION, AND OPERATING PROCEDURE*. 1999.

[71] J. J. Bloem, C. Lodi, J. Cipriano, and D. Chemisana, "An outdoor Test Reference Environment for double skin applications of Building Integrated PhotoVoltaic Systems," *Energy and Buildings*, vol. 50, pp. 63–73, Jul. 2012, doi: 10.1016/j.enbuild.2012.03.023.

[72] "NFRC 300-2010 Test Method for Determining the Solar Optical Properties of Glazing Materials and Systems." [Online]. Available: https://users.encs.concordia.ca/~raojw/crd/reference/reference003611.html

[73] D. Pahud, P. Gallinelli, D. Crivellin, S. Margot, R. Camponovo, and M. Belliardi, "G-box. Mesure in situ des performances énergétiques de façades transparentes et translucides," Scuola universitaria professionale della Svizzera italiana, Report, Jun. 2013. Accessed: Jul. 17, 2023. [Online]. Available: https://repository.supsi.ch/3082/

[74] P. H. Baker, "PASLINK AND DYNAMIC OUTDOOR TESTING OF THERMAL AND SOLAR PROPERTIES OF BUILDING COMPONENTS".

[75] J. H. Klems, M. Yazdanian, and G. O. Kelley, "Measured performance of selective glazings," Lawrence Berkeley National Lab. (LBNL), Berkeley, CA (United States), LBL-37747; Mo-337; CONF-951215-3, Jul. 1995. Accessed: Nov. 05, 2023. [Online]. Available: https://www.osti.gov/biblio/195752

[76] J. H. Klems, "A new method for predicting the solar heat gain of complex fenestration systems," 1995, Accessed: Nov. 05, 2023. [Online]. Available: https://escholarship.org/content/qt2g81t57w/qt2g81t57w.pdf

[77] M. Wang, J. Peng, N. Li, L. Lu, T. Ma, and H. Yang, "Assessment of energy performance of semi-transparent PV insulating glass units using a validated simulation model," *Energy*, vol. 112, pp. 538–548, Oct. 2016, doi: 10.1016/j.energy.2016.06.120.

[78] T. Baenas and M. Machado, "On the analytical calculation of the solar heat gain coefficient of a BIPV module," *Energy and Buildings*, vol. 151, pp. 146–156, Sep. 2017, doi: 10.1016/j.enbuild.2017.06.039.

[79] "ISO 10291:1994 - Glass in Building - Determination of Steady-State U Values (Thermal Transmittance) of Multiple Glazing - Guarded Hot Plate Method." ISO, Sep. 1994. [Online]. Available: https://www.iso.org/standard/18333.html

[80] "ASTM C177 Standard Test Method for Steady-State Heat Flux Measurements and Thermal Transmission Properties by Means of the Guarded-Hot-Plate Apparatus."

[81] "ASTM C209 Standard Test Methods for Cellulosic Fiber Insulating Board."

[82] T. M. Simko, R. E. Collins, F. A. Beck, and D. Arasteh, "Edge conduction in vacuum glazing," Lawrence Berkeley National Lab.(LBNL), Berkeley, CA (United States), 1995.

[83] A. C1371-04a, "Standard Test Method for Determination of Emittance of Materials Near Room Temperature Using Portable Emissometers," American Society for Testing and Materials West Conshohocken, PA, USA, 2010.

[84] "IEC 61215-1:2021 Terrestrial photovoltaic modules — design qualification and type approval Part 1: Test requirements." [Online]. Available: https://webstore.iec.ch/publication/61345

[85] "IEC 61215-2:2021 Terrestrial photovoltaic modules — design qualification and type approval, Part 2: Test procedures." [Online]. Available: https://webstore.iec.ch/publication/68602

[86] V. G. Karpov, D. Shvydka, and Y. Roussillon, "Physics of CdTe photovoltaics: from front to back," *MRS Online Proceedings Library (OPL)*, vol. 865, pp. F10-1, 2005.

[87] M. Gostein and L. Dunn, "Light soaking effects on photovoltaic modules: Overview and literature review," in *2011 37th IEEE Photovoltaic Specialists Conference*, IEEE, 2011, pp. 003126–003131.

[88] J. A. Duffie and W. A. Beckman, *Solar engineering of thermal processes*. Wiley New York, 1980.

[89] "ISO 19467:2017 Thermal performance of windows and doors — Determination of solar heat gain coefficient using solar simulator." [Online]. Available: https://www.iso.org/standard/64989.html

[90] "ASTM G173 Standard Tables for Reference Solar Spectral Irradiances: Direct Normal and Hemispherical on 37° Tilted Surface."

[91] B. Marion, "Preliminary Investigation of Methods for Correcting for Variations in Solar Spectrum Under Clear Skies," *Publications (E)*, pp. 1–53, Mar. 2010.

[92] "ASTME2112-23 Standard Practice for Installation of Exterior Windows, Doors and Skylights." [Online]. Available: https://www.astm.org/e2112-23.html

[93] "Guide to Meteorological Instruments and Methods of Observation: (CIMO guide). 2014 edition, updated in 2017." World Meteorological Organization, 2017. [Online]. Available: https://www.weather.gov/media/epz/mesonet/CWOP-WMO8.pdf

[94] "LST: 673: 2011; Glass in Building—Determination... - Google Scholar." Accessed: Jul. 30, 2023. [Online]. Available: https://scholar.google.com/scholar_lookup?title=EN%20673%3A2011%20Glass%20in%20Building.%20Determination%20of%20Thermal%20Transmittance%20(U%20Value).%20Calculation%20Method&author=European%20Committee%20for%20Standardization&publication_year=2011